Experimental powder diffraction using HRPT as an example

High Resolution Powder Diffractometer for Thermal Neutrons

http://sinq.web.psi.ch/hrpt

Vladimir Pomjakushin

Laboratory for Neutron Scattering, PSI

Plan

- Introduction to neutron scattering/diffraction 2-16
- Powder neutron diffraction (ND) @ PSI/SINQ 17-24
- Experimental powder diffraction using HRPT (High Resolution Powder Diffractometer for Thermal Neutrons) as an example 25-54
- Examples of results 55-66

1994 Nobel Prize in Physics

Clifford G. Shull
1915 – 2001, USA

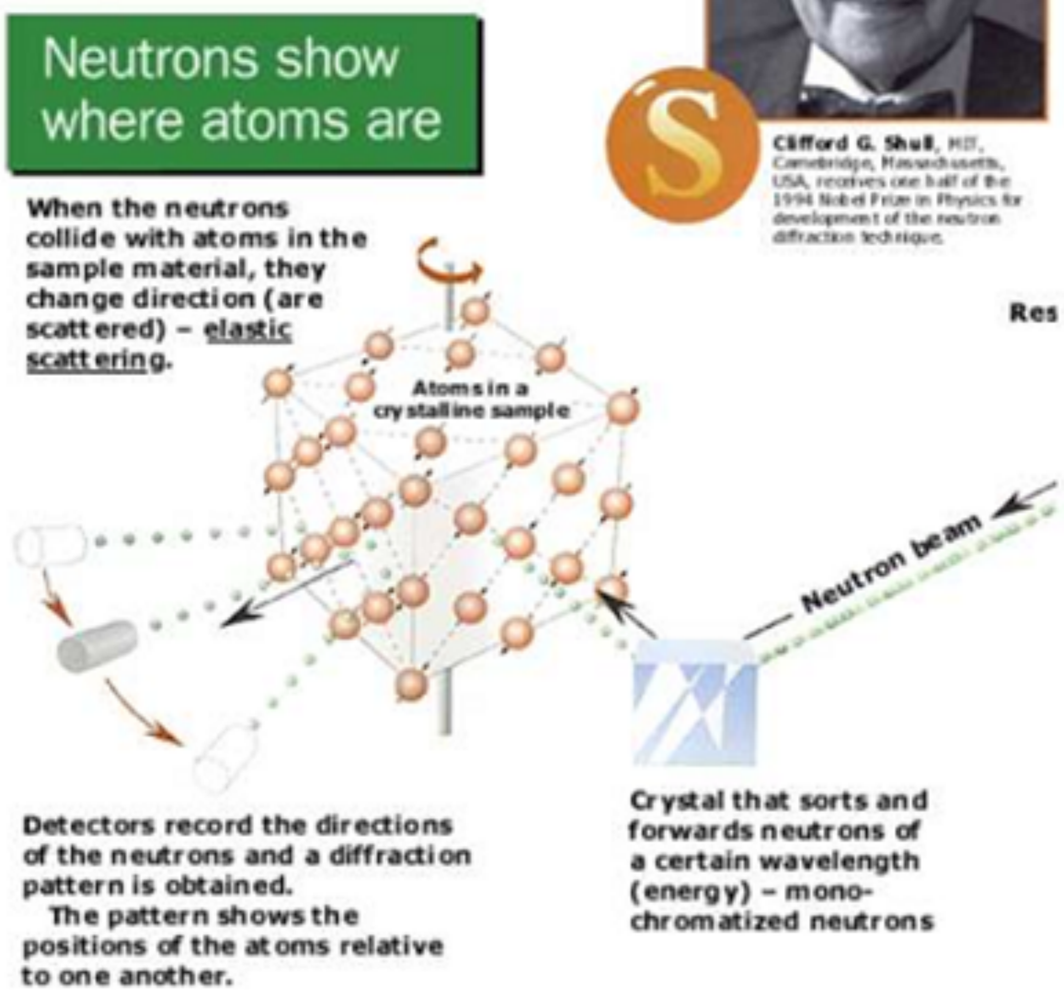

Bertram N. Brockhouse
1918 – 2003, Canada

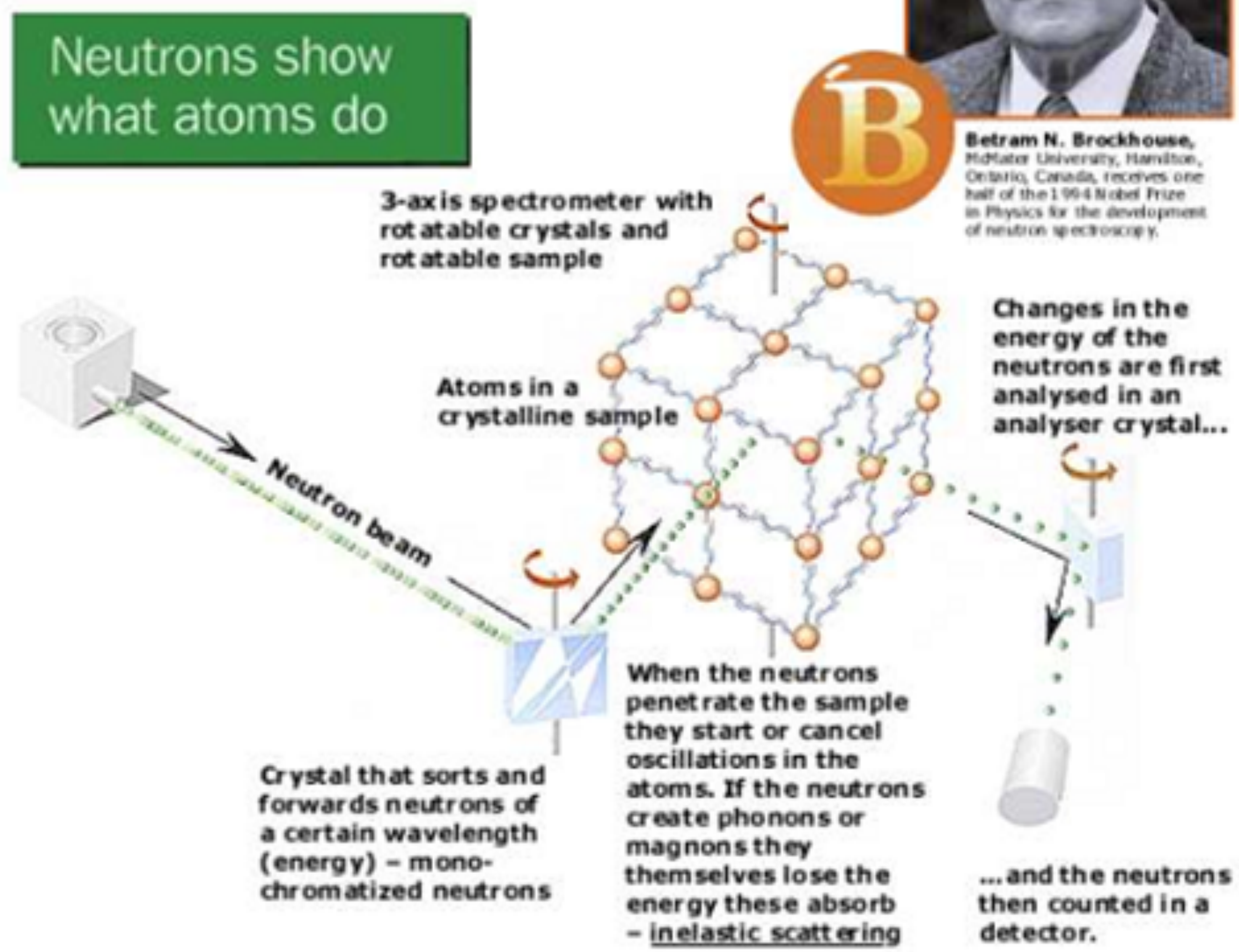

http://www.nobelprize.org/nobel_prizes/physics/laureates/1994/illpres/neutrons.html

Neutron sources for condensed matter studies

I. Continuous neutron sources

W = 10 – 100 MW
Const in time

SINQ, Switzerland
ILL, France
LLB, France
VVR-M, Russia
IR-8, Russia,
BENSC, Germany
FRM II, Germany
BNC, Hungary
NPI, Czechia
NIST, USA
ORNL, USA
…

II. Pulsed neutron sources

Short pulse → II-*a*. SPS

Long pulse → II-*b*. LPS

II-*a*. SPS

W = 0.01 – 1 MW
Pulsed in time
$\Delta t_0 \approx (15 - 100)\ \mu s$

ISIS, UK
LANSCE, USA
SNS, USA
KENS, Japan
J-SNS, Japan

II-*b*. LPS

W = 2 – 5 MW
Pulsed in time
$\Delta t_0 \approx (300 - 1000)\ \mu s$

IBR-2M, Russia
ESS, Europe
LANSCE (new)
???

courtesy of A. Balagurov

Steady state reactor or spallation source / Pulsed neutron source

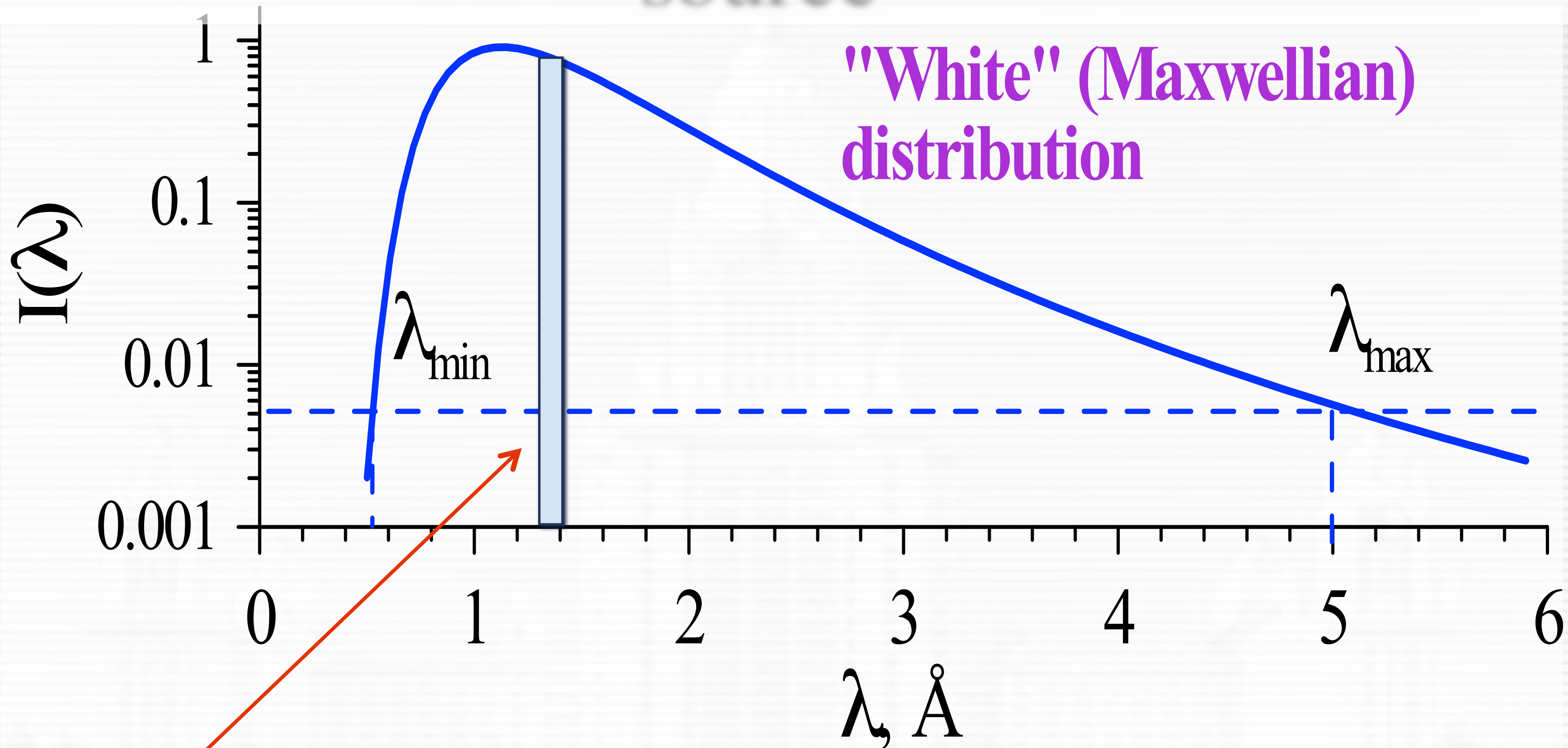

<u>Monochromatic incident beam:</u>

$\lambda = \text{const} \approx 1.4$ Å, $\Delta\lambda/\lambda \approx 0.01$,

<u>Source</u>: W = (10 – 100) MW = const,

Scan over scattering angle,

Wide angle range is needed.

courtesy of A. Balagurov

Steady state reactor or spallation source / Pulsed neutron source

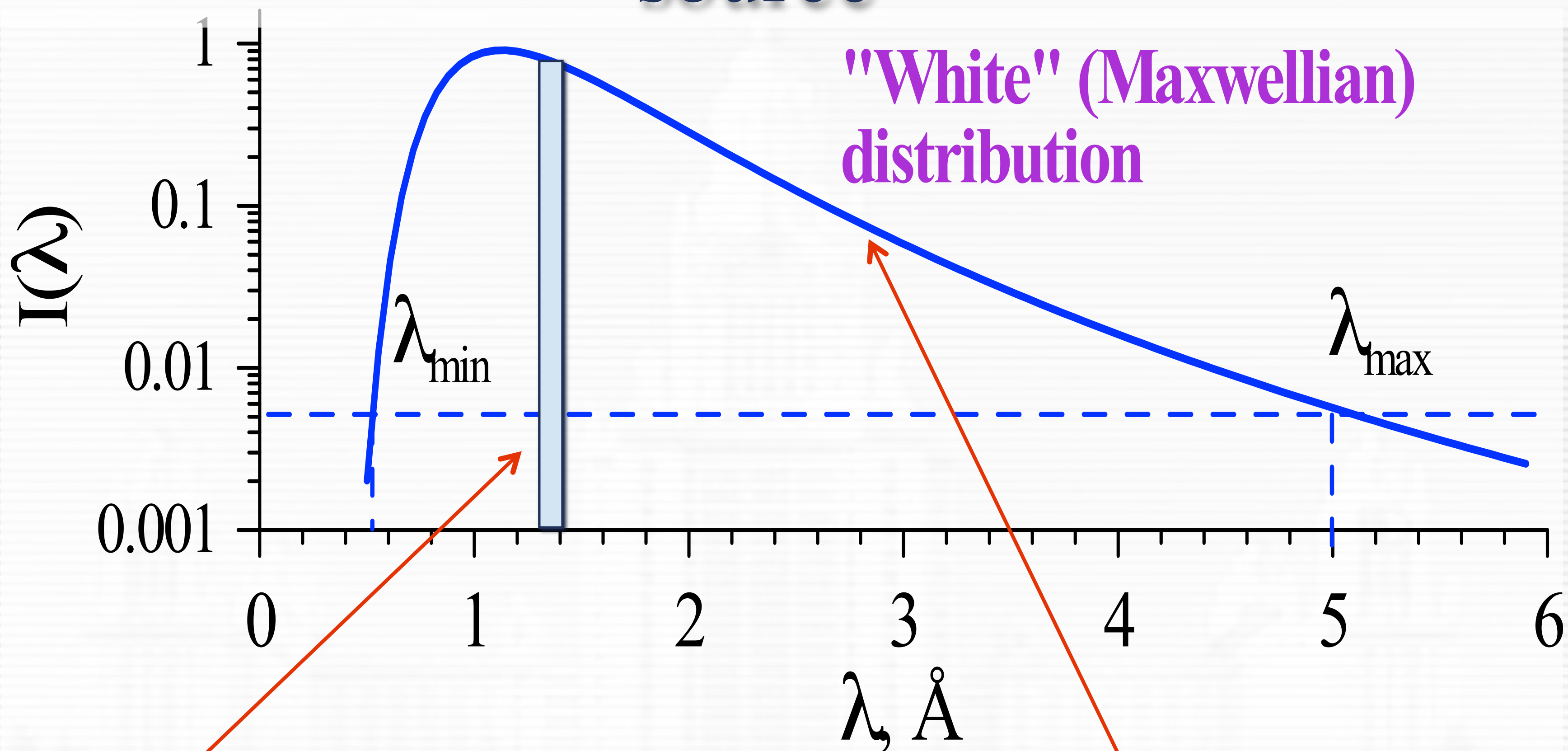

Monochromatic incident beam:

$\lambda = \text{const} \approx 1.4$ Å, $\Delta\lambda/\lambda \approx 0.01$,

Source: W = (10 – 100) MW = const,

Scan over scattering angle,

Wide angle range is needed.

Polychromatic incident beam:

$\lambda_{min} \leq \lambda \leq \lambda_{max}$, $\Delta\lambda \approx 5$ Å,

Source: W = (0.01 – 2) MW, pulsed,

Scan over time of flight (TOF),

Fixed angle geometry.

courtesy of A. Balagurov

Geometry of diffractometer with λ = const

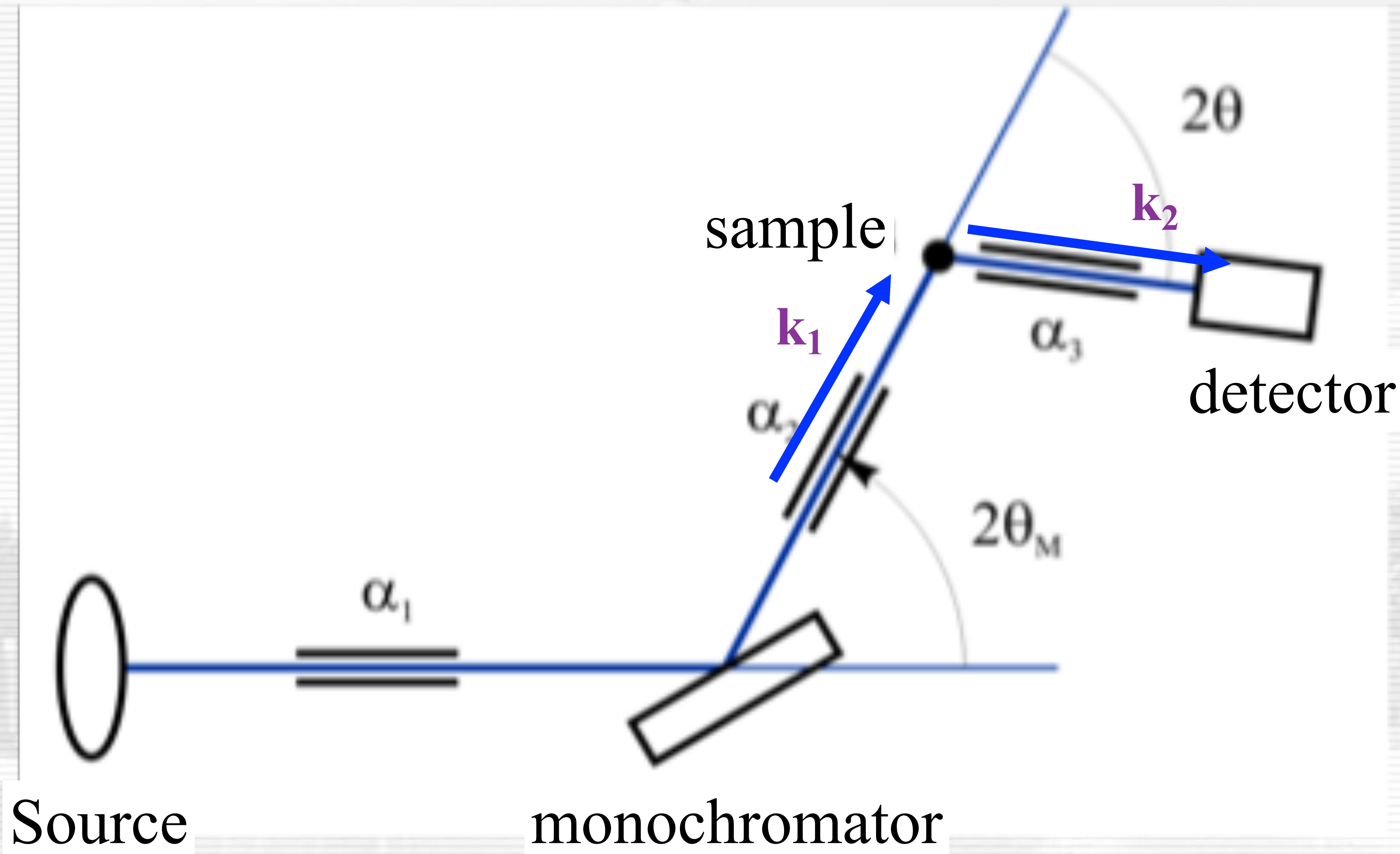

Elastic and inelastic neutron scattering

Momentum transfer
$q=k_2-k_1$

Energy transfer ($E_0 \approx 0.025$ eV)

↓

Always takes place

courtesy of A. Balagurov

Elastic and inelastic neutron scattering

Momentum transfer
$q = k_2 - k_1$

Always takes place

Energy transfer ($E_0 \approx 0.025$ eV)

to atom,
$\Delta E/E_0 \sim 1$, "inelastic"

to collective mode,
$\Delta E/E_0 \sim 1$, "inelastic"

courtesy of A. Balagurov

Elastic and inelastic neutron scattering

Momentum transfer
$q = k_2 - k_1$

Always takes place

Energy transfer ($E_0 \approx 0.025$ eV)

to atom,
$\Delta E/E_0 \sim 1$, "inelastic"

to collective mode,
$\Delta E/E_0 \sim 1$, "inelastic"

to crystal,
$\Delta E/E_0 \sim 10^{-24}$ ($\Delta E = 0$)
"elastic scattering"

$E_i = E_f$

$|k_i| = |k_f|$

courtesy of A. Balagurov

Specifics of thermal neutron interaction with matter
Scattering amplitude or length

courtesy of A. Balagurov

Specifics of thermal neutron interaction with matter
Scattering amplitude or length

- *b* nuclear coherent scattering length does not depend on **q** (thermal factors)

courtesy of A. Balagurov

Specifics of thermal neutron interaction with matter
Scattering amplitude or length

- *b* nuclear coherent scattering length does not depend on **q** (thermal factors)
- no regularity in *b* dependence on atomic number

courtesy of A. Balagurov

Specifics of thermal neutron interaction with matter
Scattering amplitude or length

- *b* nuclear coherent scattering length does not depend on **q** (thermal factors)

- no regularity in *b* dependence on atomic number
  light atoms in presence of heavy atoms: H-O, Mn-O, U-H, …

courtesy of A. Balagurov

Specifics of thermal neutron interaction with matter
Scattering amplitude or length

- *b* nuclear coherent scattering length does not depend on **q** (thermal factors)

- no regularity in *b* dependence on atomic number
  light atoms in presence of heavy atoms: H-O, Mn-O, U-H, …
  neighbours discrimination: O-N, Co-Fe, …)

courtesy of A. Balagurov

Specifics of thermal neutron interaction with matter
Scattering amplitude or length

- *b* nuclear coherent scattering length does not depend on **q** (thermal factors)

- no regularity in *b* dependence on atomic number
  light atoms in presence of heavy atoms: H-O, Mn-O, U-H, …
  neighbours discrimination: O-N, Co-Fe, …)

- no regularity in *b* dependence on nuclear mass (isotope contrasting)

courtesy of A. Balagurov

Specifics of thermal neutron interaction with matter
Scattering amplitude or length

- *b* nuclear coherent scattering length does not depend on **q** (thermal factors)

- no regularity in *b* dependence on atomic number
  light atoms in presence of heavy atoms: H-O, Mn-O, U-H, …
  neighbours discrimination: O-N, Co-Fe, …)

- no regularity in *b* dependence on nuclear mass (isotope contrasting)
  $b_H = -0.37$ $\quad\quad$ $b_{Fe\text{-}56} = 1.01$

courtesy of A. Balagurov

Specifics of thermal neutron interaction with matter
Scattering amplitude or length

- *b* nuclear coherent scattering length does not depend on **q** (thermal factors)

- no regularity in *b* dependence on atomic number

  light atoms in presence of heavy atoms: H-O, Mn-O, U-H, …

  neighbours discrimination: O-N, Co-Fe, …)

- no regularity in *b* dependence on nuclear mass (isotope contrasting)

  $b_H = -0.37$ $b_{Fe\text{-}56} = 1.01$

  $b_D = 0.67$ $b_{Fe\text{-}57} = 0.23$

courtesy of A. Balagurov

Specifics of thermal neutron interaction with matter
Scattering amplitude or length

- *b* nuclear coherent scattering length does not depend on **q** (thermal factors)

- no regularity in *b* dependence on atomic number

  light atoms in presence of heavy atoms: H-O, Mn-O, U-H, …

  neighbours discrimination: O-N, Co-Fe, …)

- no regularity in *b* dependence on nuclear mass (isotope contrasting)

  $b_H = -0.37$ $b_{Fe\text{-}56} = 1.01$

  $b_D = 0.67$ $b_{Fe\text{-}57} = 0.23$

- *b* can be < 0 ("zero" matrix without coherent scattering from container)

courtesy of A. Balagurov

Specifics of thermal neutron interaction with matter
Scattering amplitude or length

- *b* nuclear coherent scattering length does not depend on **q** (thermal factors)

- no regularity in *b* dependence on atomic number
  light atoms in presence of heavy atoms: H-O, Mn-O, U-H, …
  neighbours discrimination: O-N, Co-Fe, …)

- no regularity in *b* dependence on nuclear mass (isotope contrasting)
  $b_H = -0.37$ $b_{Fe\text{-}56} = 1.01$
  $b_D = 0.67$ $b_{Fe\text{-}57} = 0.23$

- *b* can be < 0 ("zero" matrix without coherent scattering from container)

- large magnetic scattering amplitude (magnetic structure)

courtesy of A. Balagurov

Specifics of thermal neutron interaction with matter
Scattering amplitude or length

- *b* nuclear coherent scattering length does not depend on **q** (thermal factors)

- no regularity in *b* dependence on atomic number

  light atoms in presence of heavy atoms: H-O, Mn-O, U-H, …

  neighbours discrimination: O-N, Co-Fe, …)

- no regularity in *b* dependence on nuclear mass (isotope contrasting)

  $b_H = -0.37$ $\qquad$ $b_{Fe\text{-}56} = 1.01$

  $b_D = 0.67$ $\qquad$ $b_{Fe\text{-}57} = 0.23$

- *b* can be < 0 (“zero” matrix without coherent scattering from container)

- large magnetic scattering amplitude (magnetic structure)

- small absorption (high penetration)

courtesy of A. Balagurov

Real space/lattice. Translational symmetry

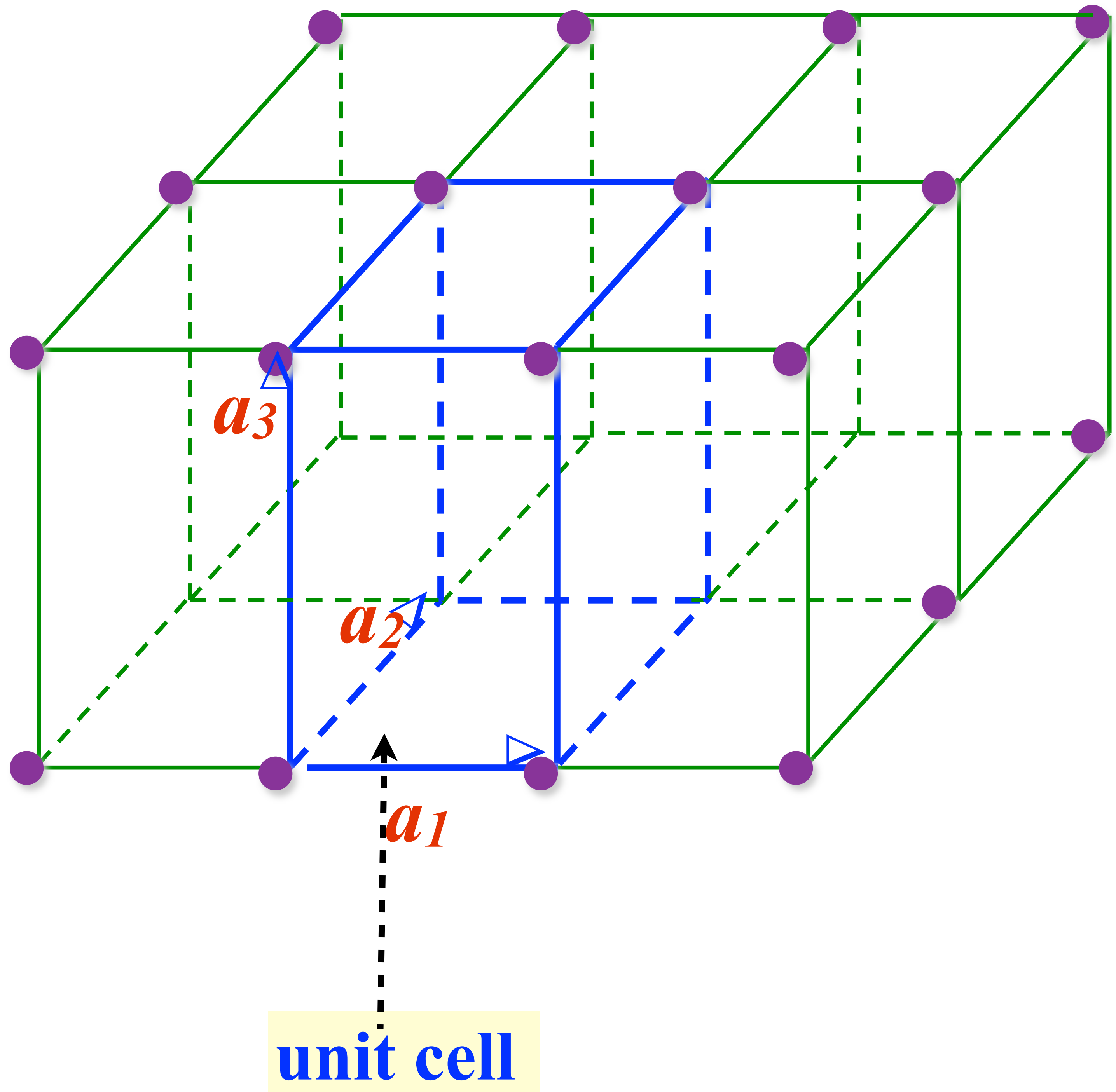

Reciprocal space/lattice

$\{a_i\}$ – basis in the real crystal space

$\{b_i\}$ – basis in the reciprocal space

Reciprocal space/lattice

$\{\boldsymbol{a}_i\}$ – **basis in the real crystal space**

$\{\boldsymbol{b}_i\}$ – **basis in the reciprocal space**

$$\boldsymbol{b}_1=[\boldsymbol{a}_2\boldsymbol{a}_3]/V_c,\quad \boldsymbol{b}_2=[\boldsymbol{a}_3\boldsymbol{a}_1]/V_c,\quad \boldsymbol{b}_3=[\boldsymbol{a}_1\boldsymbol{a}_2]/V_c,$$

$$V_c=\boldsymbol{a}_1[\boldsymbol{a}_2\boldsymbol{a}_3]$$

$$\boldsymbol{a}_i\cdot\boldsymbol{b}_j = \delta_{ij} = 1 \text{ for } i=j,\ 0 \text{ for } i\neq j$$

Reciprocal space/lattice

$\{\boldsymbol{a}_{\mathrm{i}}\}$ – **basis in the real crystal space**

$\{\boldsymbol{b}_{\mathrm{i}}\}$ – **basis in the reciprocal space**

$\boldsymbol{b}_1=[\boldsymbol{a}_2\boldsymbol{a}_3]/\mathrm{V}_c$, $\boldsymbol{b}_2=[\boldsymbol{a}_3\boldsymbol{a}_1]/\mathrm{V}_c$, $\boldsymbol{b}_3=[\boldsymbol{a}_1\boldsymbol{a}_2]/\mathrm{V}_c$,

$\mathrm{V}_c=\boldsymbol{a}_1[\boldsymbol{a}_2\boldsymbol{a}_3]$

$\boldsymbol{a}_{\mathrm{i}}\cdot\boldsymbol{b}_{\mathrm{j}} = \delta_{\mathrm{ij}} = 1$ for $\mathrm{i=j}$, 0 for $\mathrm{i\neq j}$

$\mathbf{T} = \mathrm{n}_1\boldsymbol{a}_1 + \mathrm{n}_2\boldsymbol{a}_2 + \mathrm{n}_3\boldsymbol{a}_3$ – crystal lattice if $\mathrm{n_i}$ is integer

$\mathbf{H} = \mathrm{h}_1\boldsymbol{b}_1 + \mathrm{h}_2\boldsymbol{b}_2 + \mathrm{h}_3\boldsymbol{b}_3$ – reciprocal lattice $\mathrm{h_i}$ is integer

$\mathbf{T}_\mathrm{n}\cdot\mathbf{H}_\mathrm{h} = \mathrm{n}_1\mathrm{h}_1 + \mathrm{n}_2\mathrm{h}_2 + \mathrm{n}_3\mathrm{h}_3 = \mathrm{m}$ – **integer**

(h, k, l) – **Miller indexes**

$\mathbf{H} \perp \{h_1\ h_2\ h_3\}$, $d_{\mathrm{hkl}} = 1/|\mathbf{H}_{\mathrm{hkl}}|$

$|\mathbf{H}_{\mathrm{hkl}}| = (\mathbf{H}\cdot\mathbf{H})^{1/2}$

Neutron scattering on periodic structure

Position of the scatterer

$\mathbf{R} = \quad \mathbf{R}_m \quad + \quad \mathbf{r}_j$

Position of object origin — Position of scatterer in object

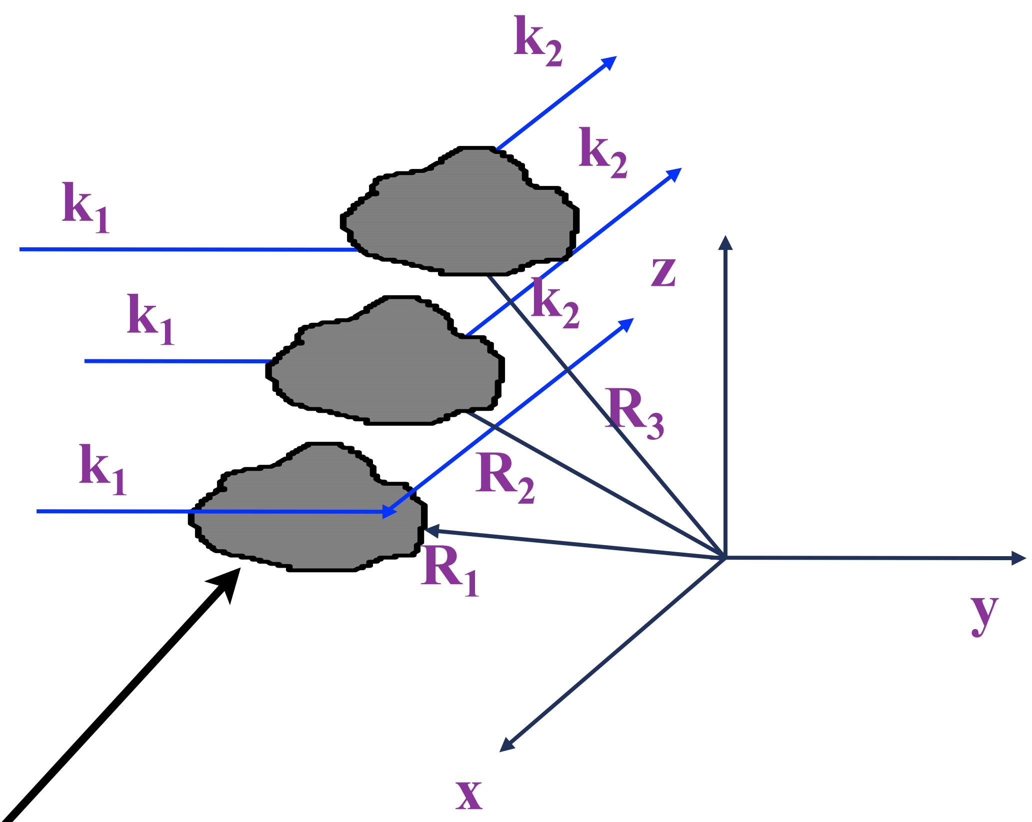

an object

Neutron scattering on periodic structure

Position of the scatterer

$\mathbf{R} = \mathbf{R}_m + \mathbf{r}_j$

Position of object origin — Position of scatterer in object

scattering wave amplitude

$\langle \mathbf{k}_1 | V | \mathbf{k}_2 \rangle = b(\mathbf{R})\exp(i\mathbf{Rq})$, $\quad \mathbf{q} = \mathbf{k}_2 - \mathbf{k}_1$

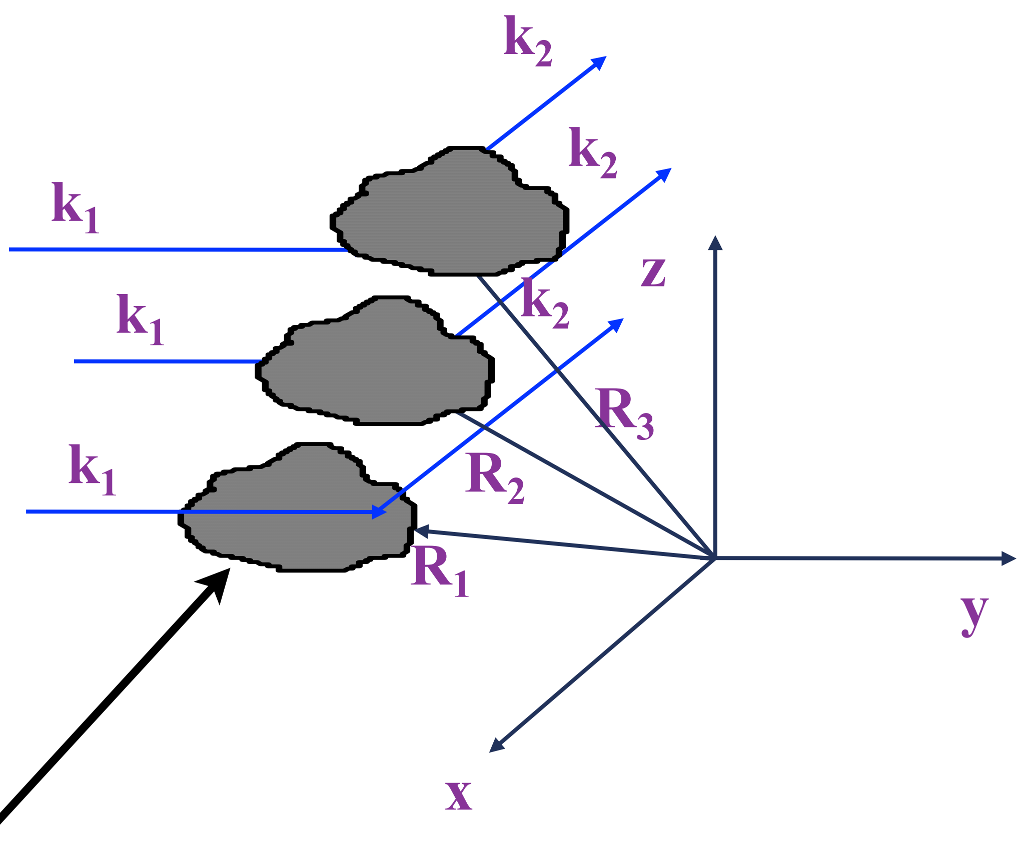

an object

Neutron scattering on periodic structure

Position of the scatterer

$\mathbf{R} = \mathbf{R}_m + \mathbf{r}_j$

Position of object origin — Position of scatterer in object

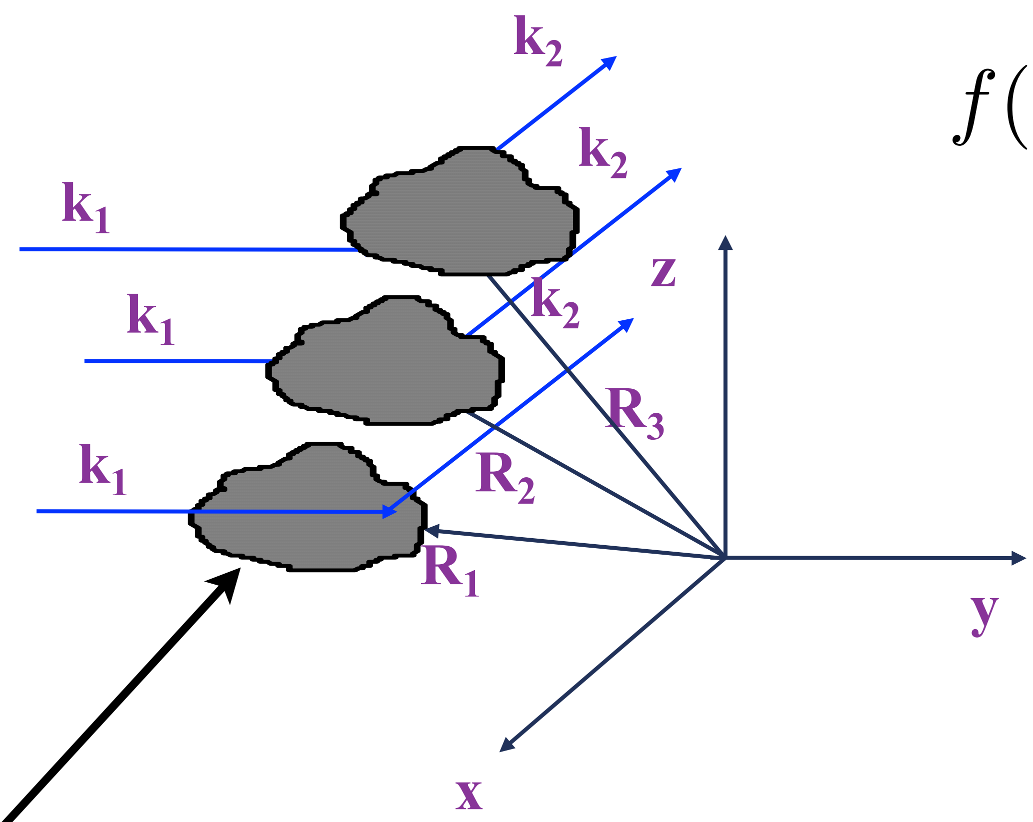

an object

scattering wave amplitude

$<\mathbf{k}_1|V|\mathbf{k}_2> = b(\mathbf{R})\exp(i\mathbf{Rq})$, $\quad \mathbf{q} = \mathbf{k_2} - \mathbf{k_1}$

Sum of wave amplitude from all objects

$$f(\mathbf{q}) \propto \sum_m \exp(i\mathbf{q}\mathbf{R}_m) \cdot \sum_j b(\mathbf{r}_j) \exp(i\mathbf{q}\mathbf{r}_j)$$

Neutron scattering on periodic structure

Position of the scatterer

$\mathbf{R} = \mathbf{R}_m + \mathbf{r}_j$

Position of object origin — Position of scatterer in object

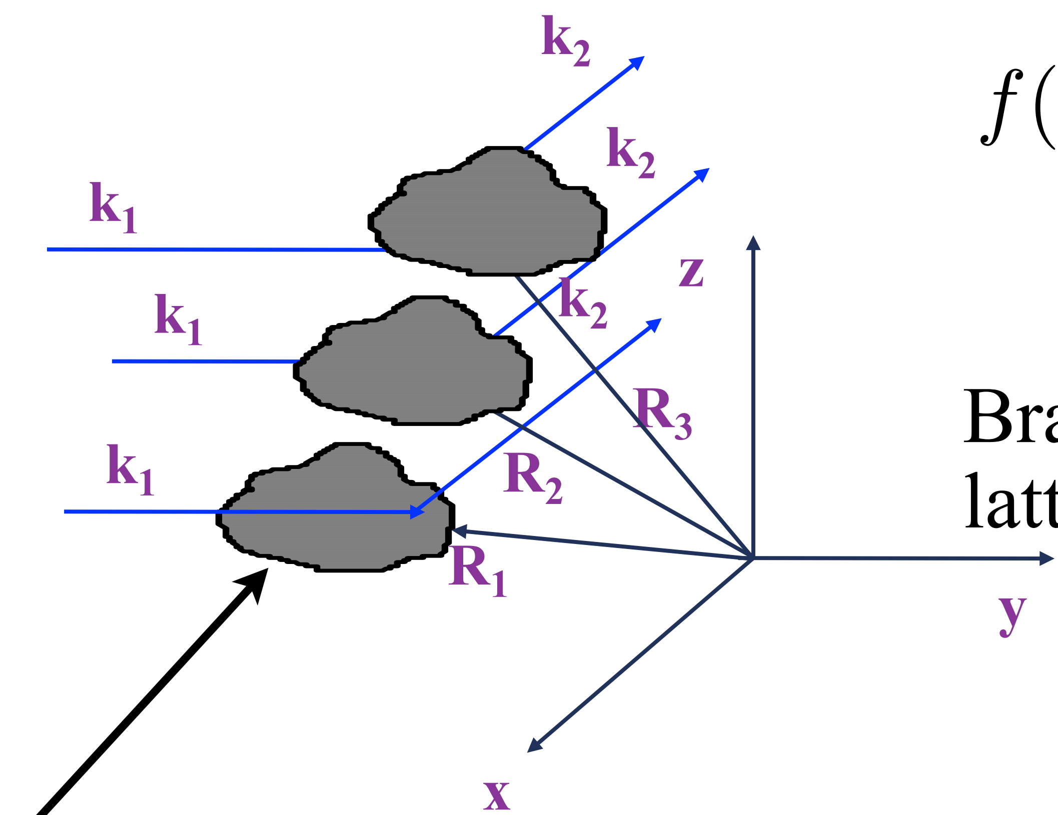

an object

scattering wave amplitude

$<\mathbf{k}_1|V|\mathbf{k}_2> = b(\mathbf{R})\exp(i\mathbf{R}\mathbf{q})$, $\quad \mathbf{q} = \mathbf{k}_2 - \mathbf{k}_1$

Sum of wave amplitude from all objects

$$f(\mathbf{q}) \propto \sum_m \exp(i\mathbf{q}\mathbf{R}_m) \cdot \sum_j b(\mathbf{r}_j)\exp(i\mathbf{q}\mathbf{r}_j)$$

$\delta(\mathbf{q} - 2\pi\mathbf{H})$

Bragg peak at reciprocal lattice nodes

same value for any $\mathbf{R}_m$

Structure factor: unique property of the object

$$F(\mathbf{q}) = \sum_j b(\mathbf{r}_j)\exp(i\mathbf{q}\mathbf{r}_j)$$

Neutron scattering on periodic structure

Position of the scatterer

$\mathbf{R} = \mathbf{R}_m + \mathbf{r}_j$

Position of object origin — Position of scatterer in object

scattering wave amplitude

$<\mathbf{k}_1|V|\mathbf{k}_2> = b(\mathbf{R})\exp(i\mathbf{R}\mathbf{q})$, $\quad \mathbf{q} = \mathbf{k}_2 - \mathbf{k}_1$

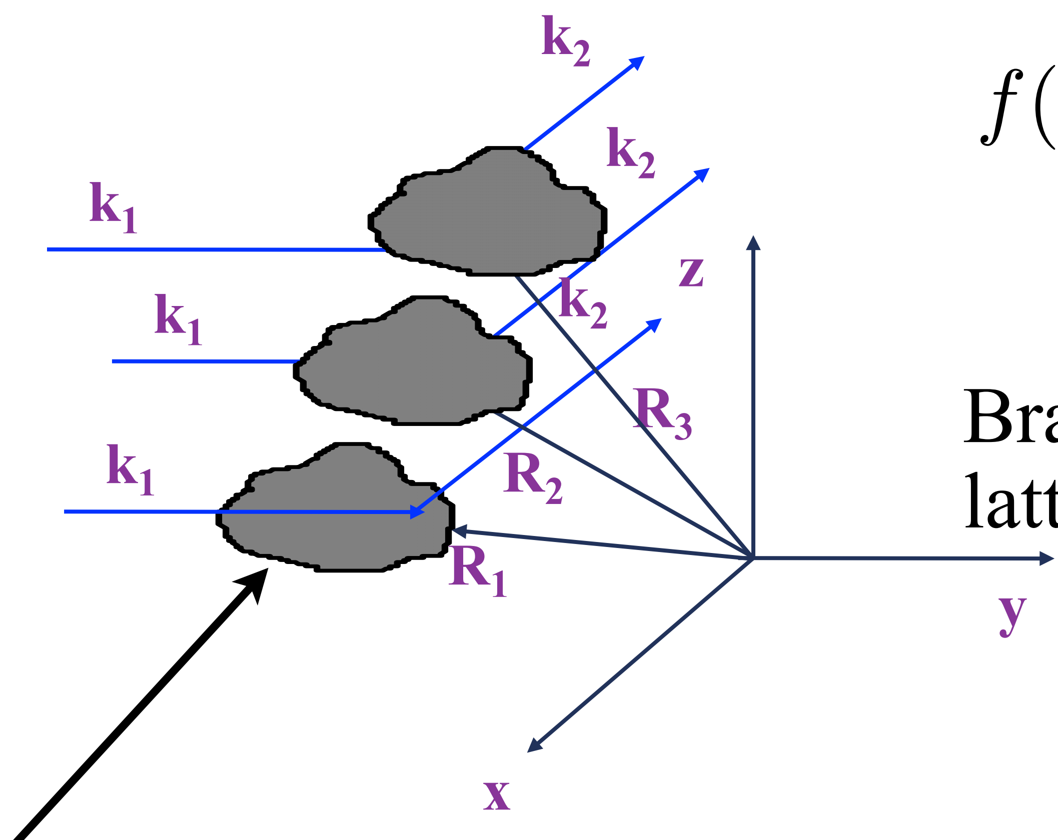

an object

Sum of wave amplitude from all objects

$$f(\mathbf{q}) \propto \sum_m \exp(i\mathbf{q}\mathbf{R}_m) \cdot \sum_j b(\mathbf{r}_j)\exp(i\mathbf{q}\mathbf{r}_j)$$

$\sum_m \exp(i\mathbf{q}\mathbf{R}_m) \rightarrow \delta(\mathbf{q} - 2\pi\mathbf{H})$

Bragg peak at reciprocal lattice nodes

$\sum_j b(\mathbf{r}_j)\exp(i\mathbf{q}\mathbf{r}_j) \rightarrow$ same value for any $\mathbf{R}_m$

Structure factor: unique property of the object

$$\boxed{F(\mathbf{q}) = \sum_j b(\mathbf{r}_j)\exp(i\mathbf{q}\mathbf{r}_j)}$$

Intensity in the detector

$$I = \frac{d\sigma}{d\Omega} \propto |f(\mathbf{q})|^2 \propto |F(\mathbf{q})|^2 \delta(\mathbf{q} - 2\pi\mathbf{H})$$

Ewald sphere construction for λ=const

$$\boxed{f \sim F \cdot \delta(q - 2\pi H)}$$

$$\boxed{q = k_2 - k_1 = 2\pi H}$$

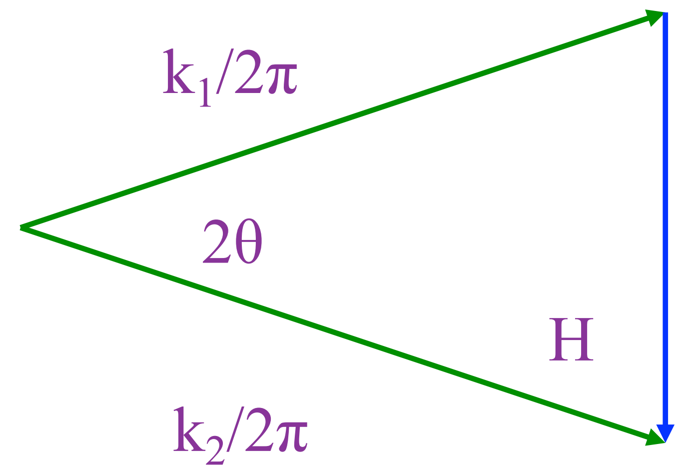

$H = h_1 b_1 + h_2 b_2 + h_3 b_3$ – reciprocal lattice vector

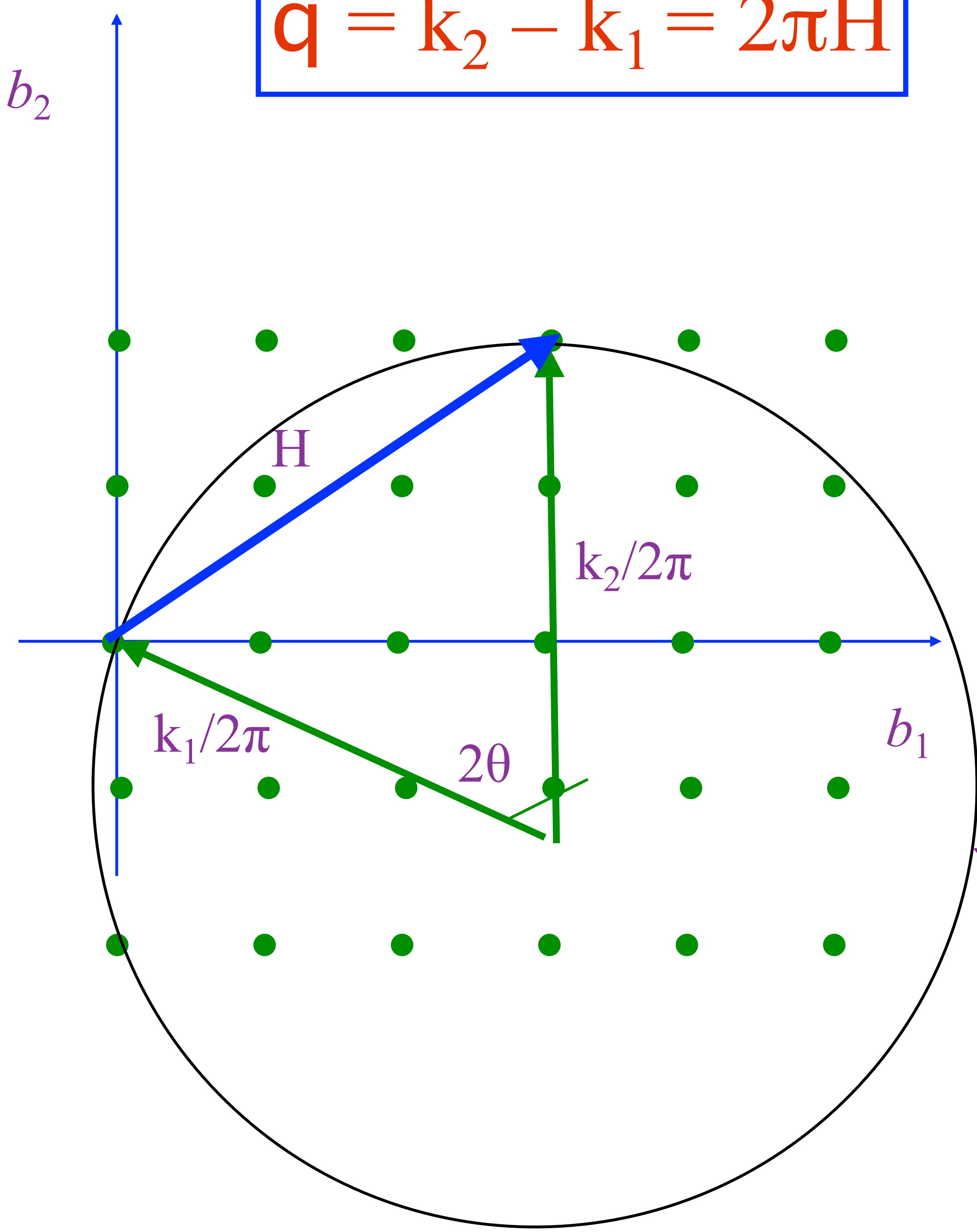

Ewald reflection sphere

Paul Peter Ewald
23.01.1888, Germany
22.08.1985, USA

Ewald sphere construction for λ=const

$$\boxed{f \sim F\cdot\delta(q - 2\pi H)}$$

$$\boxed{q = k_2 - k_1 = 2\pi H}$$

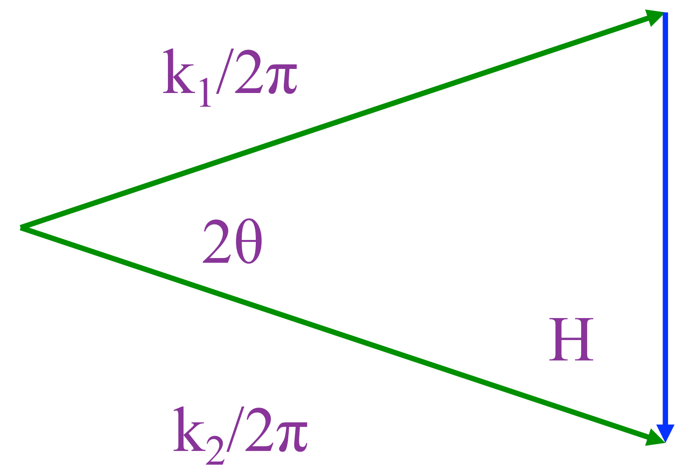

$H = h_1 b_1 + h_2 b_2 + h_3 b_3$ – reciprocal lattice vector

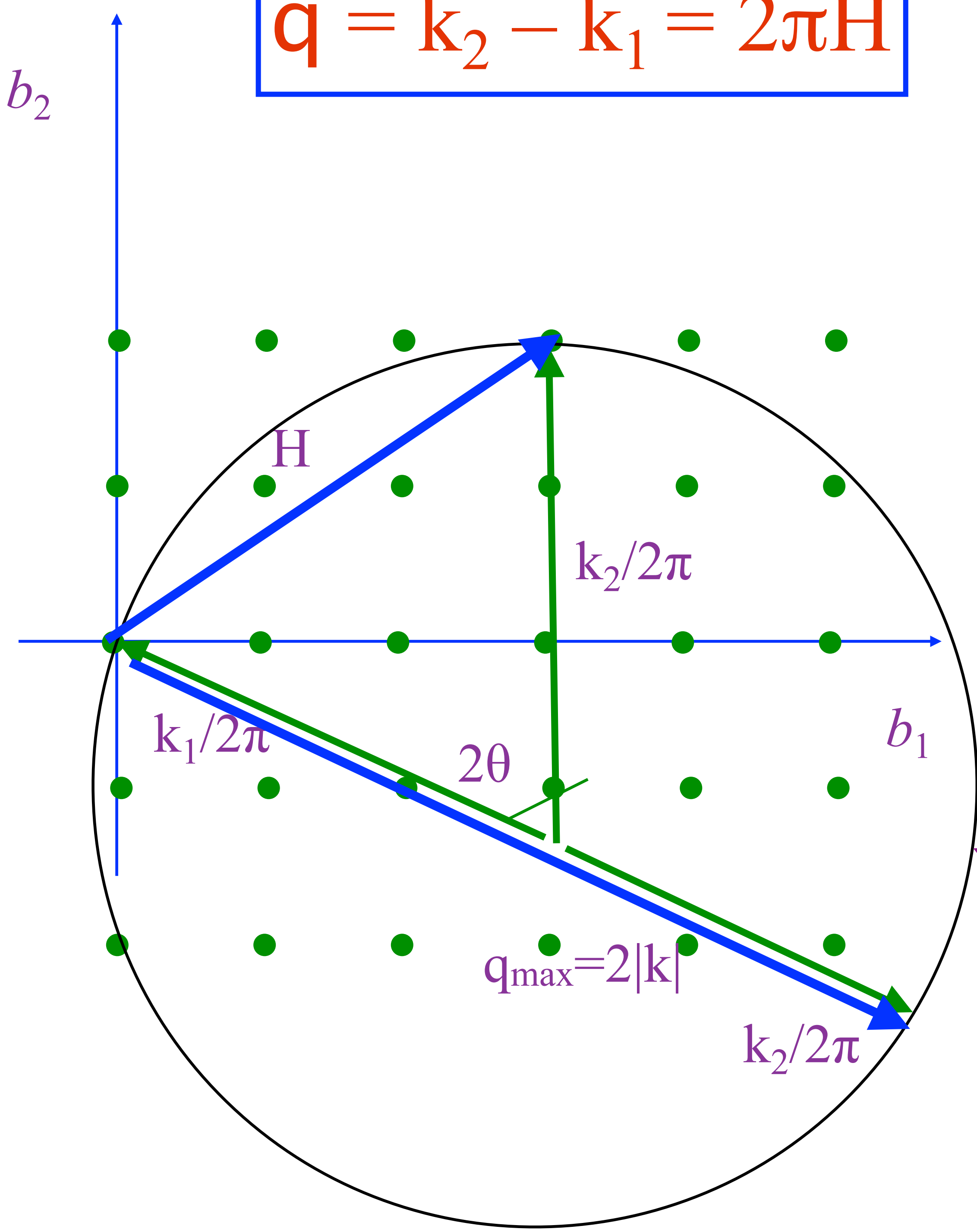

Ewald reflection sphere

Paul Peter Ewald
23.01.1888, Germany
22.08.1985, USA

Elastic scattering as Fourier transform of a structure

Intensity of scattered waves

$I(q) \sim |f(q)|^2$

Amplitude of a wave function

$I(q) \sim \int e^{iqr}\, G(r)dr$

$f(q) \sim \int e^{iqr}\, b(r)dr$

$G(r) = \int b(u)\, b(u + r)\, du$

$G(r) \sim \int e^{-iqr}\, I(q)dq$ $\longleftrightarrow$ $b(r) \sim \int e^{-iqr}\, f(q)dq$

Pair correlation function

Scattering-length density

$b(r)$ / $G(r)$ - object $\longleftrightarrow$ $f(q)$ / $I(q)$ - image

Real space $\longleftrightarrow$ Reciprocal space

courtesy of A. Balagurov

Diffraction limit and image quality

Object

$$b(r) \sim \int_0^\infty e^{-iqr} f(q)dq$$

Fourier image

$$f(q) \sim \int e^{iqr} b(r)dr$$

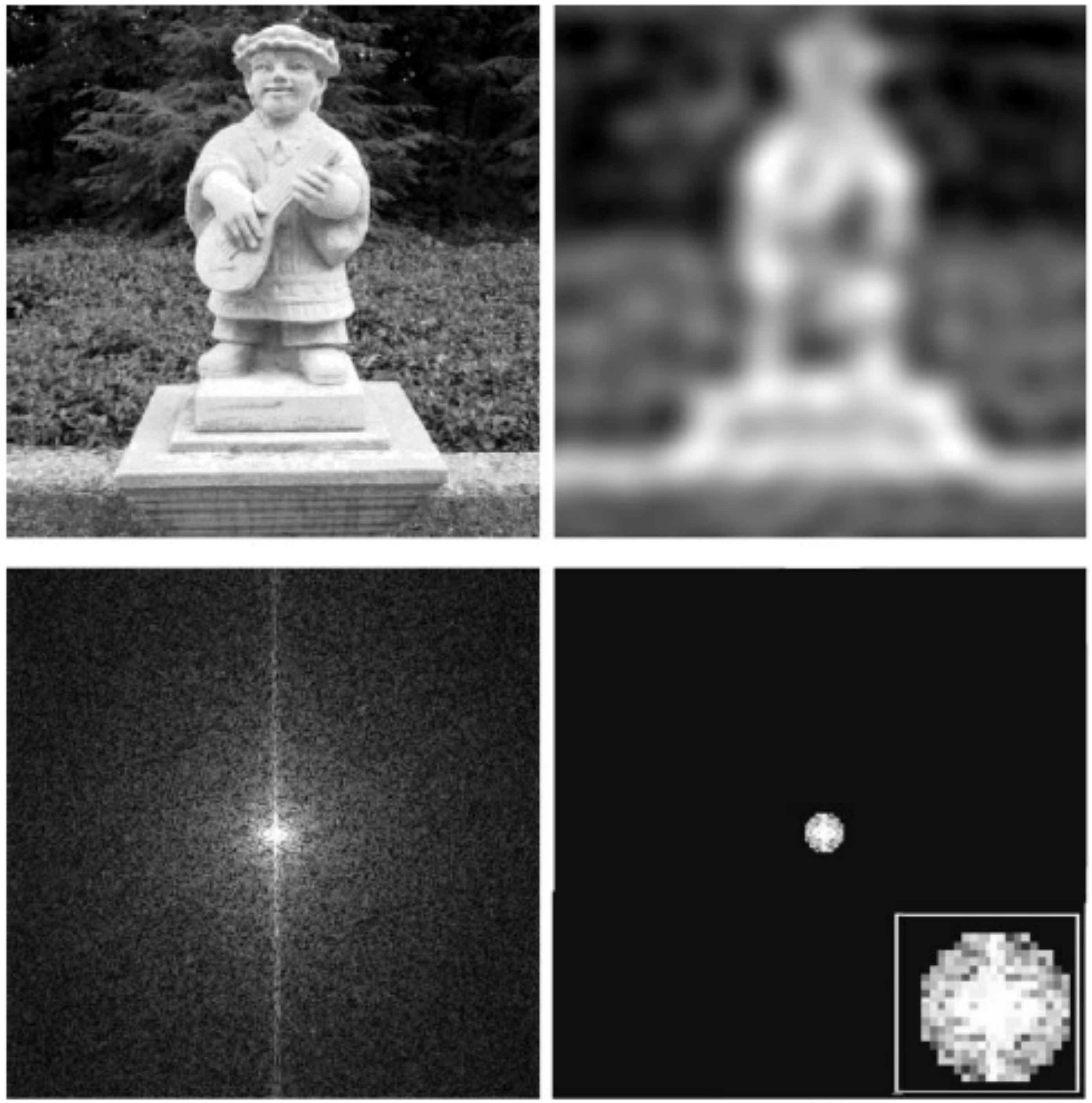

$$b(r) \sim \int_0^Q e^{-iqr} f(q)dq$$

Fourier image without high Q

courtesy of A. Balagurov

Fourier synthesis of $HgBa_2CuO_{4+\delta}$ structure

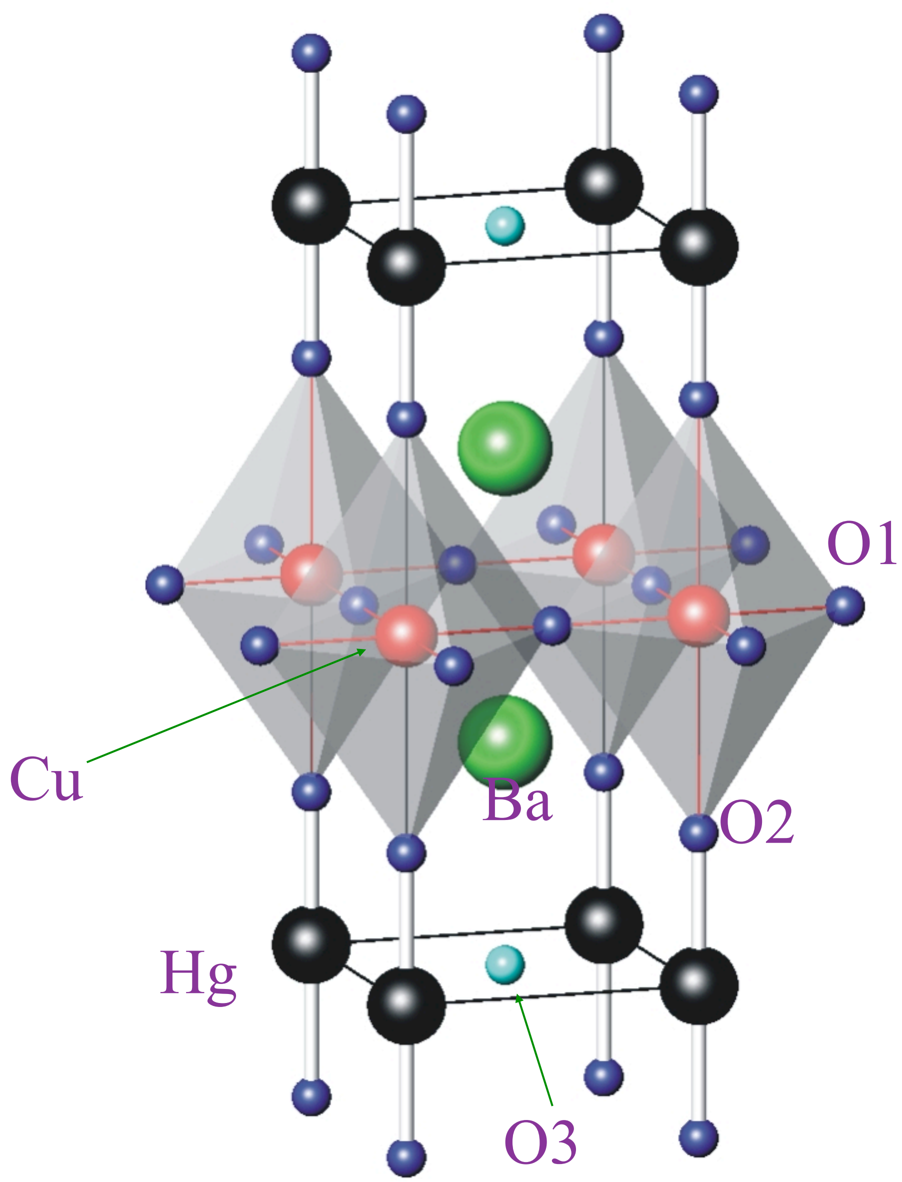

Cross-section:

$0 \le x = y \le 1,$

$0 \le z \le 0.5$

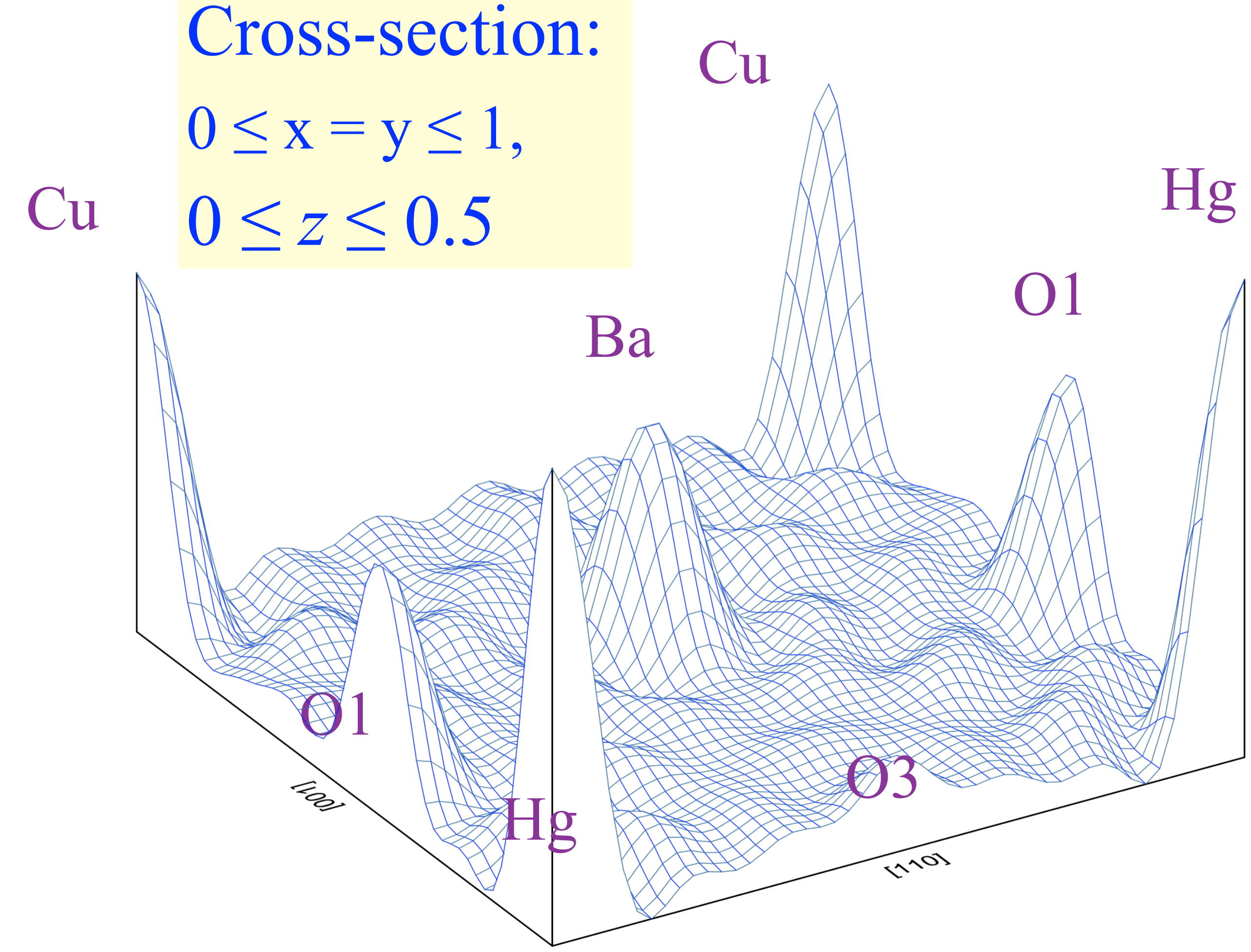

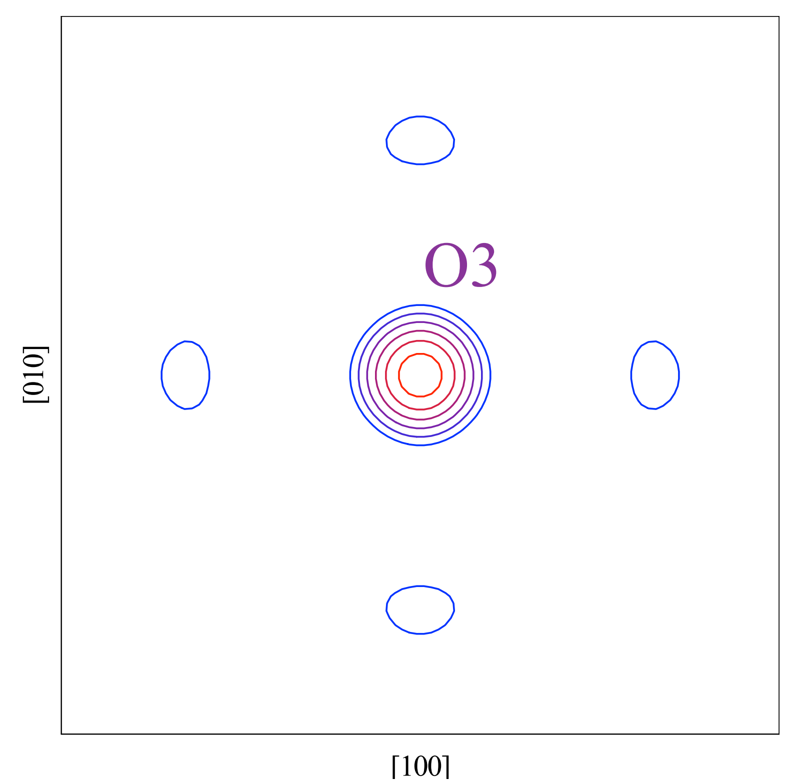

Difference synthesis.

Cross-section:

$0 \le x \le 1,$

$0 \le y \le 1,$

$z = 0$

$HgBa_2CuO_{4+\delta}$ structure: the O3 position is partially filled, $n(O3) = \delta = 0.12$.

courtesy of A. Balagurov

Diffraction limit

$$b(r) \sim \int_0^\infty e^{-iqr} f(q)dq \longrightarrow b(r) \sim \int_0^Q e^{-iqr} f(q)dq, \quad Q = q_{max}$$

$$\boxed{l_c \approx 2\pi/Q \geq \lambda_{min}/2 \ \text{ – diffraction limit}}$$

courtesy of A. Balagurov

Diffraction limit

$$b(r) \sim \int_0^{\infty} e^{-iqr} f(q)dq \longrightarrow b(r) \sim \int_0^{Q} e^{-iqr} f(q)dq, \quad Q = q_{max}$$

$$\boxed{l_c \approx 2\pi/Q \geq \lambda_{min}/2 \; - \; \text{diffraction limit}}$$

As a rule: for diffraction $\lambda_{min} \approx 1$ Å, *i.e.* $l_c \approx 0.5$ Å,

for SANS $Q \approx 0.5$ Å^{-1}, *i.e.* $l_c \approx 20$ Å.

In practice: for interatomic distances $\sigma \sim 0.002$ Å,

for lattice parameters $\sigma < 0.0001$ Å,

courtesy of A. Balagurov

Diffraction limit

$$b(r) \sim \int_0^\infty e^{-iqr} f(q)dq \longrightarrow b(r) \sim \int_0^Q e^{-iqr} f(q)dq, \quad Q = q_{max}$$

$$\boxed{l_c \approx 2\pi/Q \geq \lambda_{min}/2 \ – \text{ diffraction limit}}$$

As a rule: for diffraction $\lambda_{min} \approx 1$ Å, *i.e.* $l_c \approx 0.5$ Å,

for SANS $Q \approx 0.5$ Å^{-1}, *i.e.* $l_c \approx 20$ Å.

In practice: for interatomic distances $\sigma \sim 0.002$ Å,

for lattice parameters $\sigma < 0.0001$ Å,

Diffraction limit is overcome owing to:
- periodicity of a structure,
- parametric description of an object.

courtesy of A. Balagurov

Powder neutron diffractometers

European Portal for Neutron Scattering

http://pathfinder.neutron-eu.net

http://www.neutrons-ensa.eu/

Text

Powder neutron diffractometers

European Portal for Neutron Scattering

http://pathfinder.neutron-eu.net

http://www.neutrons-ensa.eu/

SINQ/PSI, CH	Structure: DMC, HRPT, Strain scanner: POLDI
ILL, FR	D20, D2B,... Text
LLB, FR	G41, G42
ISIS, UK	GEM, HRPD, PEARL
FRM-II, GE	SPODI
FLNP/Dubna, RU	HRFD, DN2, DN12

Powder ND at SINQ/PSI

HRPT - High Resolution Powder Diffractometer for Thermal Neutrons at SINQ

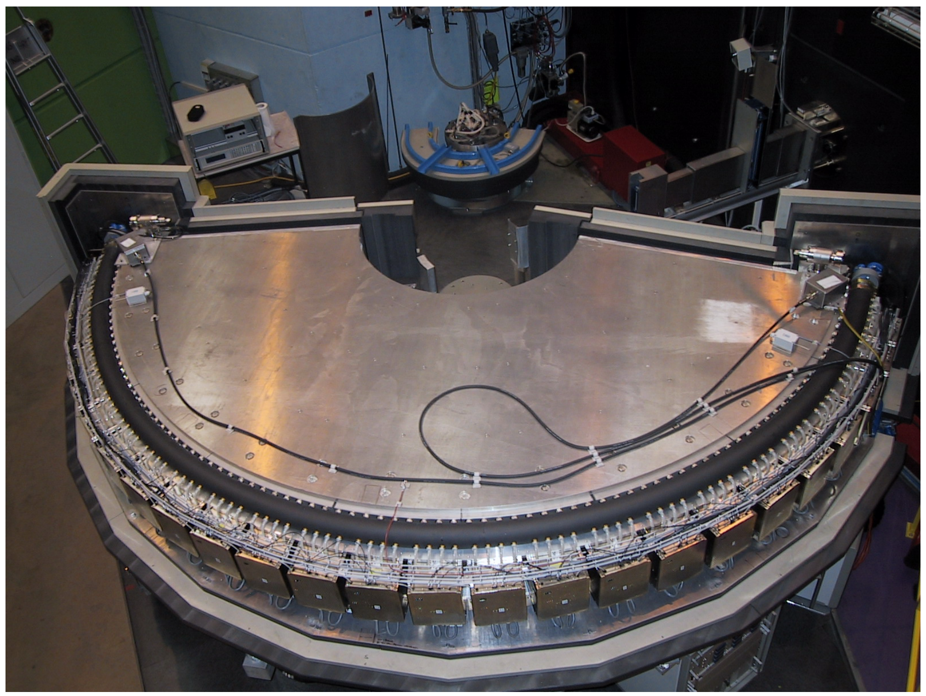

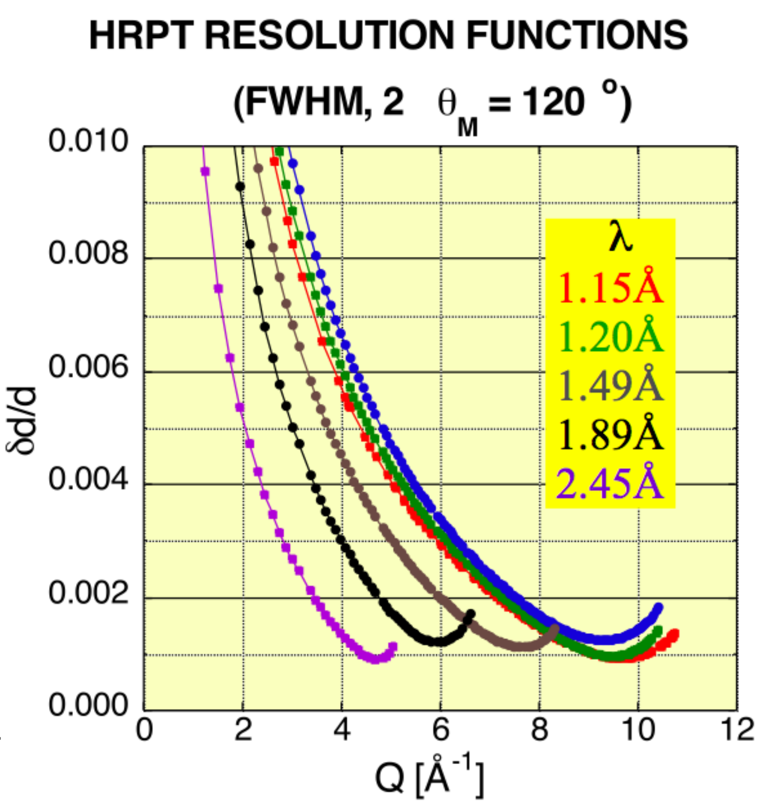

DMC - cold neutron powder diffractometer

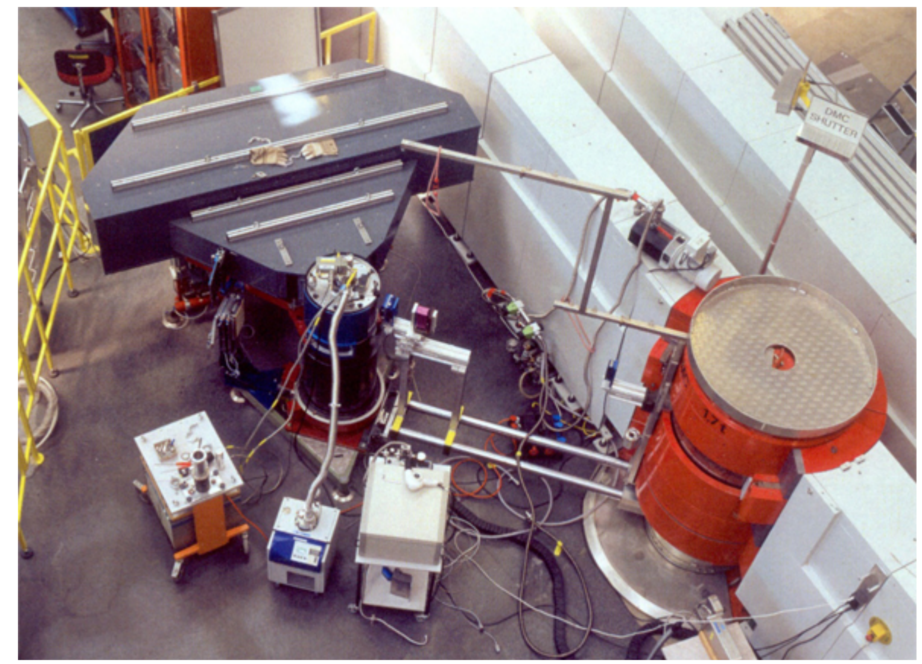

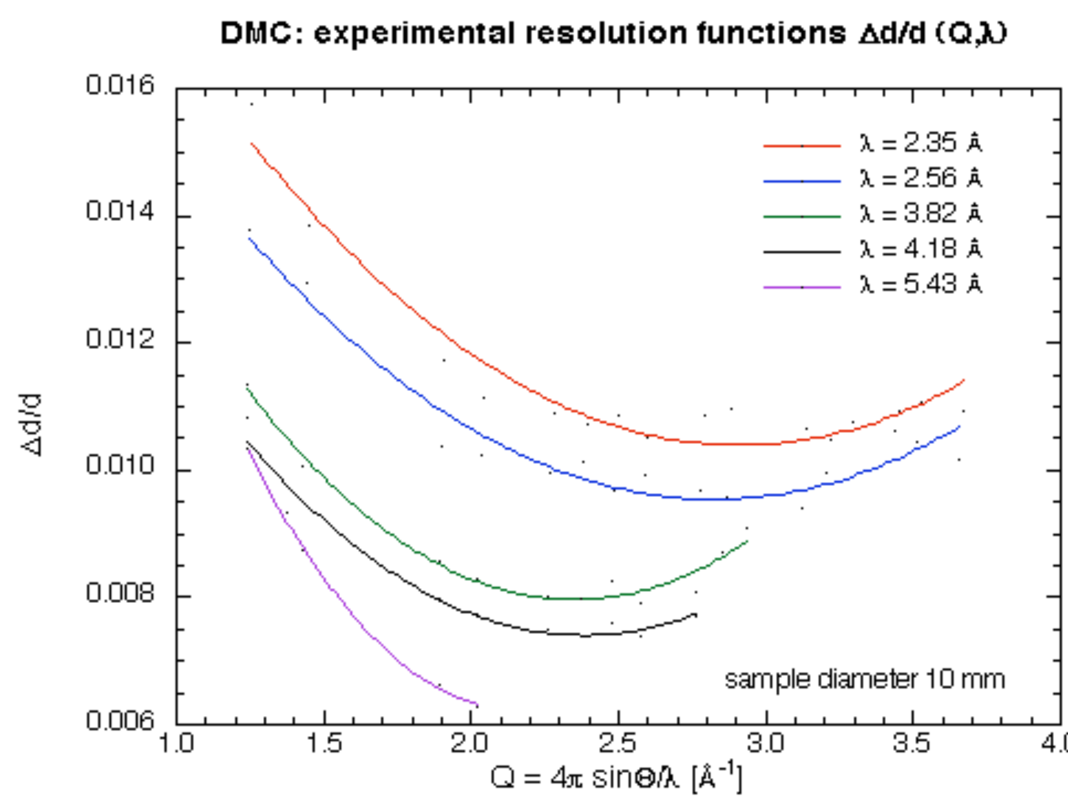

PSI n

Powder ND at SINQ/PSI

HRPT - High Resolution Powder Diffractometer for Thermal Neutrons at SINQ

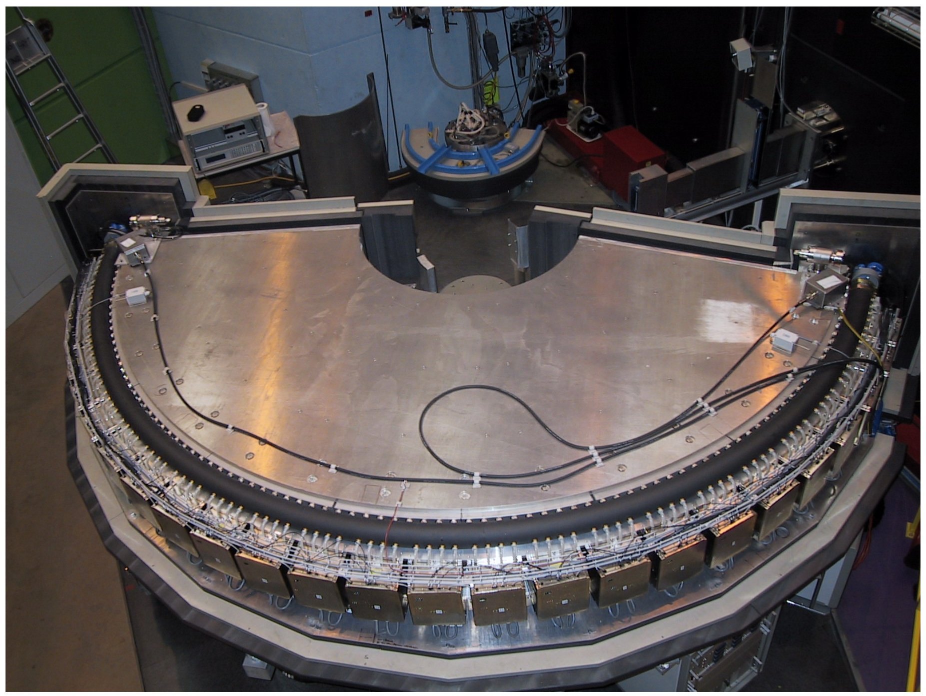

DMC - cold neutron powder diffractometer

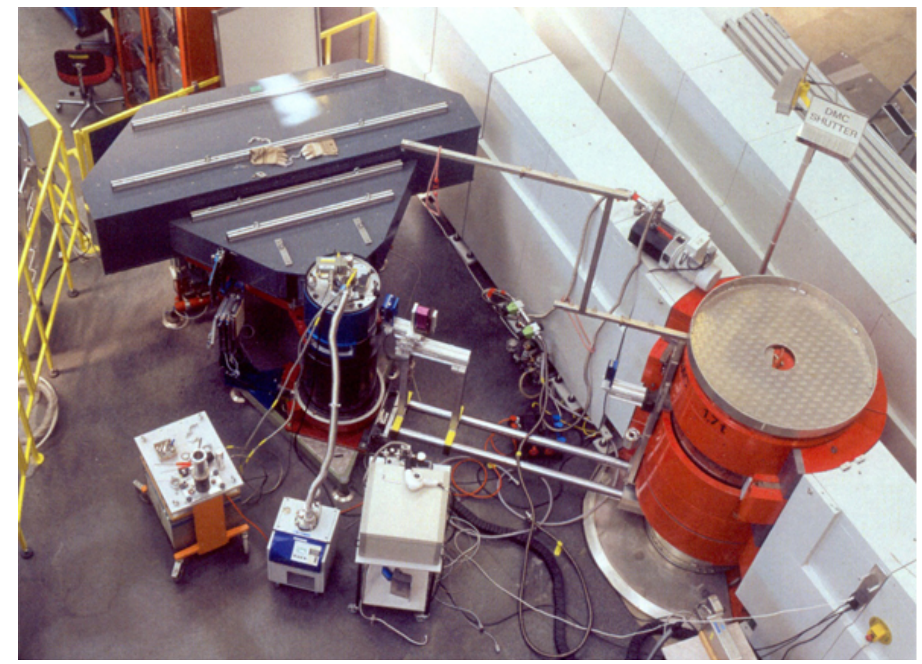

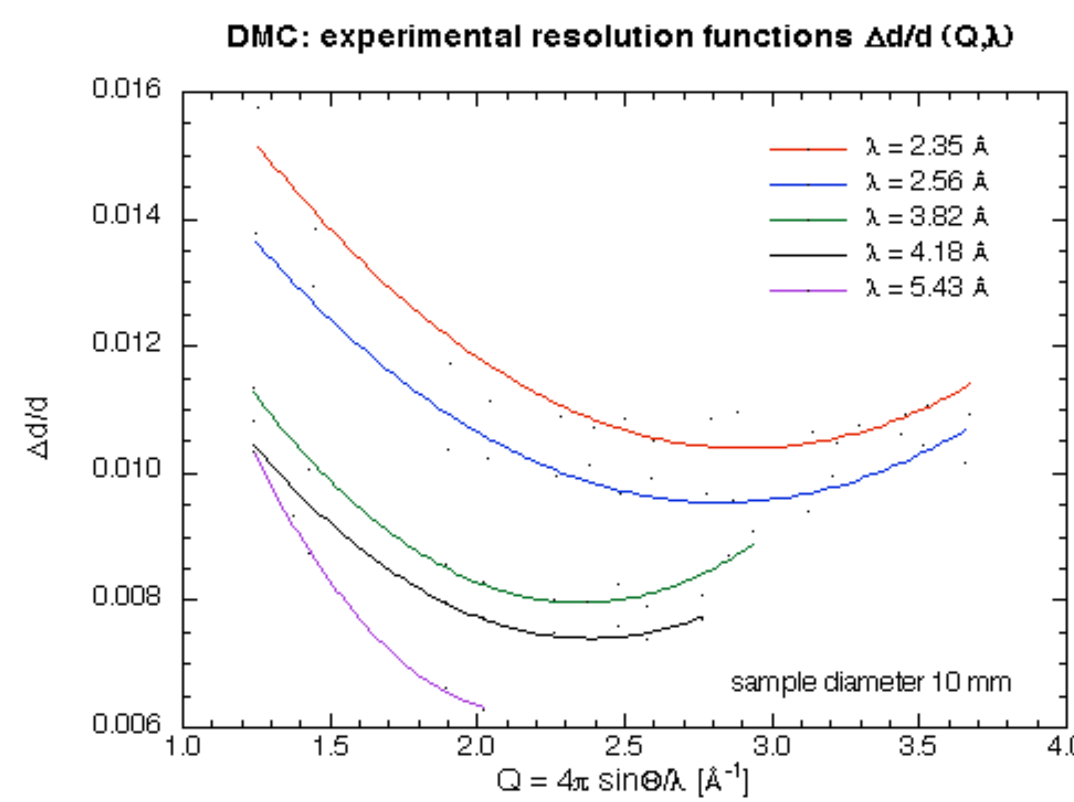

Powder ND at SINQ/PSI

HRPT - High
Diffractometer for

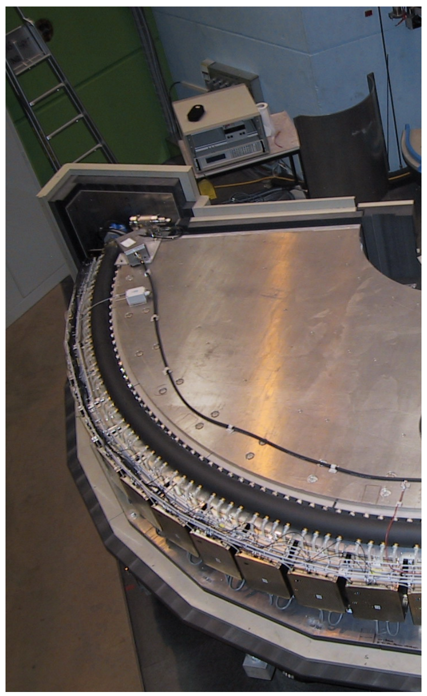

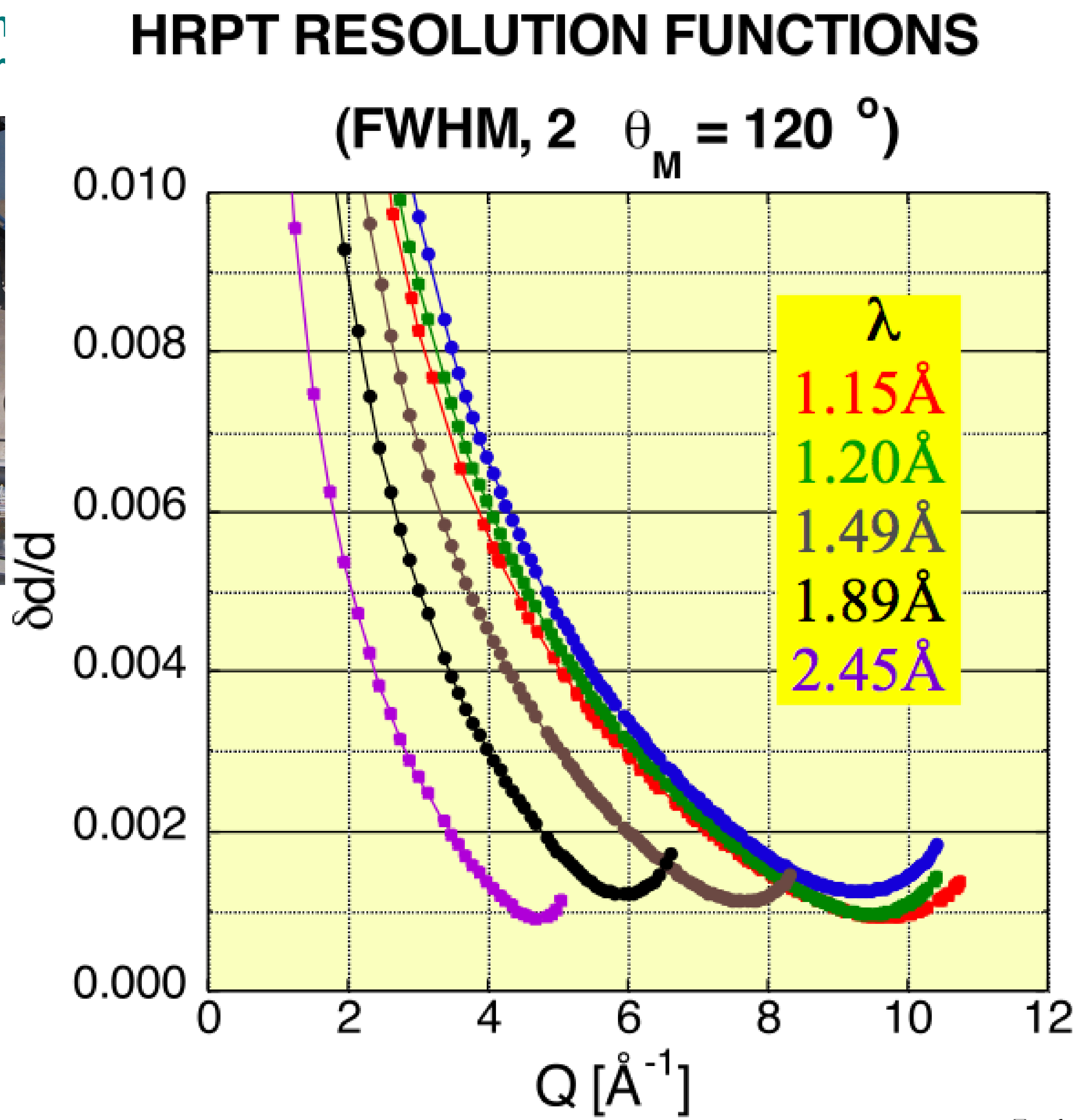

powder diffractometer

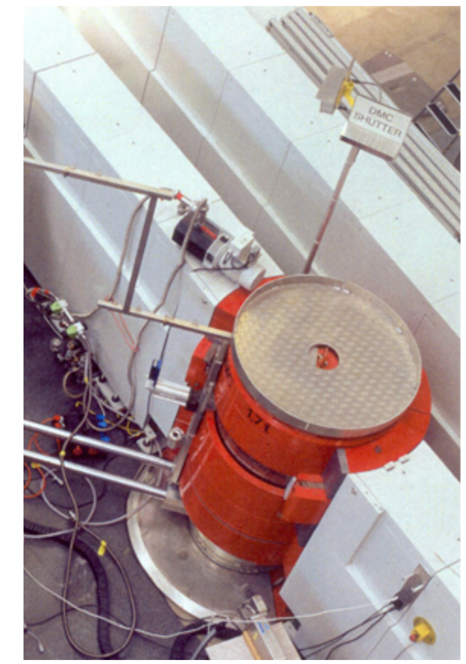

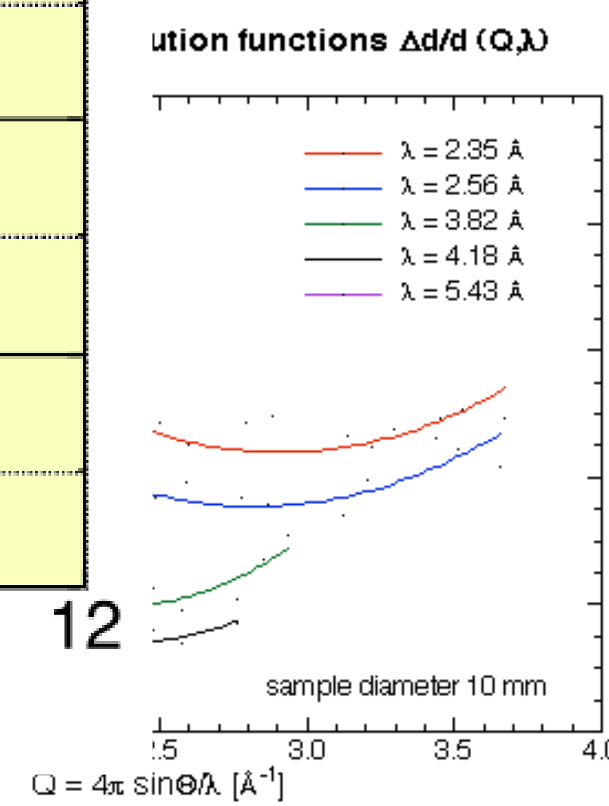

Example of HRPT diffraction pattern

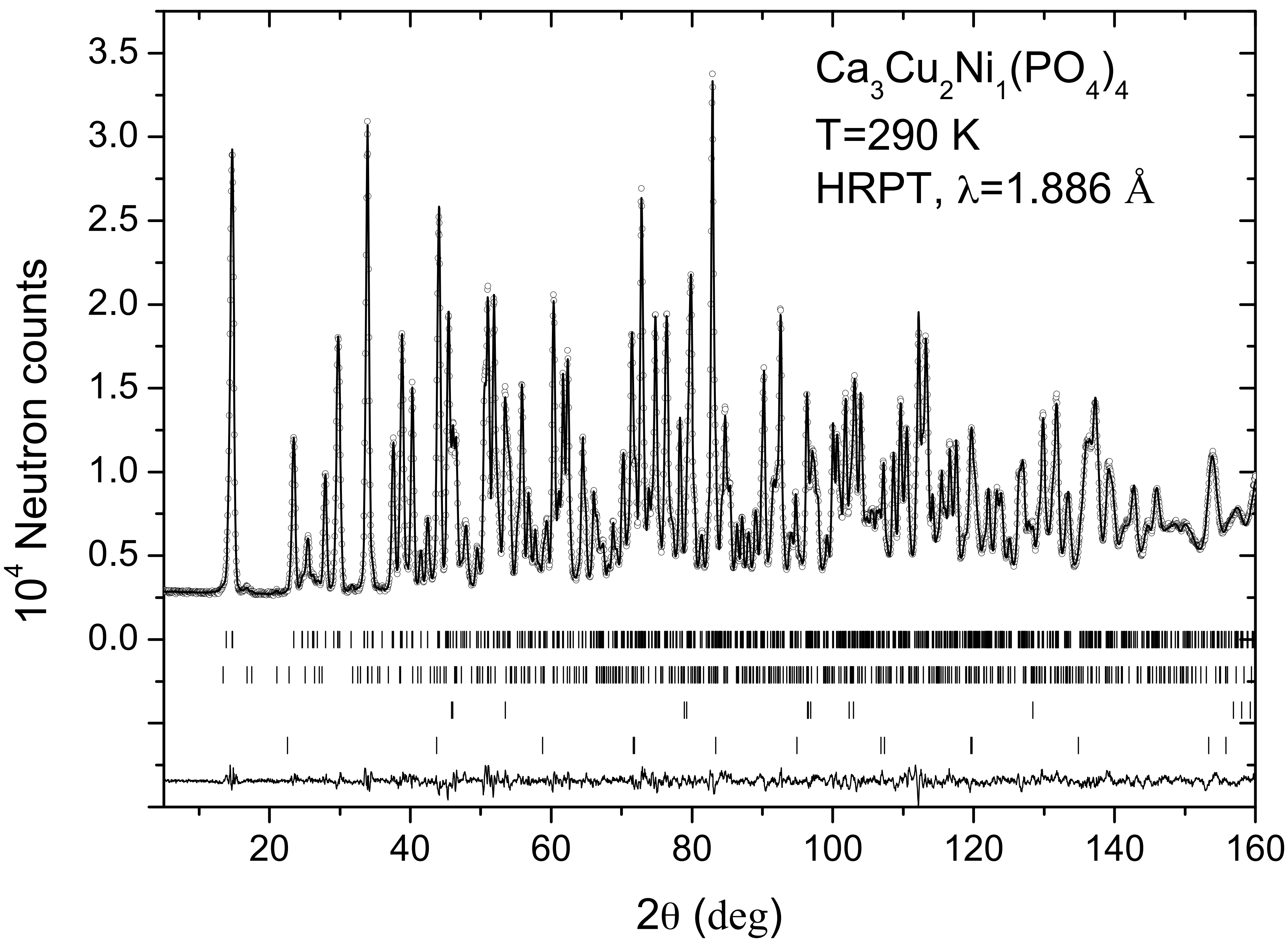

Powder ND at SINQ/PSI

HRPT - High Resolution Powder Diffractometer for Thermal Neutrons at SINQ

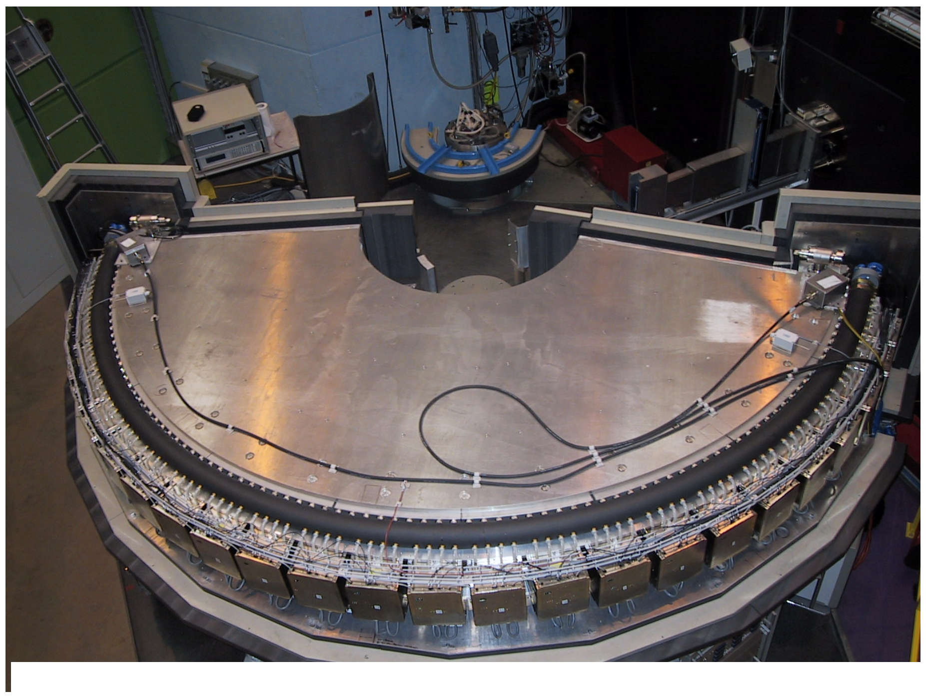

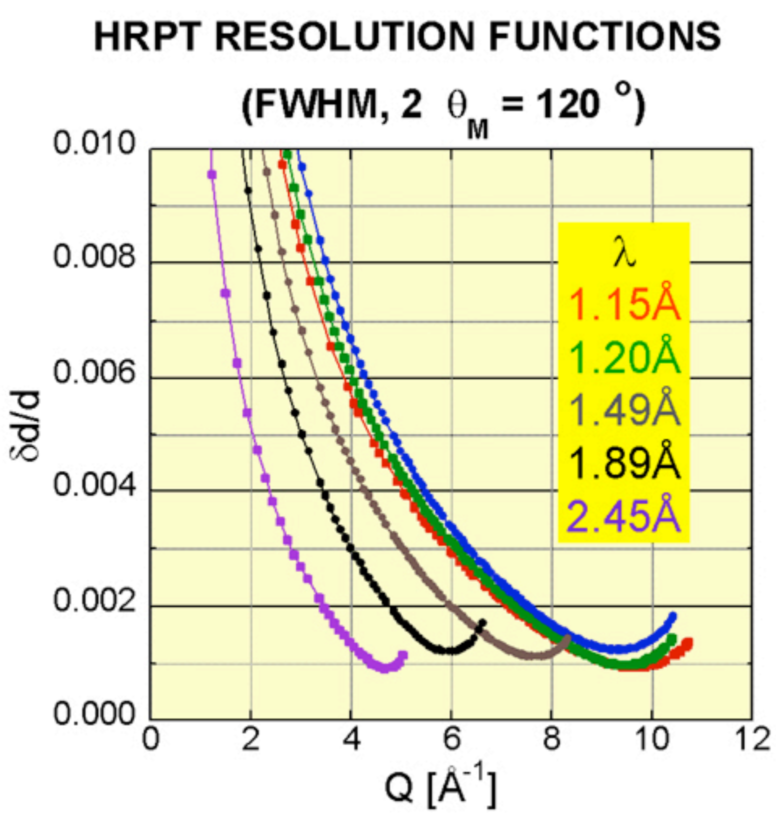

DMC - cold neutron powder diffractometer

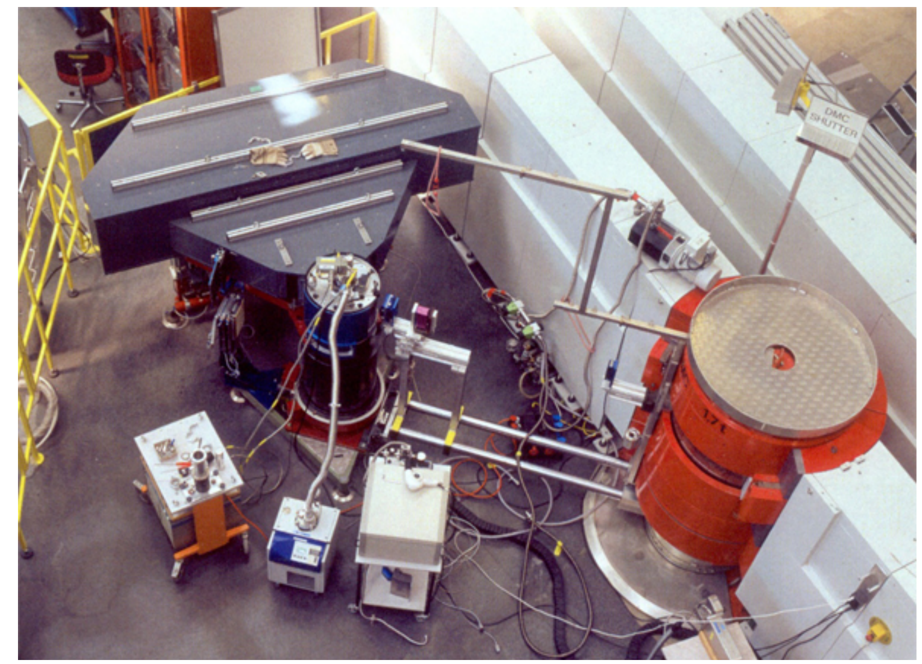

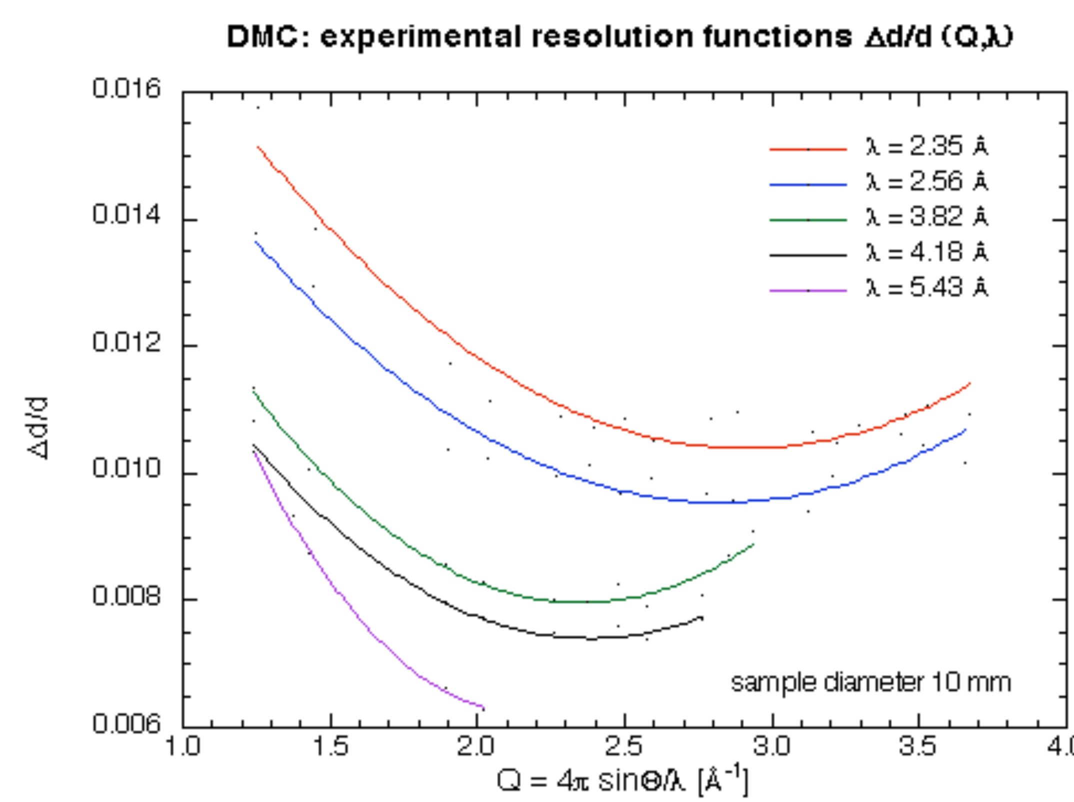

P

Powder ND at SINQ/PSI

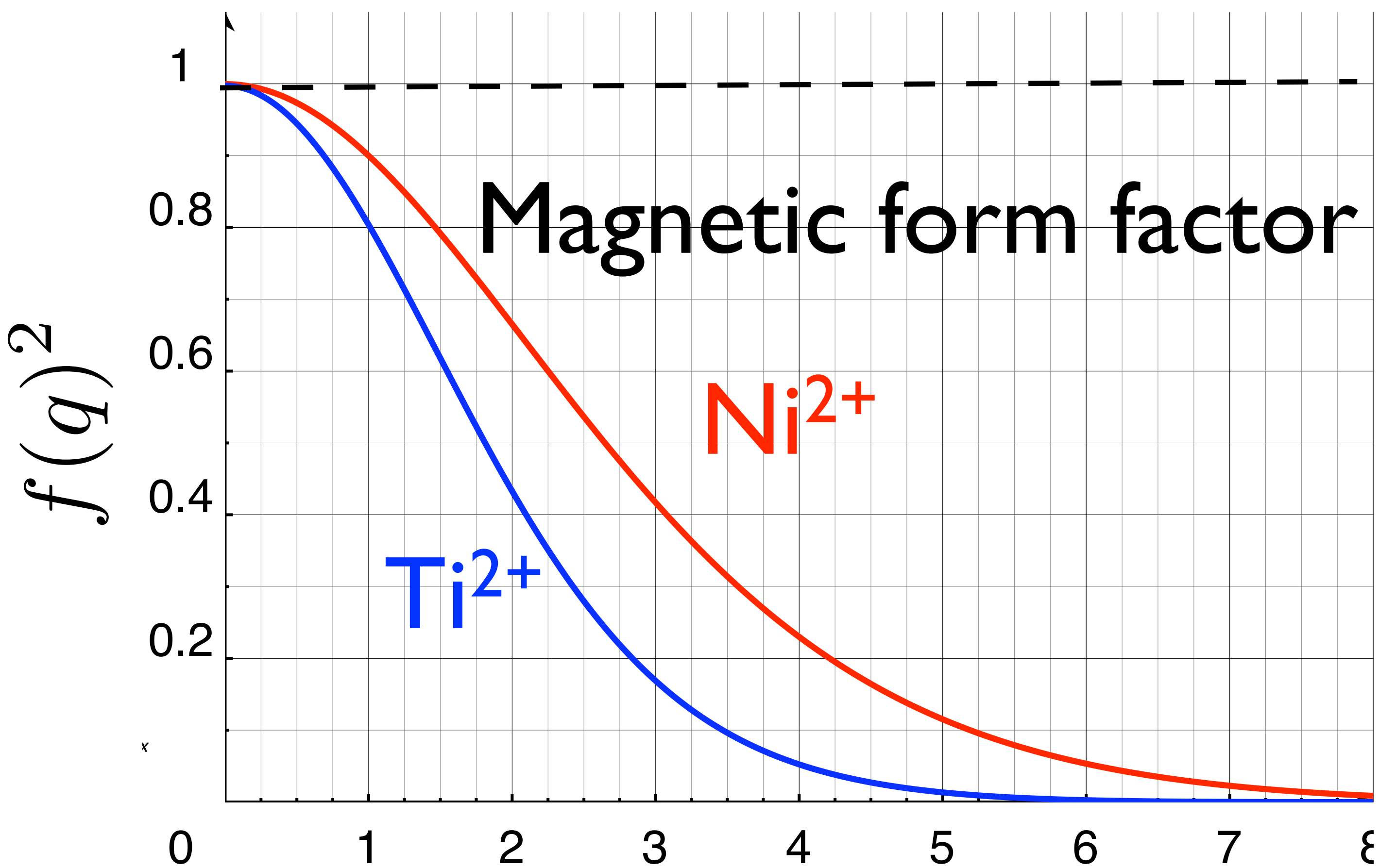

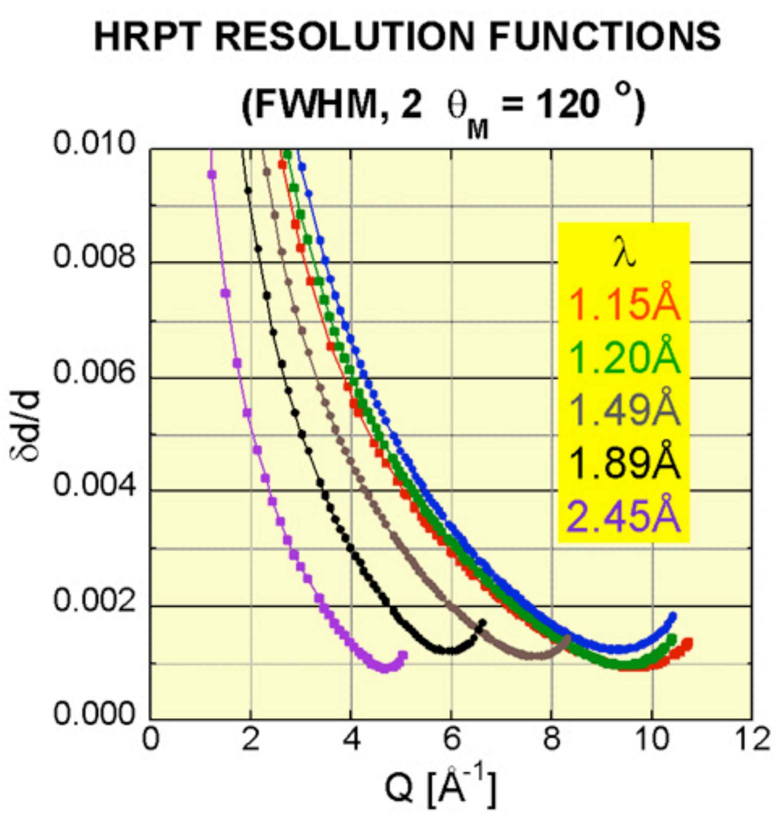

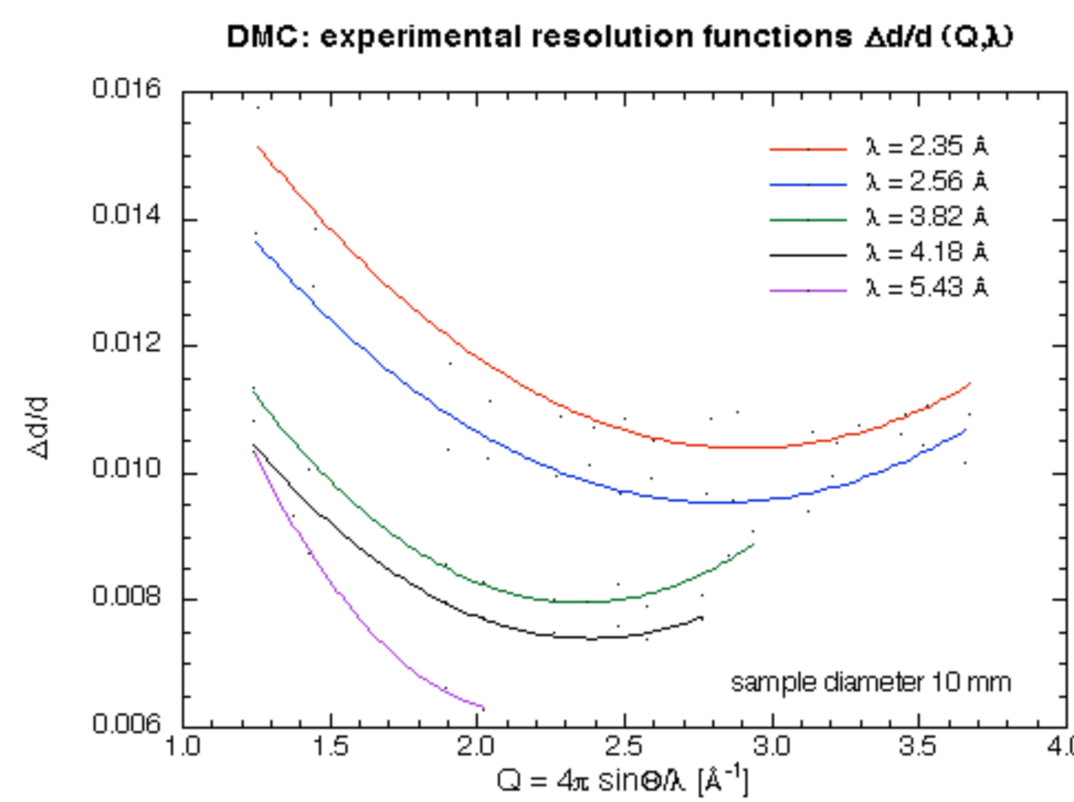

P

cf. resolution/q-range

HRPT 1.9Å

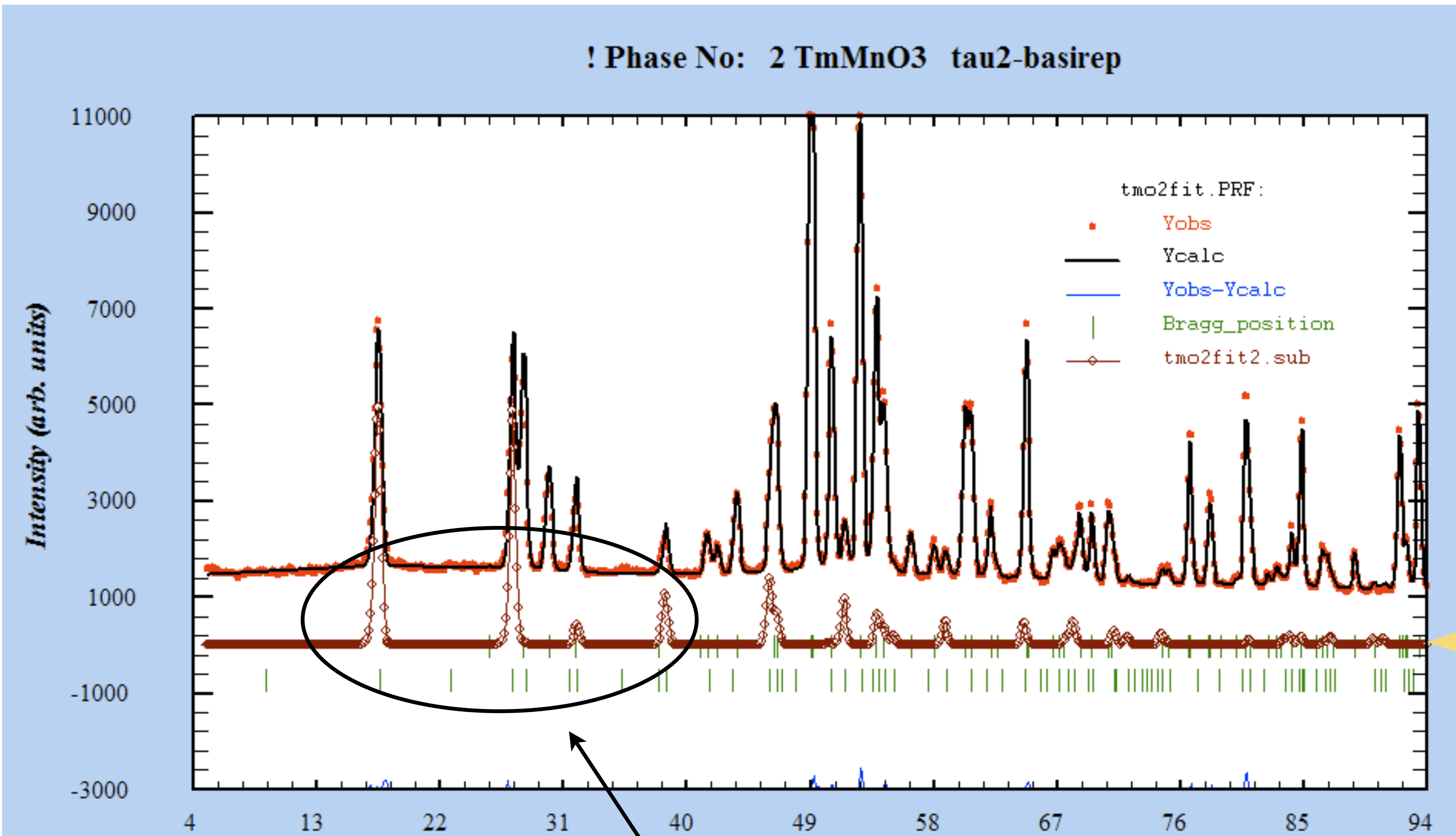

magnetic contribution

DMC range at 4.5Å

Cf. resolution/q-range

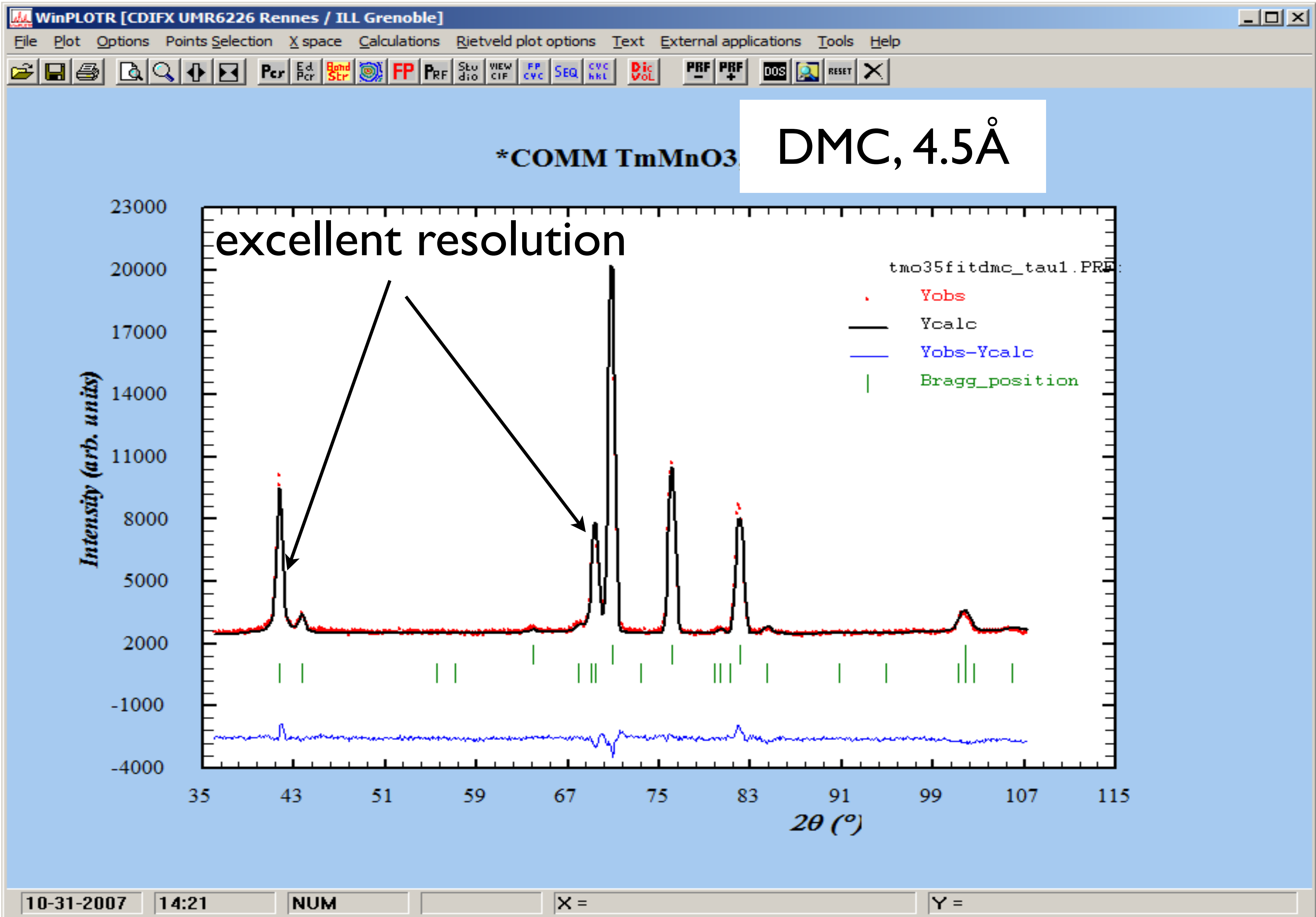

Complementarity 1.9Å HRPT and 4.5Å DMC

excellent resolution and high Q-range

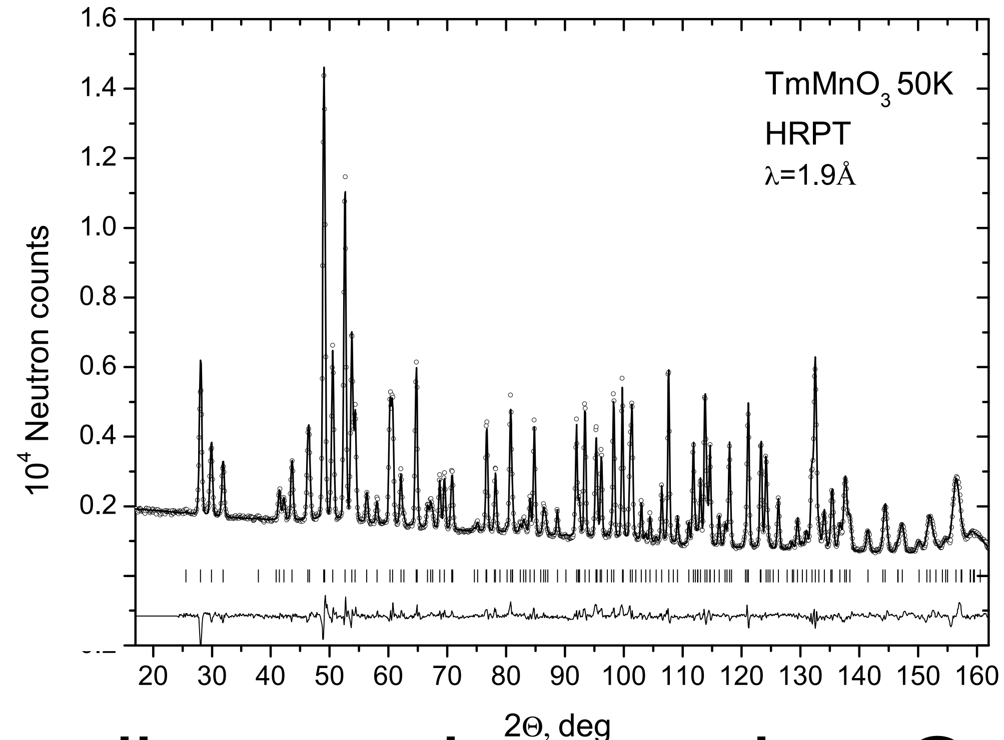

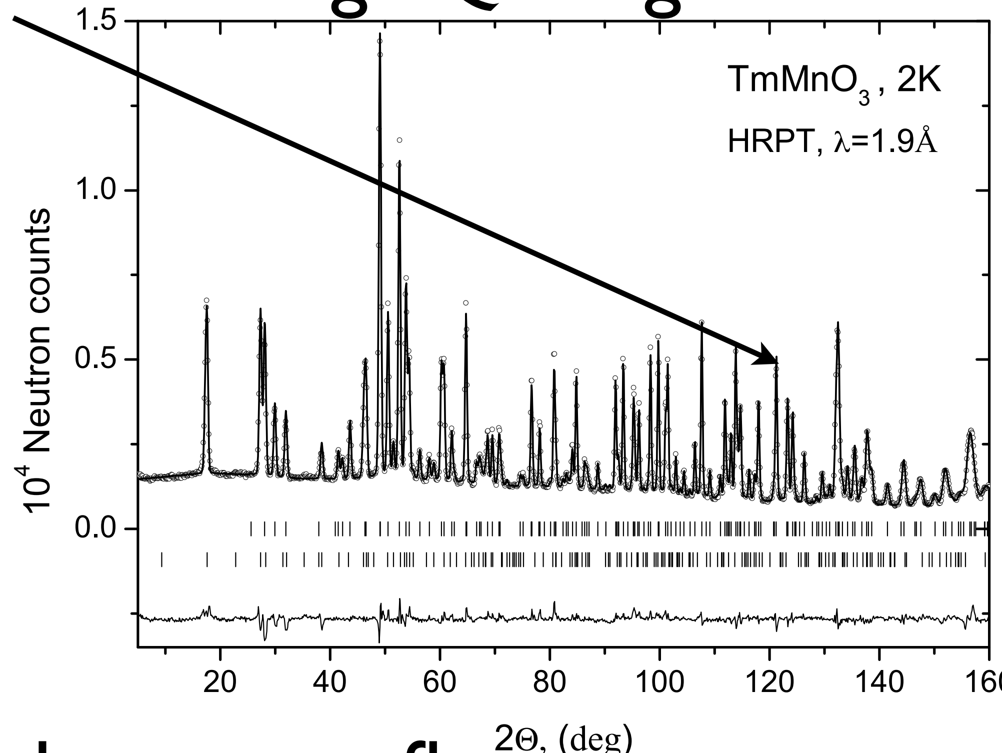

excellent resolution at low Q and high neutron flux

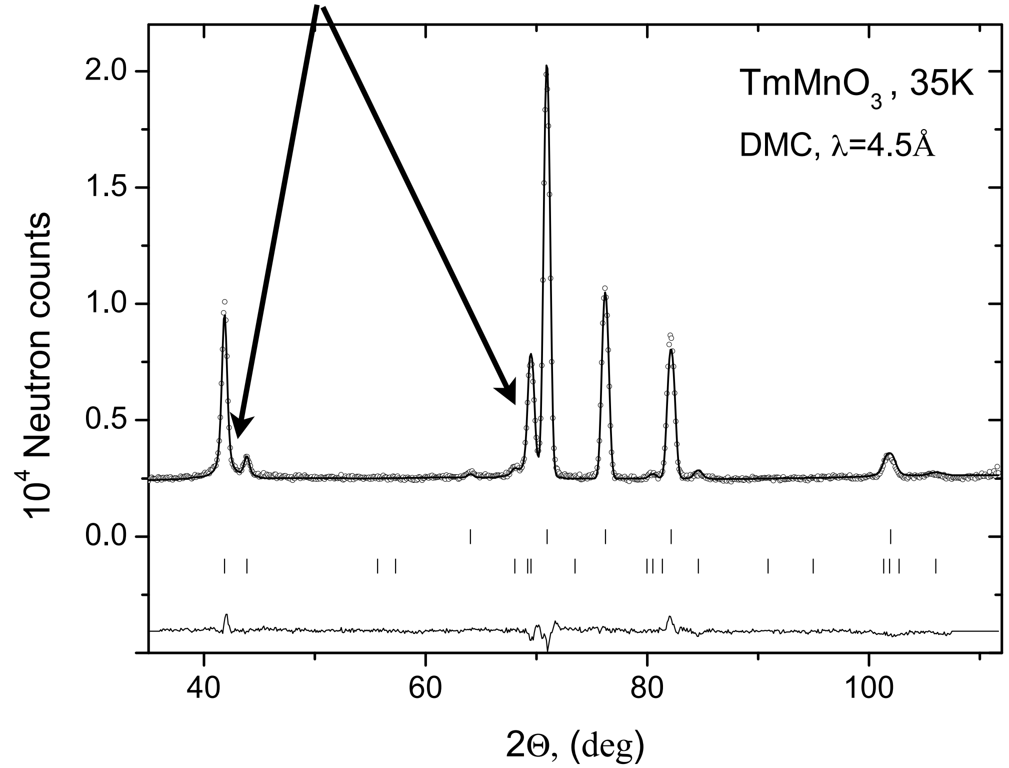

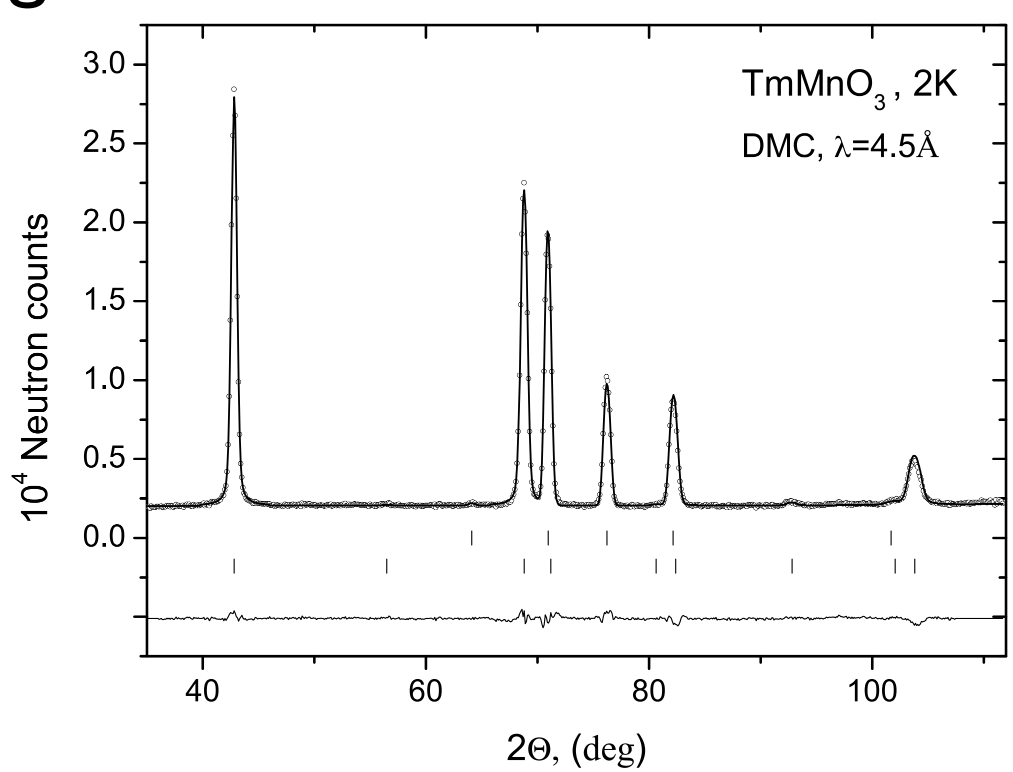

P

High Resolution Powder Diffractometer for Thermal Neutrons at PSI. Applications of HRPT

1) Precise structure refinement complementary to x-rays
2) Magnetic ordering phenomena. For small moments and/or very long-periodic structure DMC is much better.
3) Direct structure solution. Phase analysis of (new) materials

More information about HRPT

More information about HRPT

Google Switzerland

HRPT neutron

More information about HRPT

Switzerland

HRPT neutron

HRPT

Search

Advanced Search

Search: the web pages from Switzerland

Web Show options...

HRPT Properties Trust
Real Estate Investment Trust that buys, owns and leases office buildings. Information about real-estate holdings, company news and financials. Show stock quote for HRP
www.hrpreit.com/ - Cached - Similar -

Investor Relations Contact Us
Properties News
About Us Our Strategy

More results from hrpreit.com »

HRPT: High-Resolution Powder Diffractometer for Thermal Neutrons - 3 visits - 4:50pm
6 Jun 2007 ... Complementary to DMC, the multidetector diffractometer **HRPT** is designed as flexible instrument for efficient neutron powder diffraction ...
sinq.web.psi.ch/sinq/instr/**hrpt**.html - Cached - Similar -

Instrument view at SINQ target station

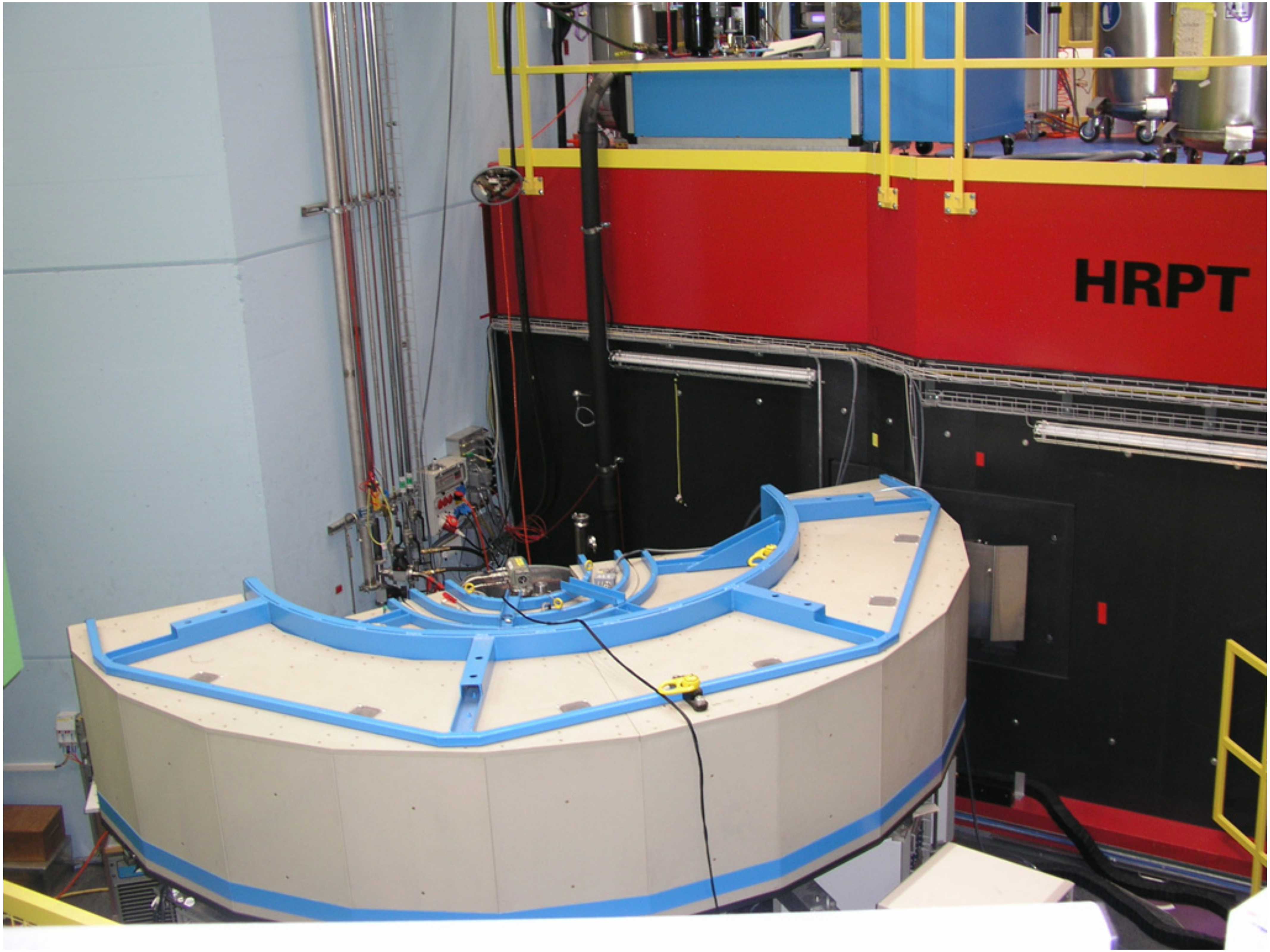

Instrument view at SINQ target station

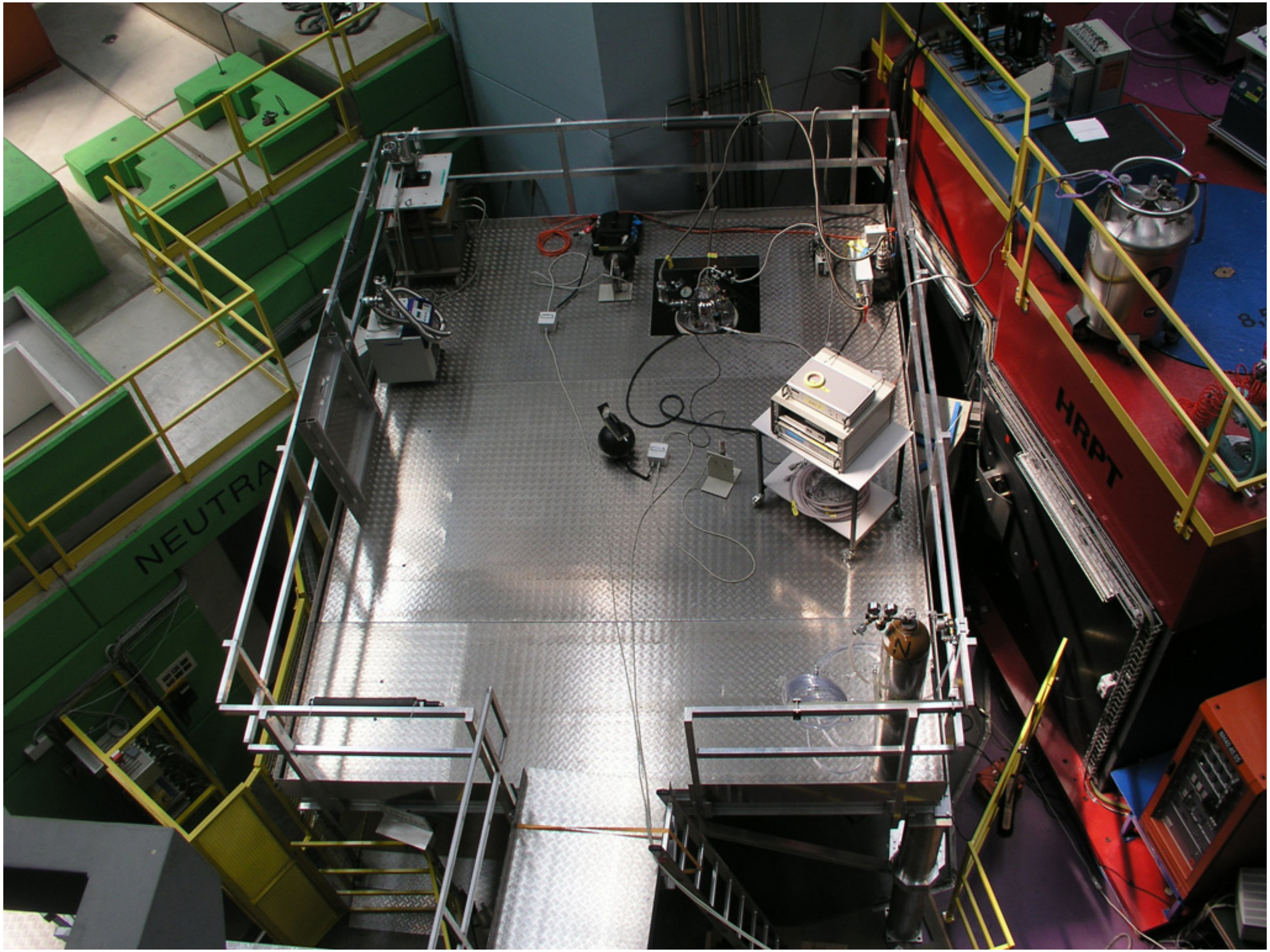

Instrument view at SINQ target station

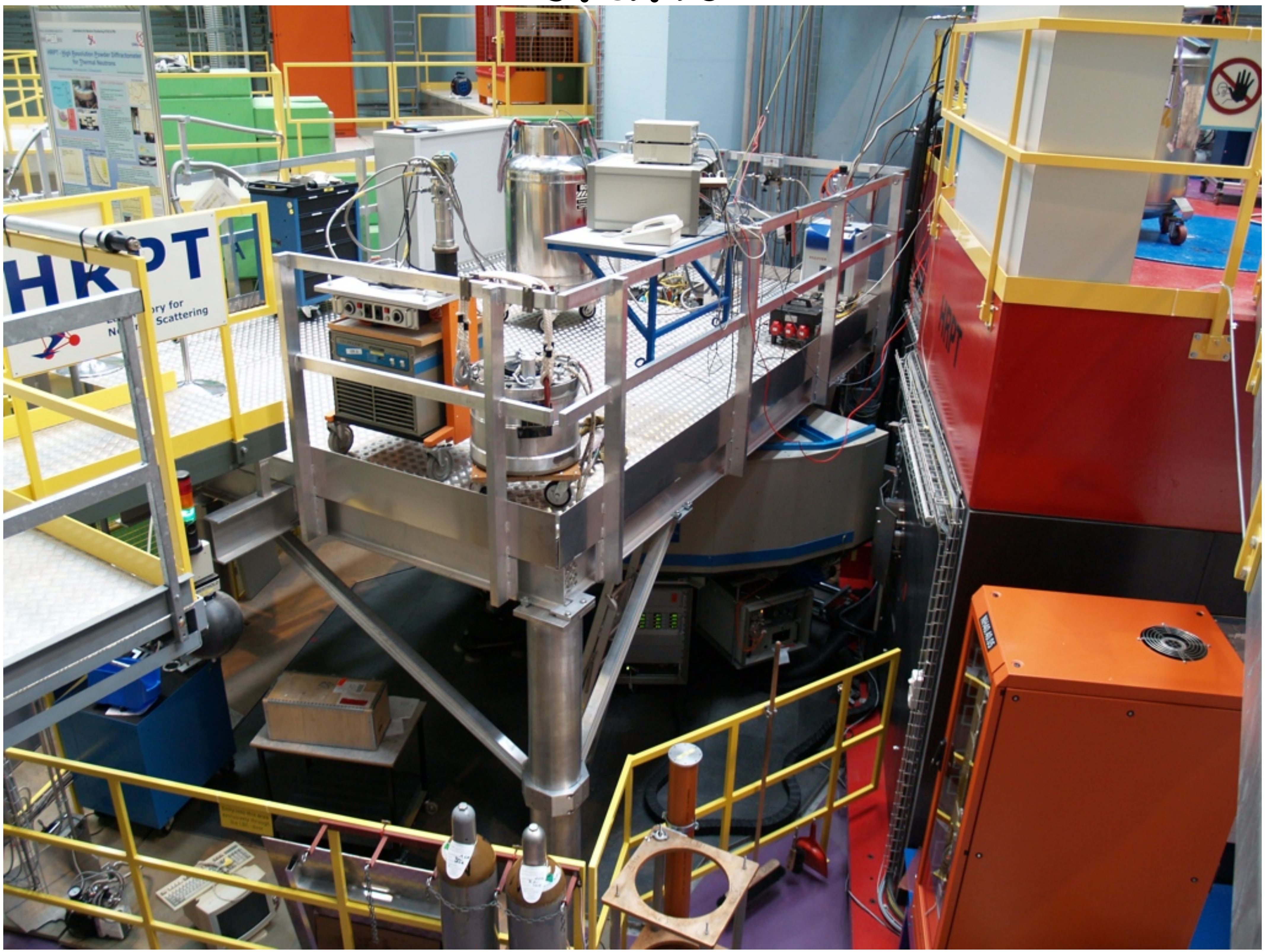

SINQ hall

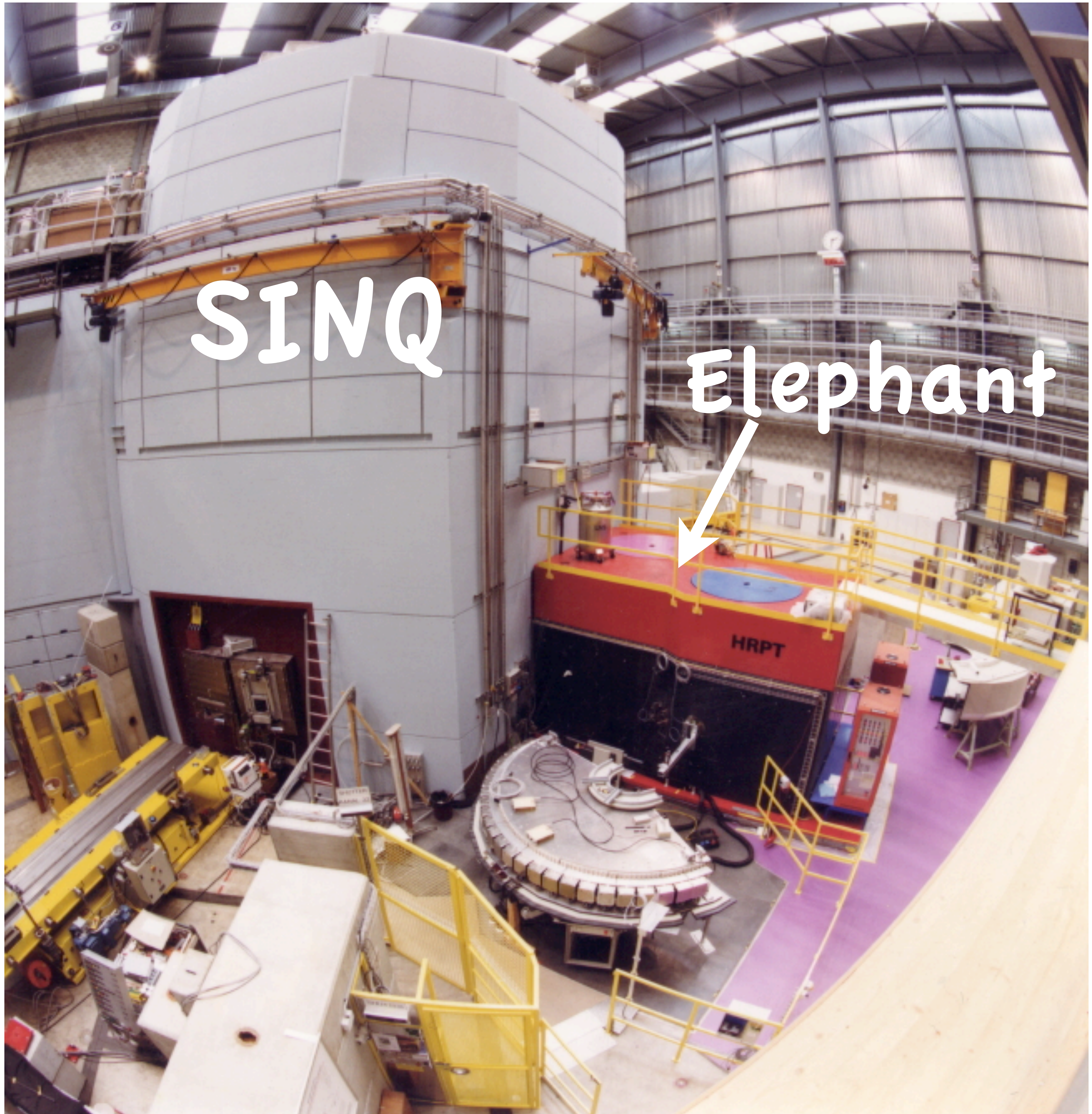

“Elephant” - shielding of primary beam (200 tons)

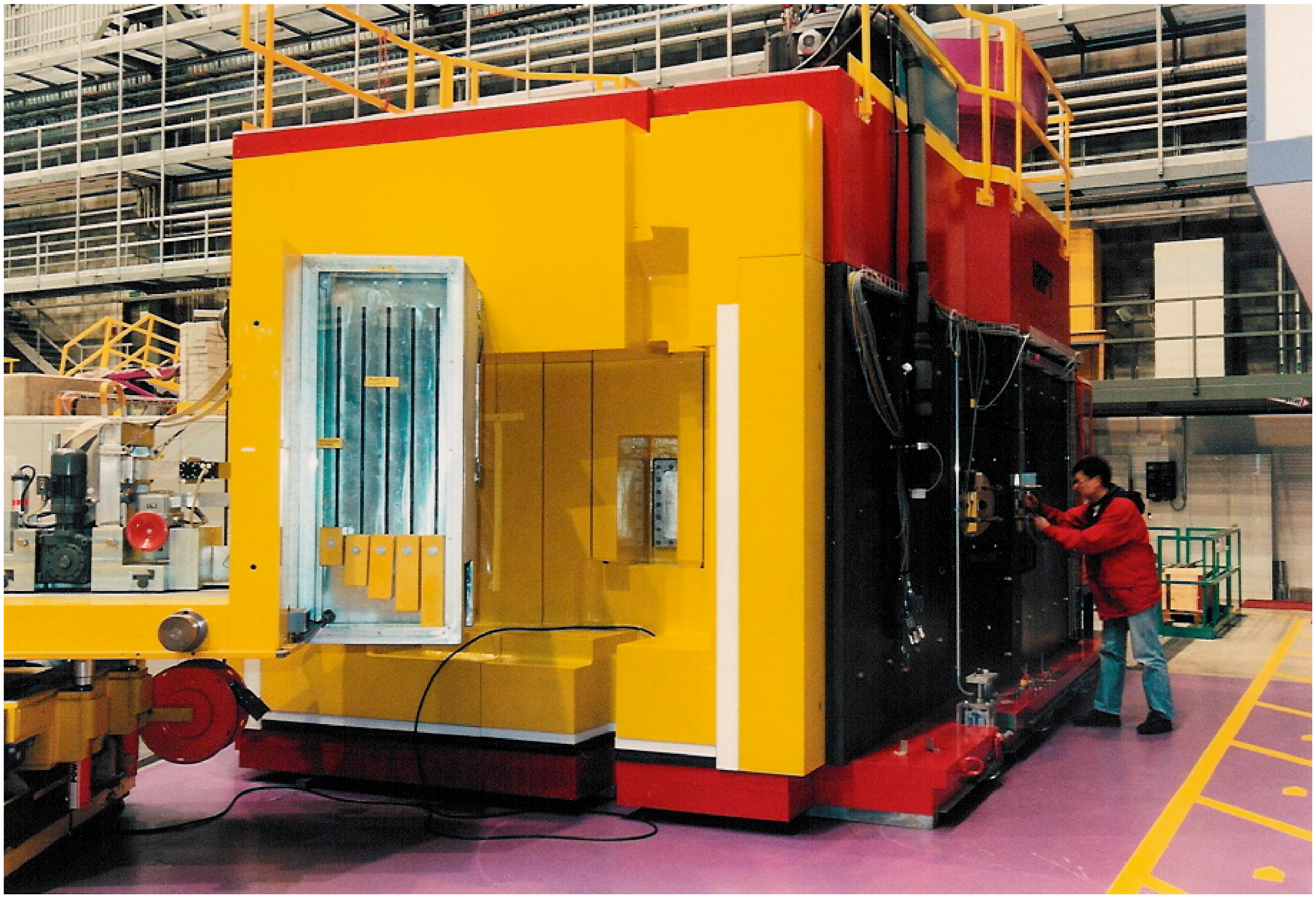

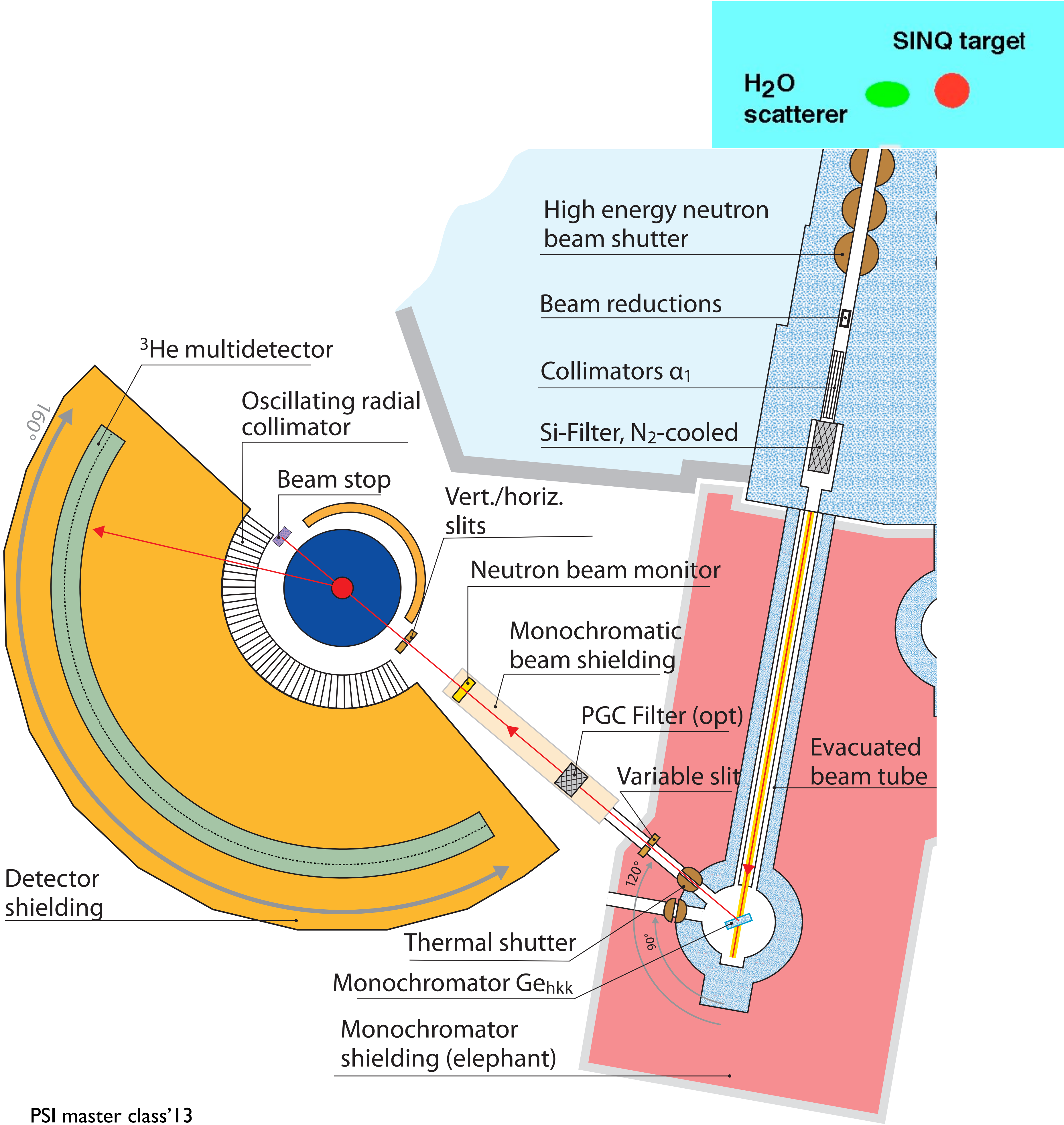
SINQ target
H_2O
scatterer
High energy neutron beam shutter
Beam reductions
Collimators α_1
Si-Filter, N_2-cooled
^{3}He multidetector
Oscillating radial collimator
Beam stop
Vert./horiz. slits
Neutron beam monitor
Monochromatic beam shielding
PGC Filter (opt)
Variable slit
Evacuated beam tube
160°
120°
90°
Detector shielding
Thermal shutter
Monochromator Ge_{hkk}
Monochromator shielding (elephant)

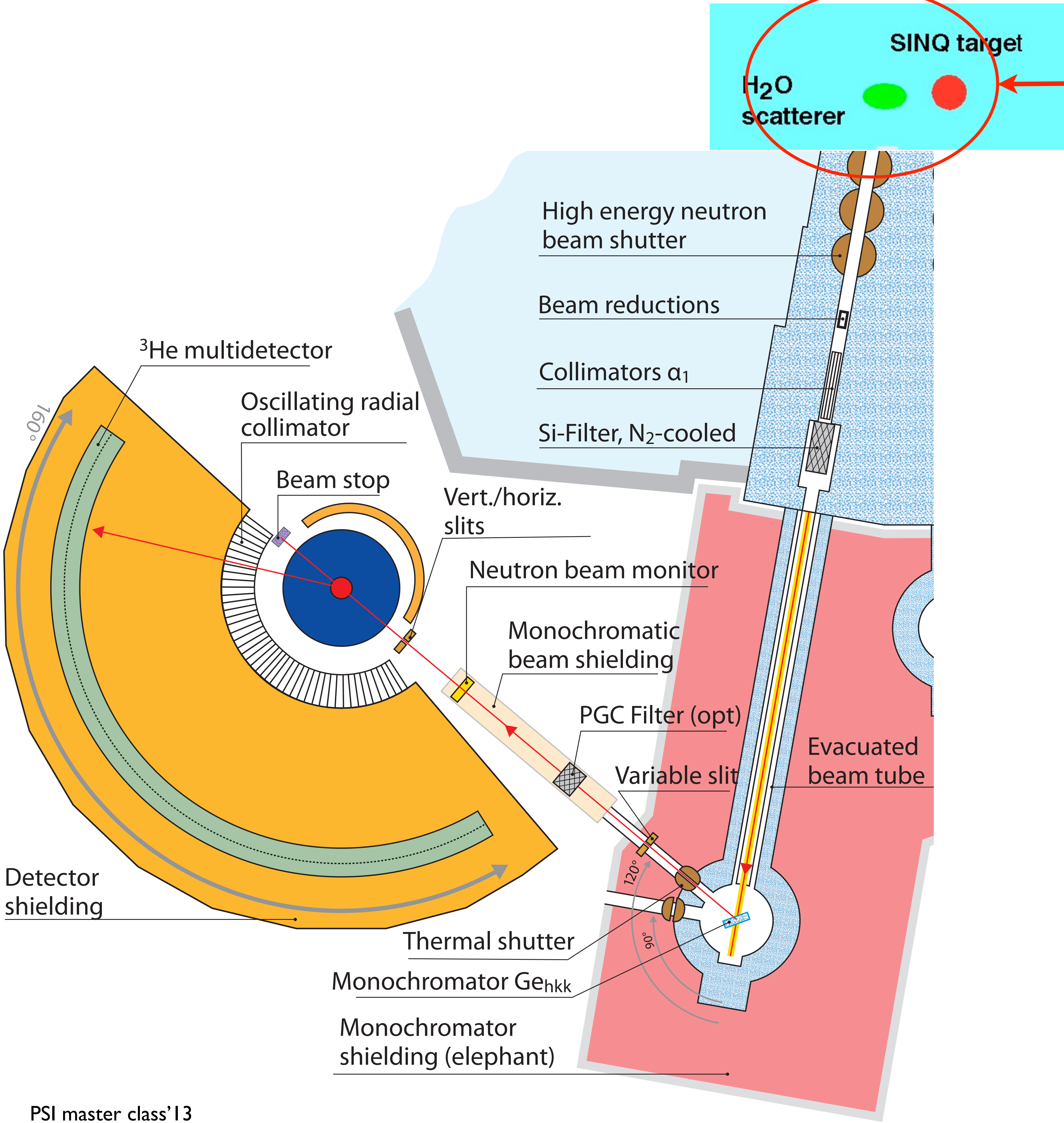

neutron flux from the moderator

Neutron flux from the D_2O moderator at HRPT/NEUTRA (white beam)

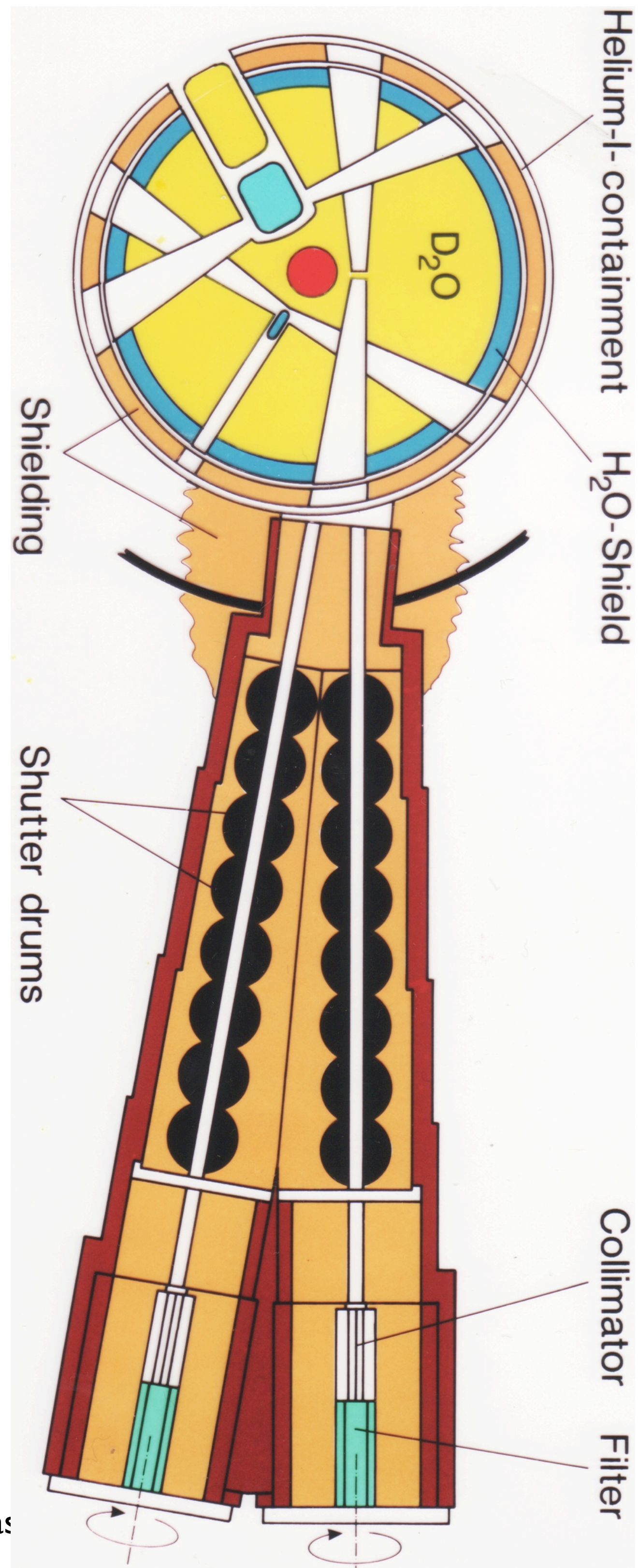

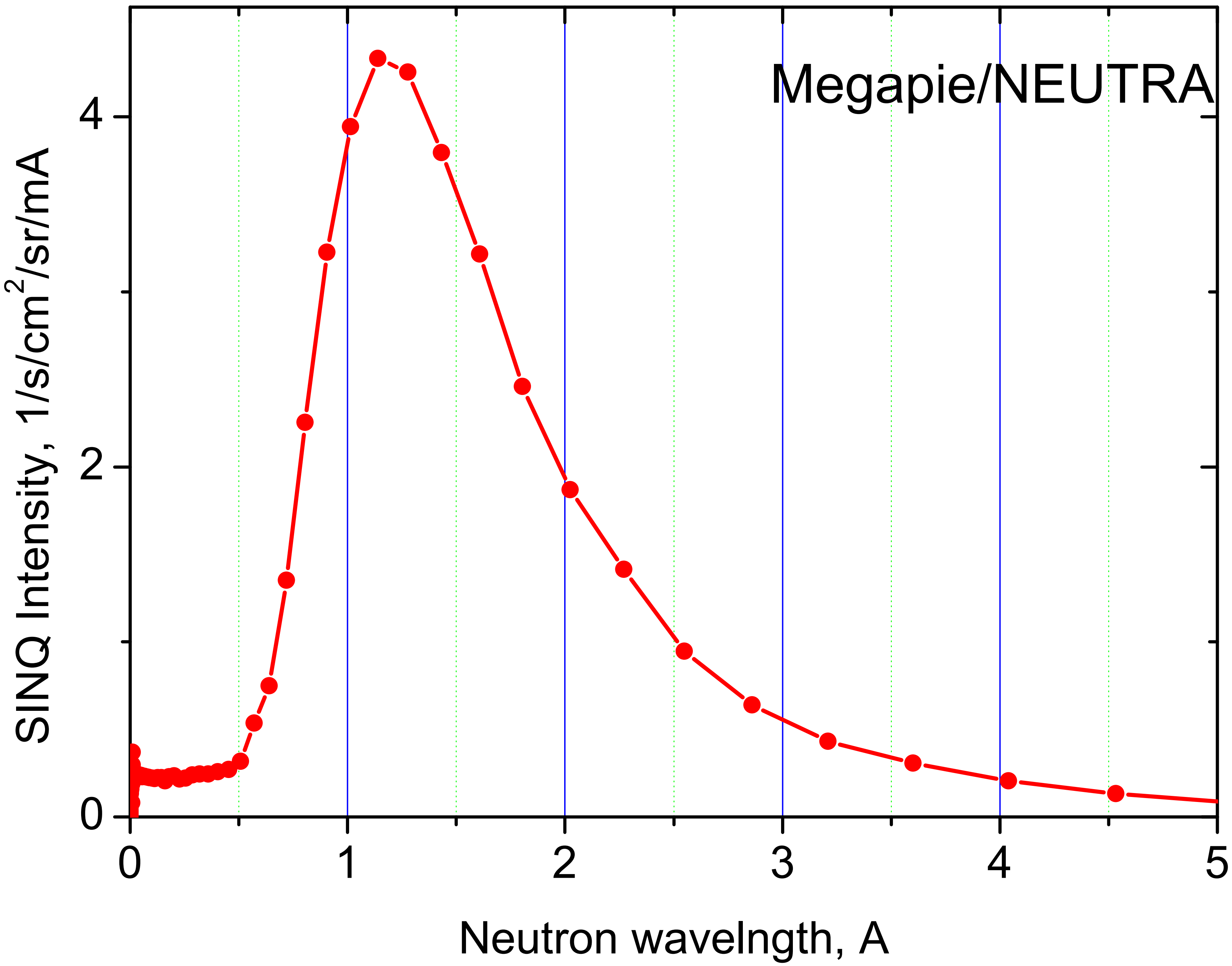

DMC flux

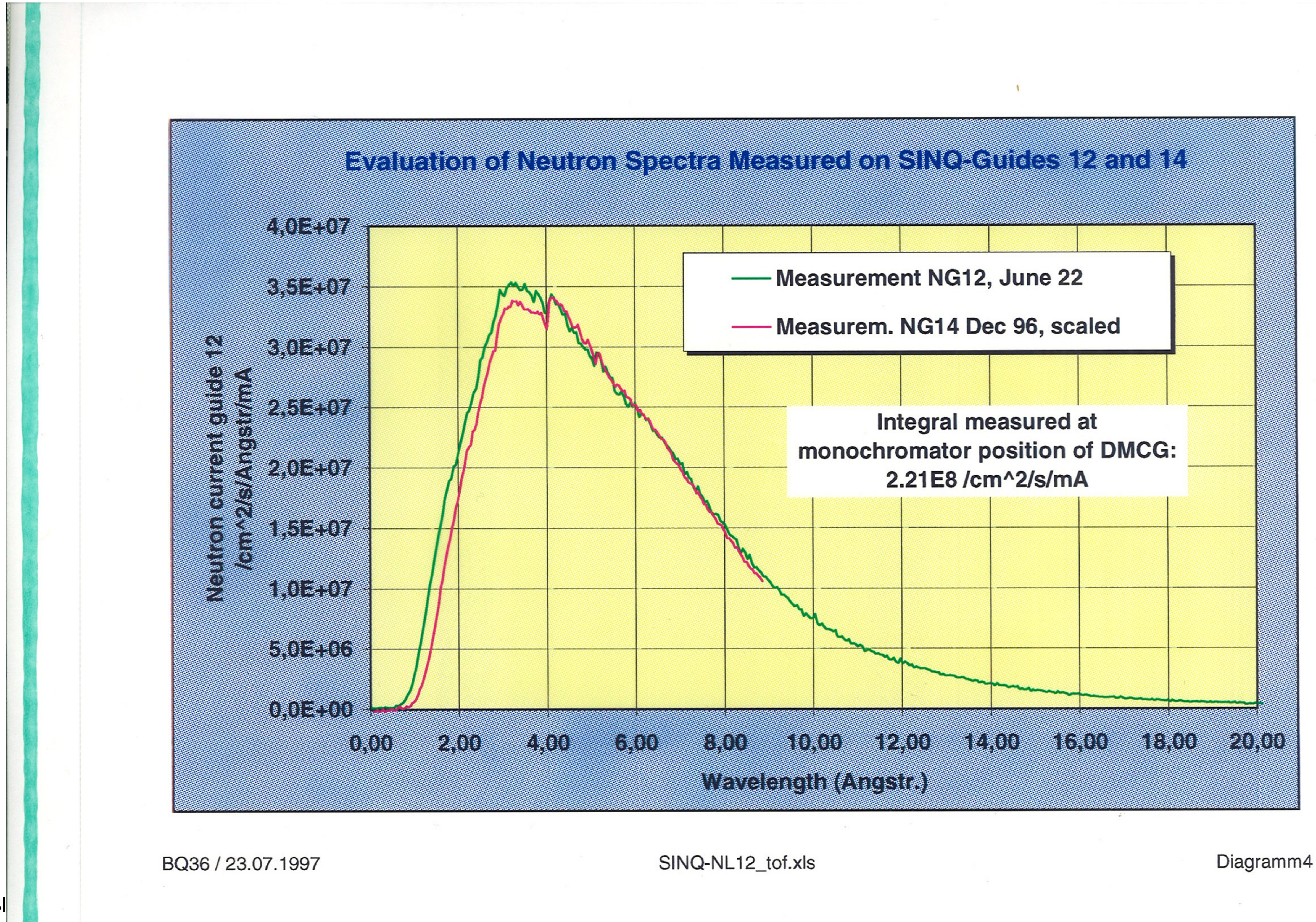

Evaluation of Neutron Spectra Measured on SINQ-Guides 12 and 14
Measurement NG12, June 22
Measurem. NG14 Dec 96, scaled
Integral measured at monochromator position of DMCG: 2.21E8 /cm^2/s/mA
Neutron current guide 12 /cm^2/s/Angstr/mA
4,0E+07
3,5E+07
3,0E+07
2,5E+07
2,0E+07
1,5E+07
1,0E+07
5,0E+06
0,0E+00
0,00
2,00
4,00
6,00
8,00
10,00
12,00
14,00
16,00
18,00
20,00
Wavelength (Angstr.)
BQ36 / 23.07.1997
SINQ-NL12_tof.xls
Diagramm4

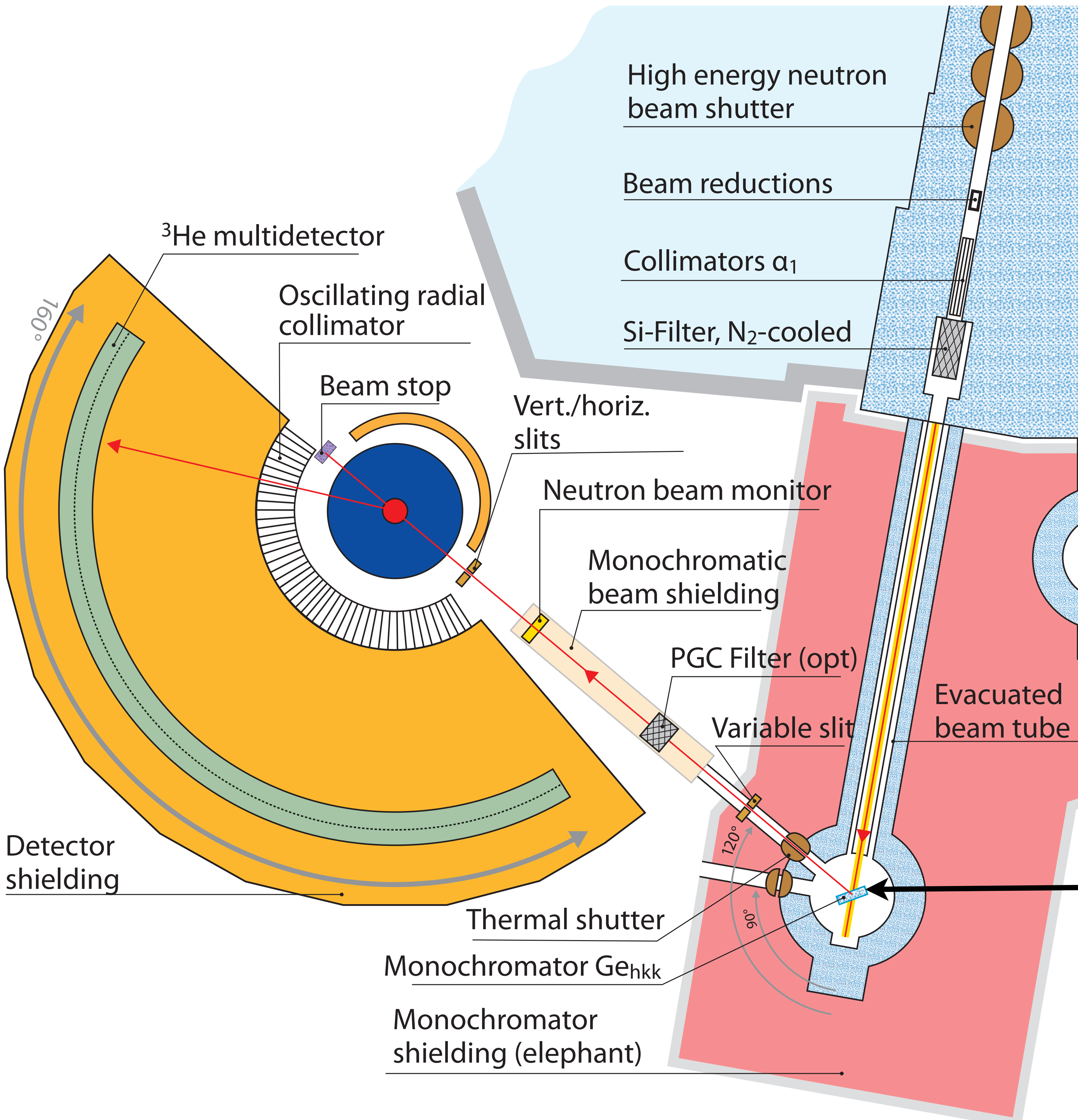

neutron monochromator
fixed 120 take off angle

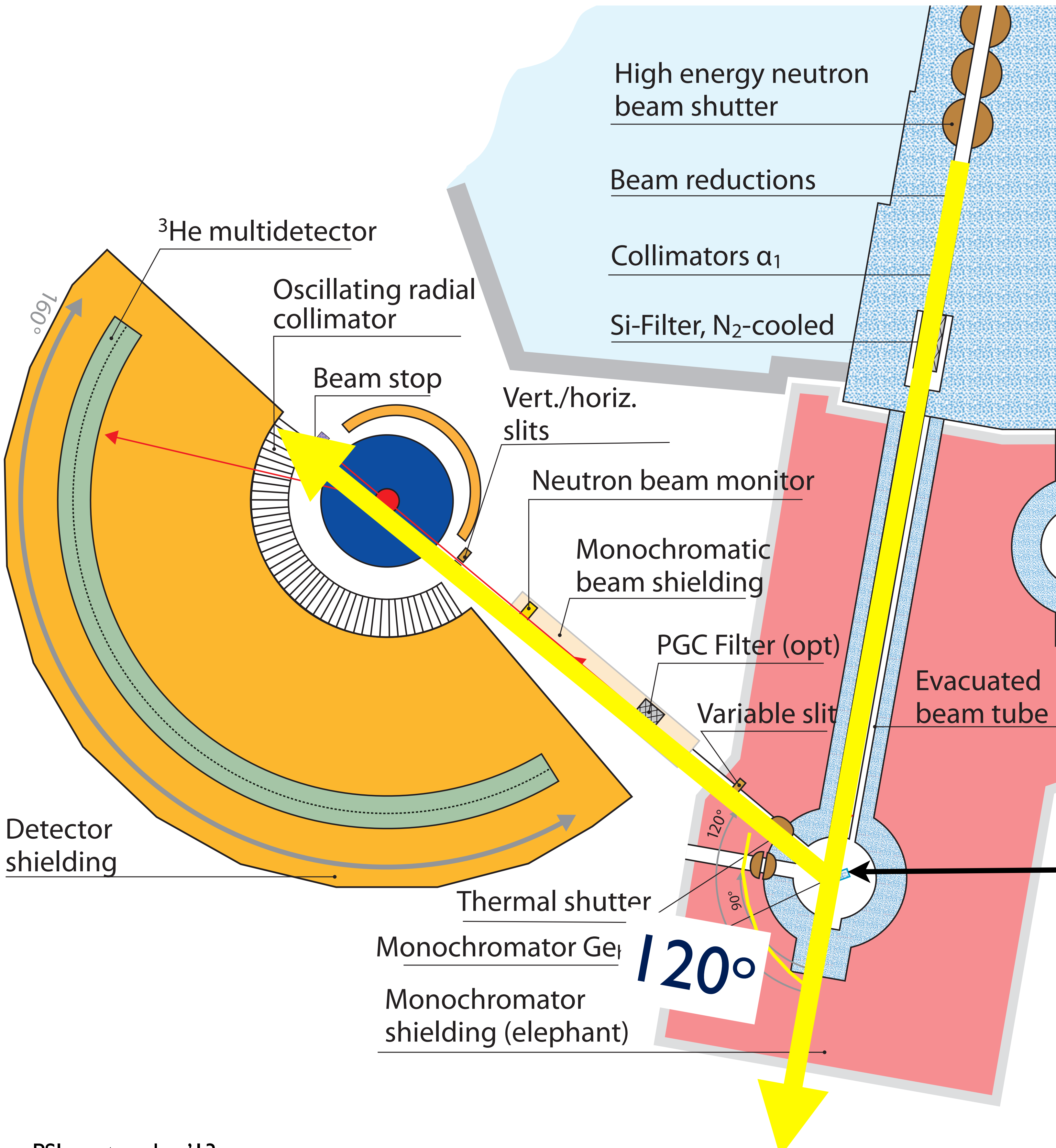

neutron monochromator
fixed 120 take off angle

Ge hkk focusing monochromator

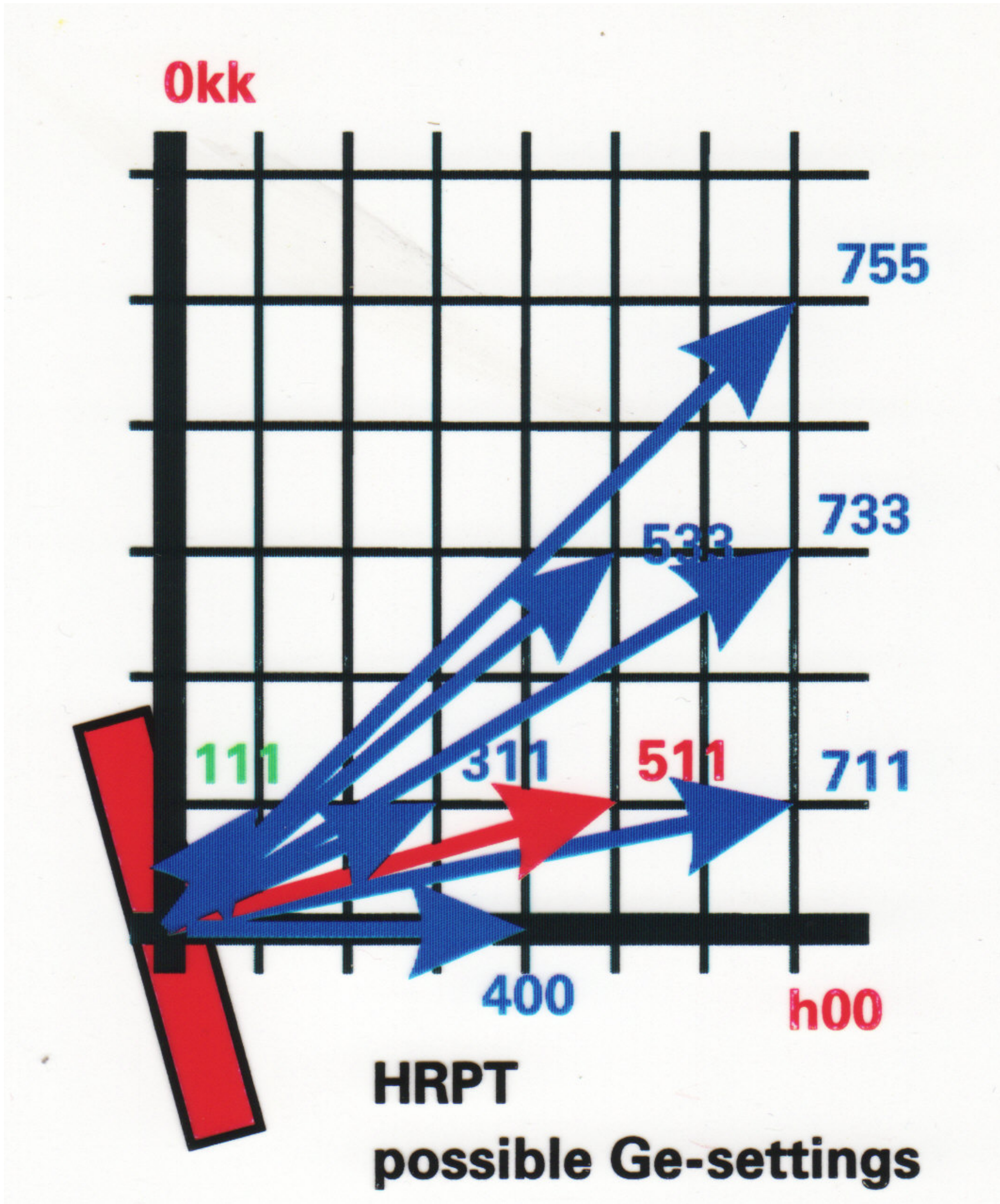

Ge hkk focusing monochromator

Monochromator hight: 11slabs*25=255mm
Beam spot hight at sample position
is smaller due to vertical focusing: 60mm
Wavelength is chosen by rotation along (hkk)
Mosaic 15'

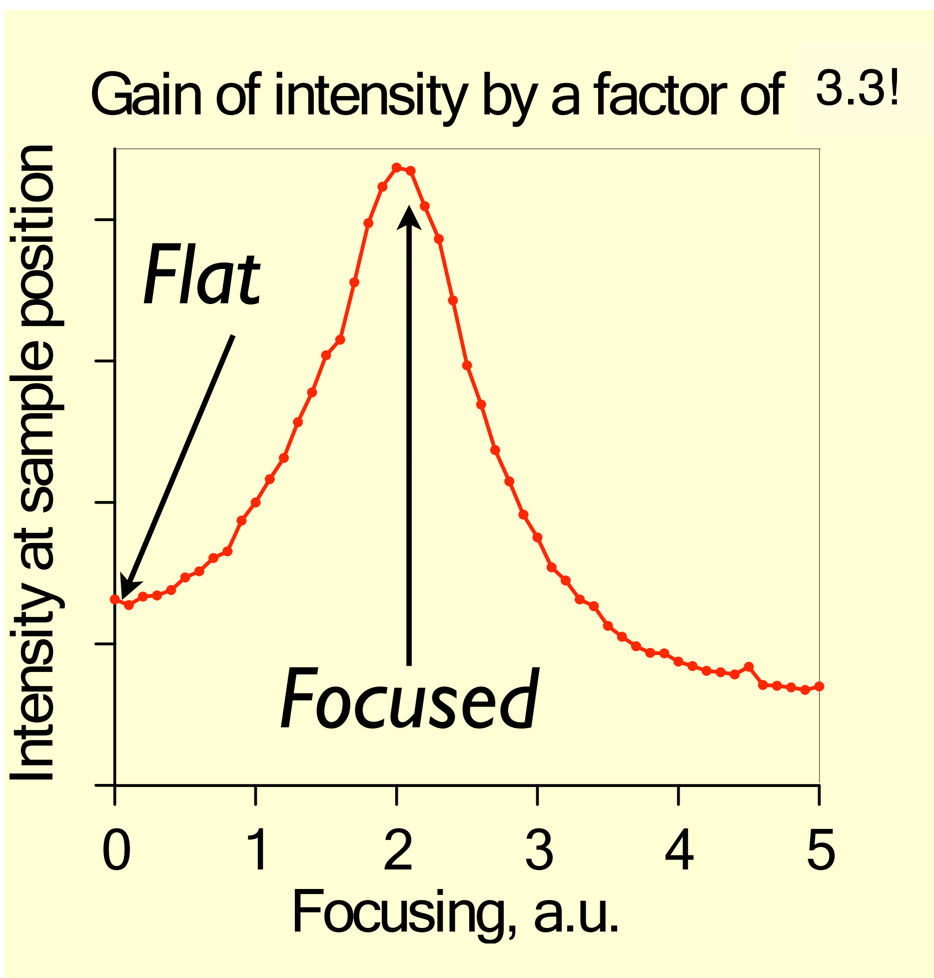

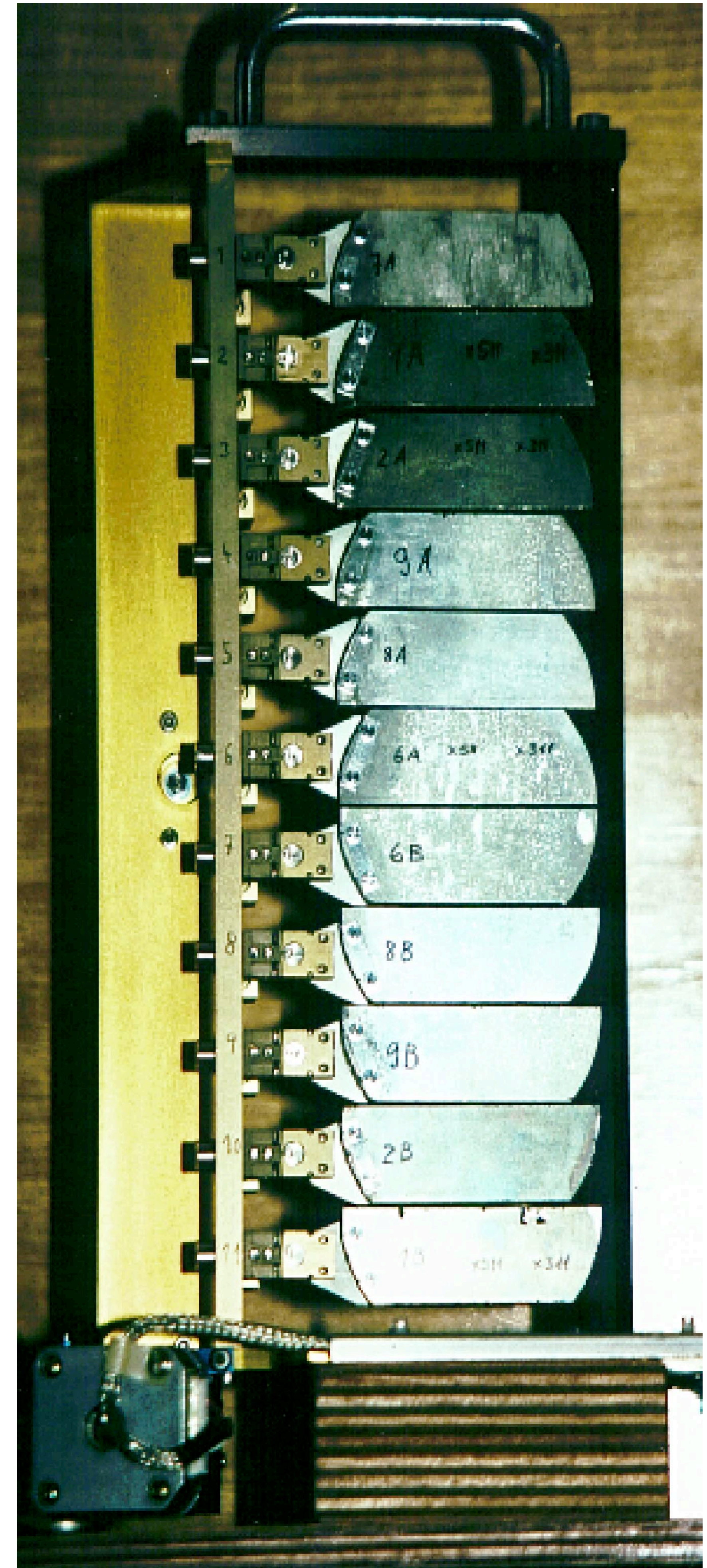

Flexible choice of wavelength, resolution/intensity

- Wavelength is selected by (hkk) plane of Ge-monochromator
- Resolution and intensity are controlled by appropriate primary/secondary collimations and take-off-angle of the monochromator (120° or 90°)

	$2\theta_M$=90°		$2\theta_M$ = 120°	
(hkk) Ge	λ, Å	Effective intensity	λ, Å	Effective intensity
311	2.40971	0.64	2.9536	~0.16
400	1.9984[4,5]		2.449[1,3]	0.19
133	1.8324	1.00	2.246[1,2]	
511	1.5384	1.55	1.886	1.0
533	1.2183	0.83	1.494	0.90
711	1.1194	0.60	1.372	0.71
733	0.9763	0.34	1.197	0.63
822	0.9419	0.48	1.154	0.79
466			1.044	0.27

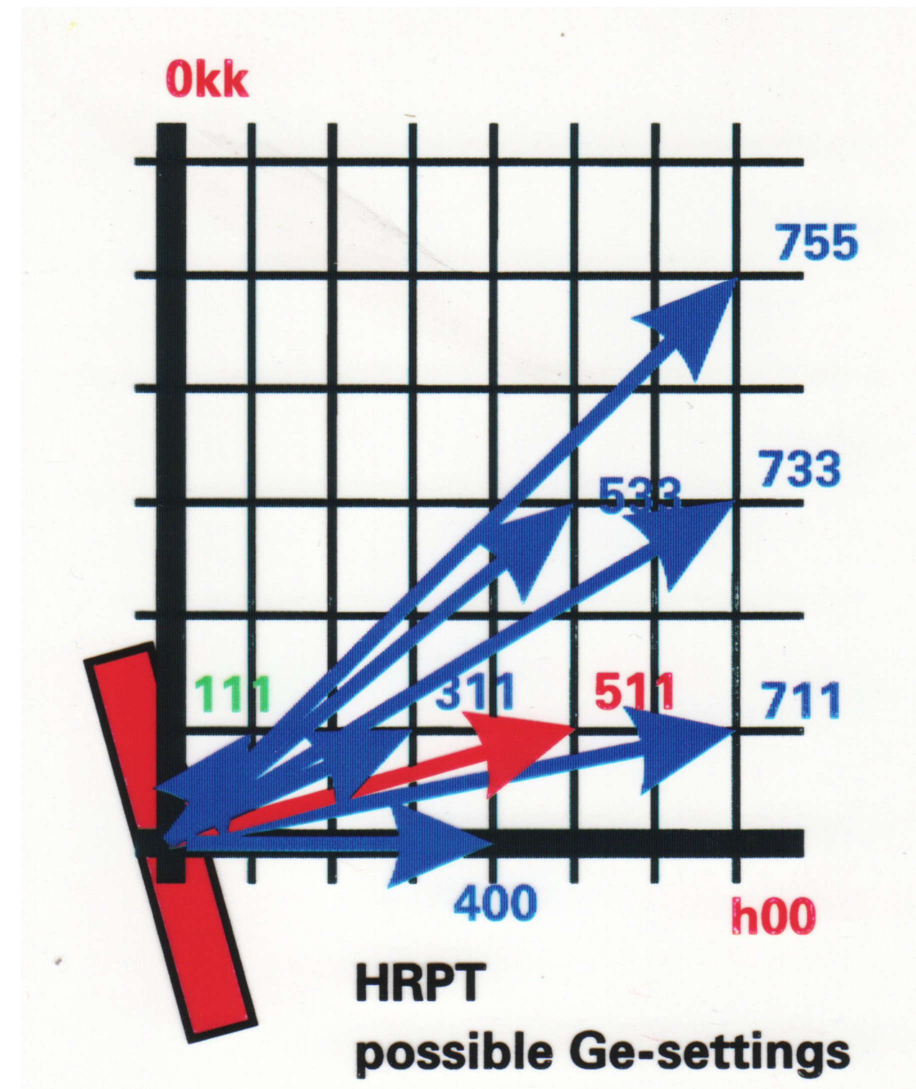

HRPT resolution
horizontal angular divergence control

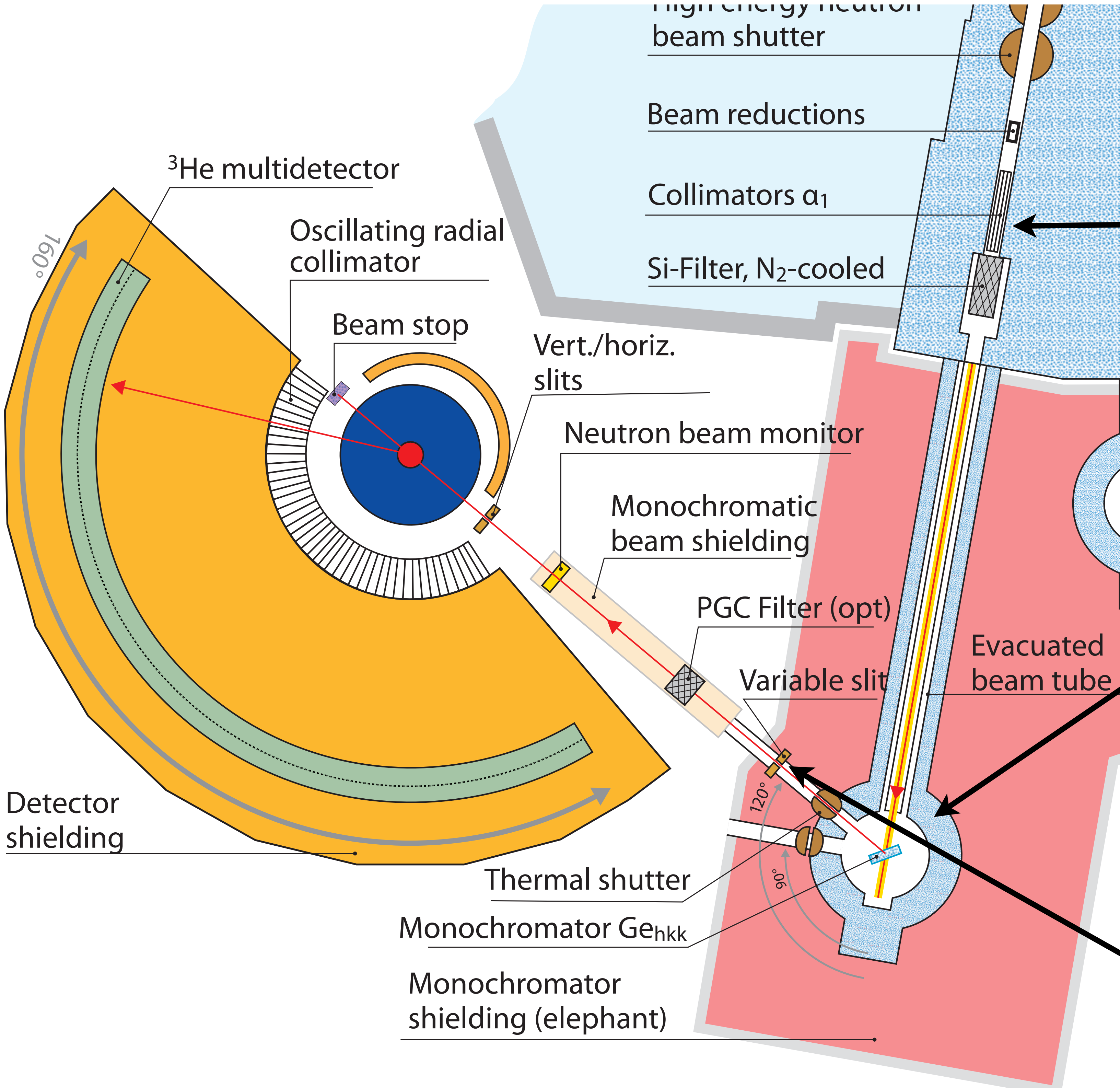

α_1

primary beam collimator(s): 6', 12', 24', 30'

α_2

mosaic spread of the monochromator 15'

α_3

slit system for monochromatic beam and sample diameter

Resolution calibration

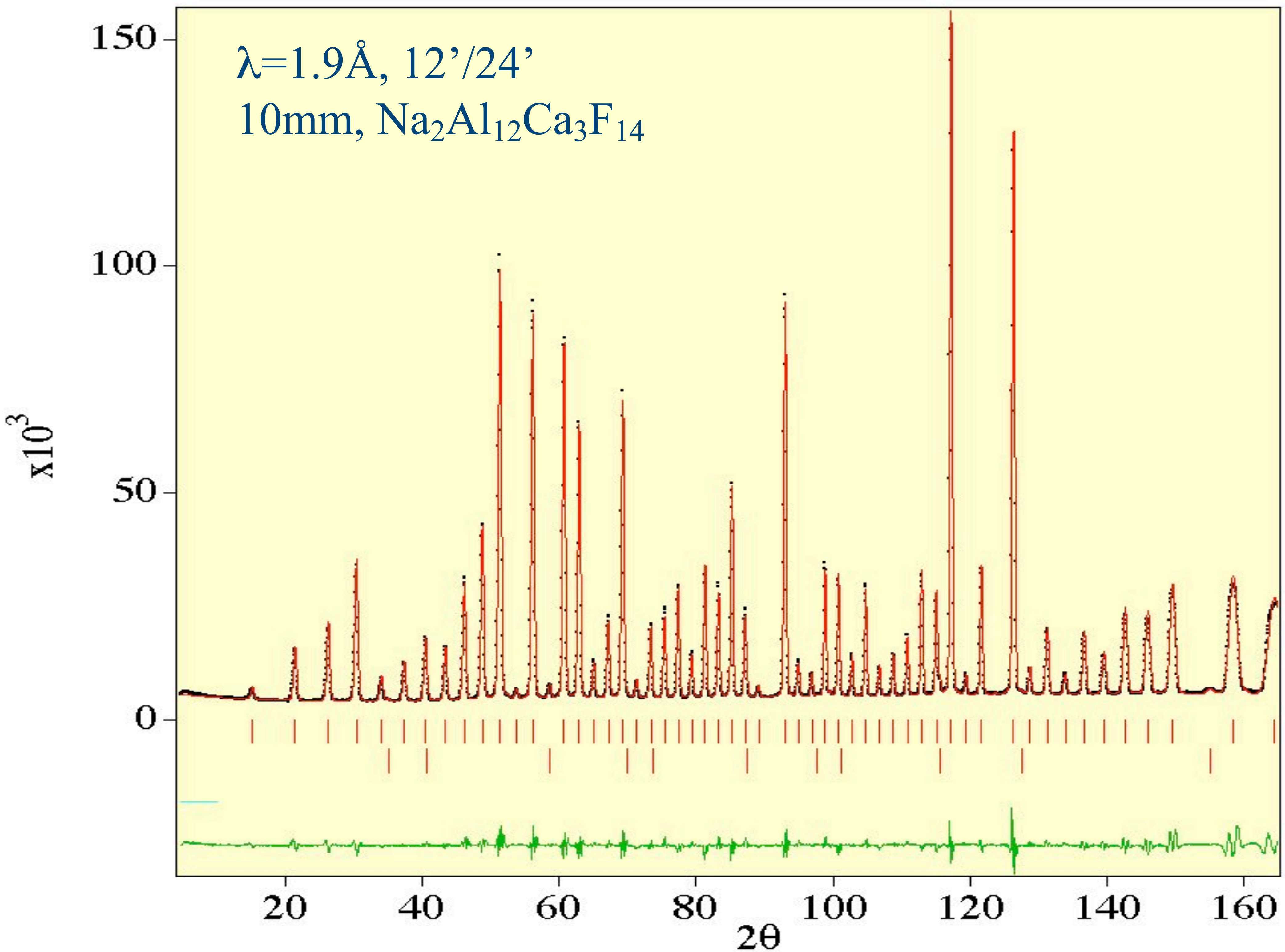

Resolution and intensity (2)

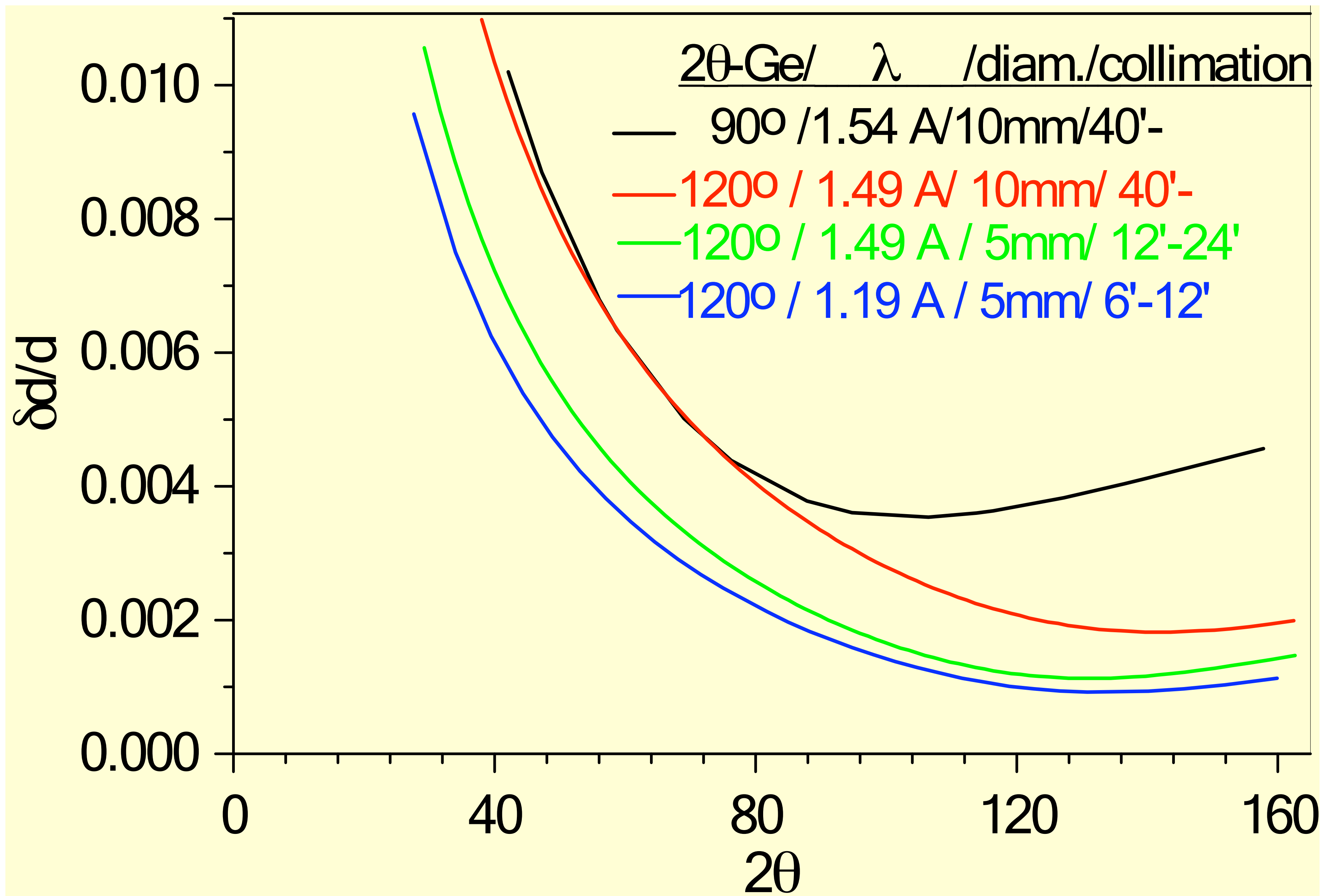

Comparison of resolution functions for different primary-secondary collimations. Typical modes are HI:40'-, MR:12'-24', HR:6'-12'. Counting rates are decreased by a factor of ~3 and ~(8-10) for MR and HR, respectively.

Detector

- ^3He (3.6 bar) + CF_4 (1.1 bar), effective detection length 3.5 cm, 15 cm hight
- Volume 100L, Voltage -6.7kV
- Efficiency 80% @ 1.5 Å
- 1600 wires with angular separation 0.1° (2.6 mm), 1500 mm to sample

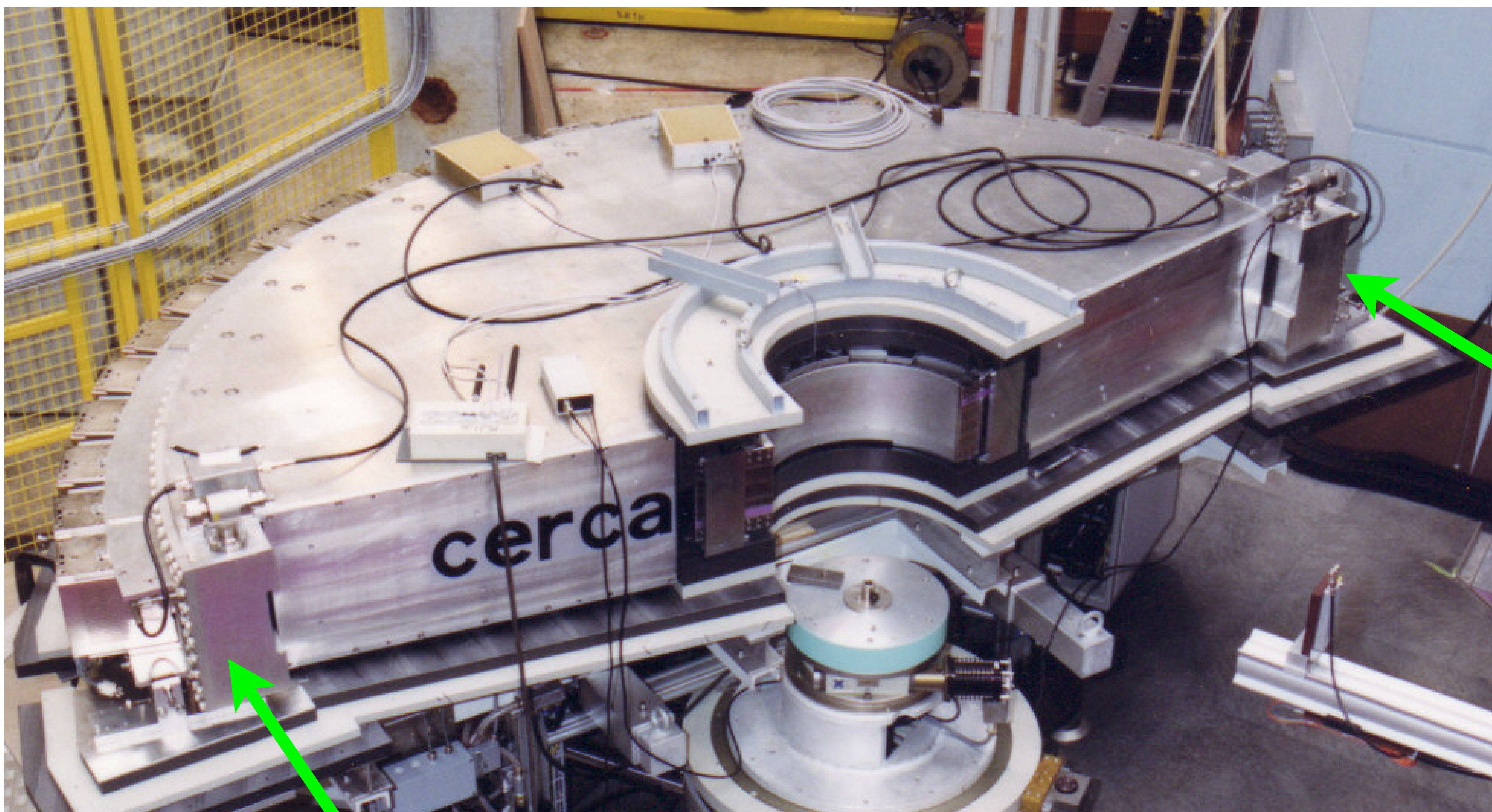

detector

Detector chamber. 1600 wires

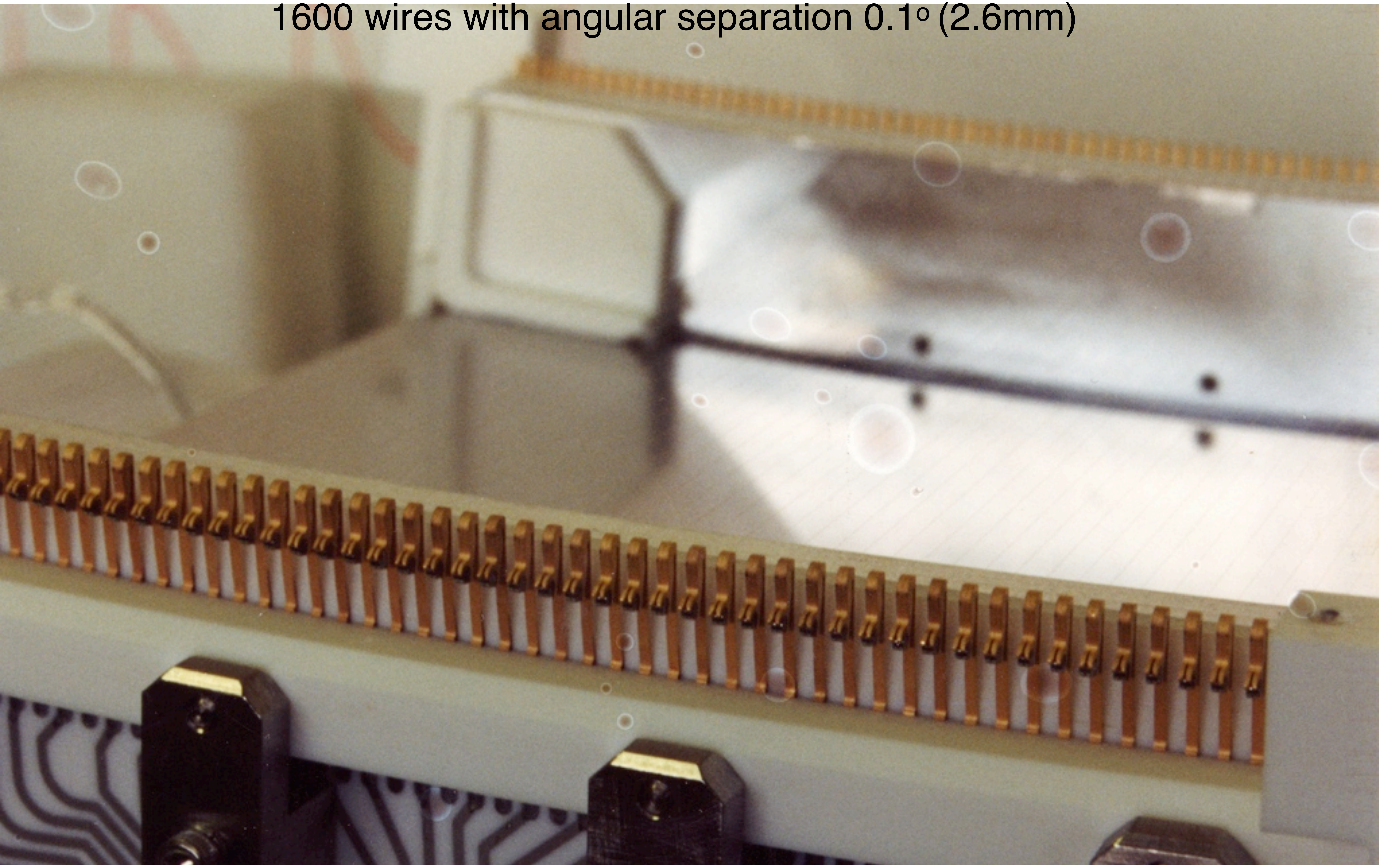

Oscillating radial collimator to avoid scattering from sample environment.

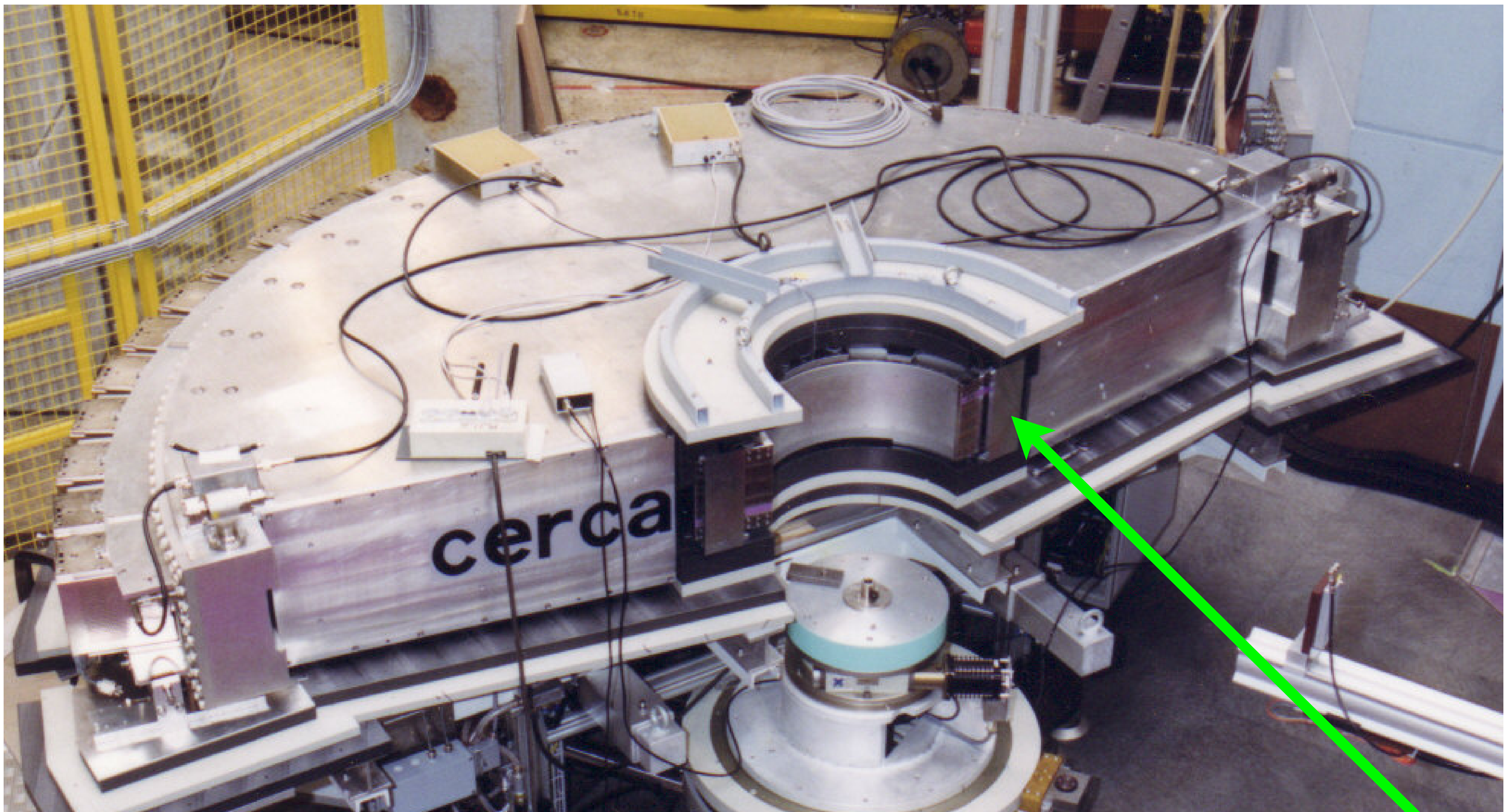

radial
collimator

HRPT radial collimators

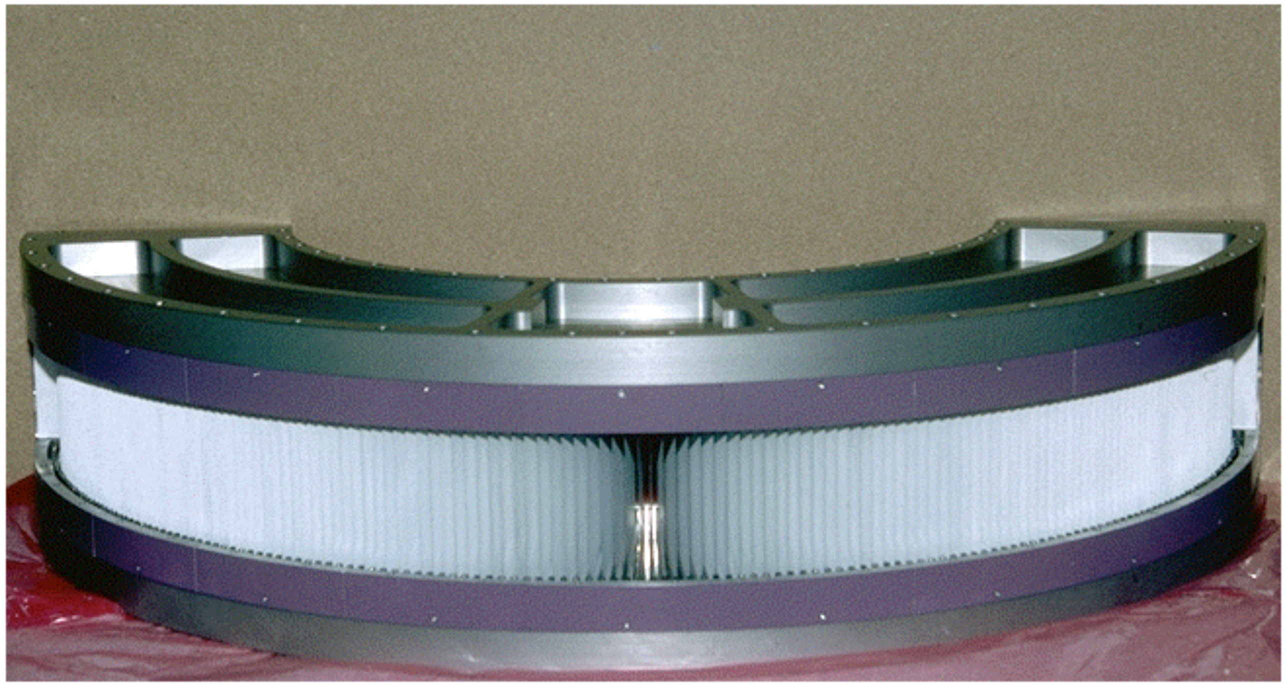

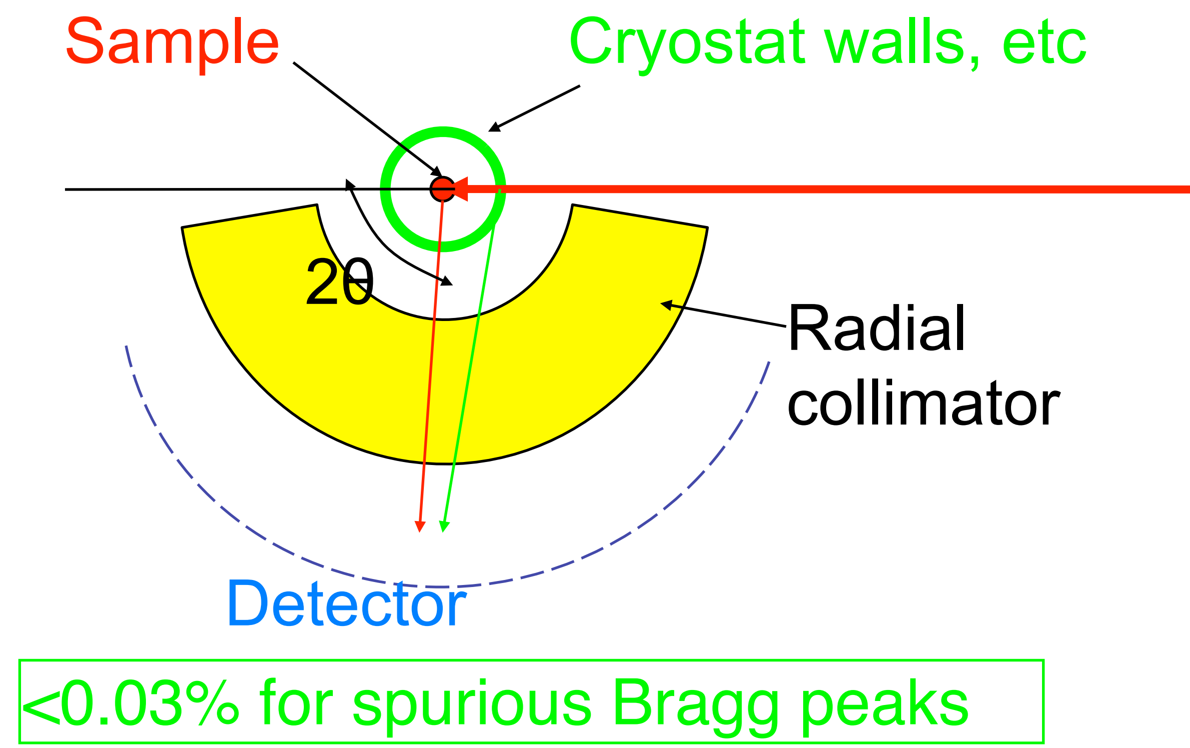

Radial collimator with the shielding.

There are two radial collimators with 14mm and 28mm full width full maximum triangular transmission function.

Samples, T, P, H and other equipment

- **standard sample container: 6-10 mm dia x 50 mm ($<4cm^3$)**
- due to low background small samples can be measured (30 mm^3)
- zero matrix high pressure cells:
  - clamp cells for 9 and 15 kbar
  - Paris Edinburgh cell 100 kbar
- standard LNS sample environment:
  - Temperature = 50 mK—1800K,
  - Magnetic field H = 4 T (vertical)
- Sample changers 4-8 samples, T=1.5-300 K

standard sample containers: 6-10 mm dia x 50 mm (<4cm^3)

Samples, T, P, H and other equipment

- standard sample container: 6-10 mm dia x 50 mm (<4cm^3)
- **due to low background small samples can be measured (30 mm^3)**
- zero matrix high pressure cells:
  - clamp cells for 9 and 15 kbar
  - Paris Edinburgh cell 100 kbar
- standard LNS sample environment:
  - Temperature = 50 mK—1800K,
  - Magnetic field H = 4 T (vertical)
- Sample changers 4-8 samples, T=1.5-300 K

Samples, T, P, H and other equipment

- standard sample container: 6-10 mm dia x 50 mm (<4cm^3)
- due to low background small samples can be measured (30 mm^3)
- **zero matrix high pressure cells:**
  - **clamp cells for 9 and 15 kbar**
  - **Paris Edinburgh cell 100 kbar**
- standard LNS sample environment:
  - Temperature = 50 mK—1800K,
  - Magnetic field H = 4 T (vertical)
- Sample changers 4-8 samples, T=1.5-300 K

clamp cells for 9 and 14 kbar

Paris Edinburgh cell 100 kbar

[Th. Straessle et al]

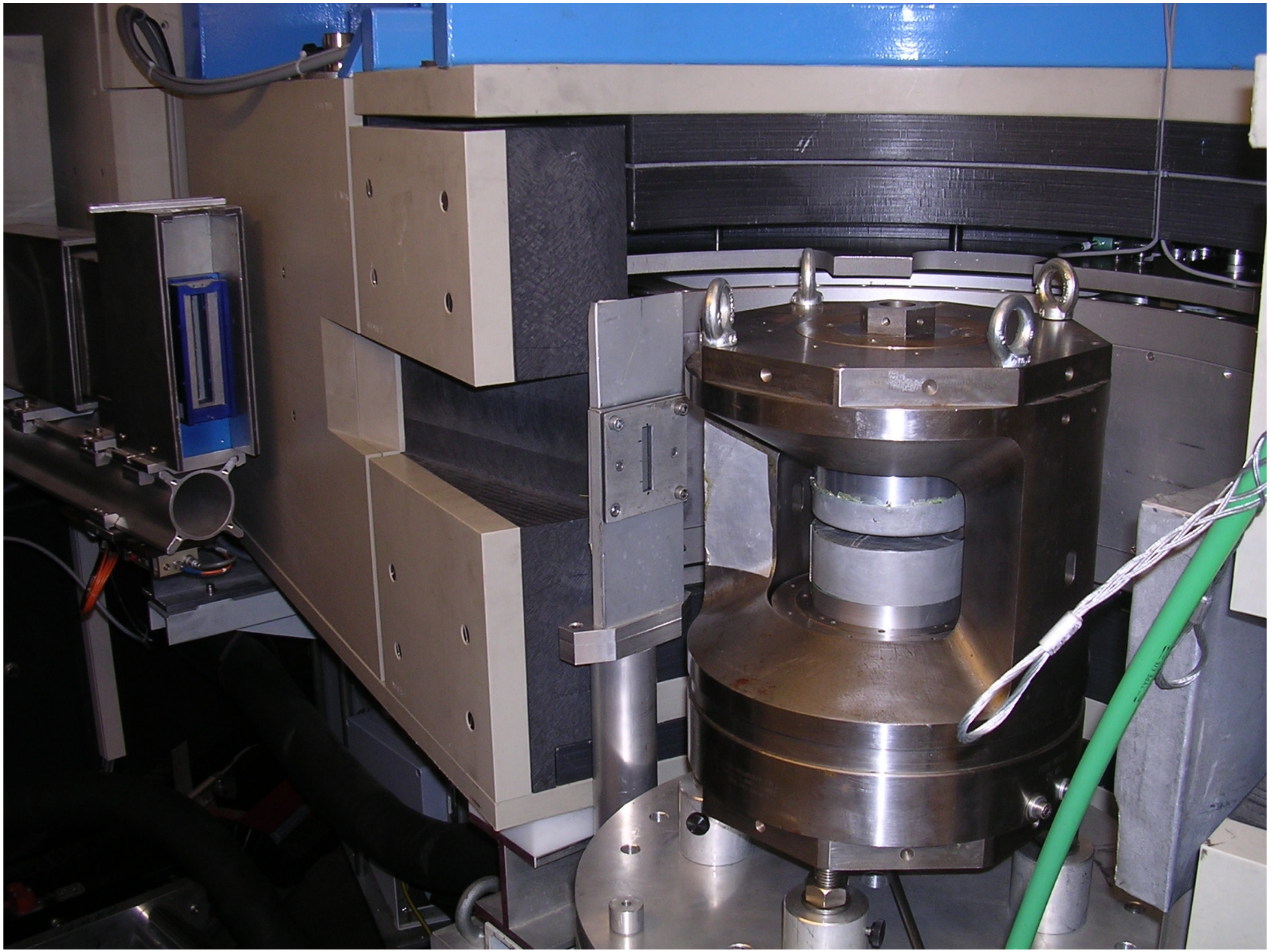

Samples, T, P, H and other equipment

- standard sample container: 6-10 mm dia x 50 mm (<$4cm^3$)
- due to low background small samples can be measured (30 mm^3)
- zero matrix high pressure cells:
  - clamp cells for 9 and 15 kbar
  - Paris Edinburgh cell 100 kbar
- **standard LNS sample environment:**
  - **Temperature = 50 mK—1800K,**
  - **Magnetic field H = 6 T (vertical)**
  - **Automatic He, N_2 refilling systems**
- Sample changers 4-8 samples, T=1.5-300 K

Samples, T, P, H and other equipment

- standard sample container: 6-10 mm dia x 50 mm (<4cm^3)
- due to low background small samples can be measured (30 mm^3)
- zero matrix high pressure cells:
  - clamp cells for 9 and 15 kbar
  - Paris Edinburgh cell 100 kbar
- standard LNS sample environment:
  - Temperature = 50 mK—1800K,
  - Magnetic field H = 4 T (vertical)
  - Automatic He, N_2 refilling systems
- **Sample changers 4-8 samples, T=1.5-300 K**

HRPT room temperature 8-sample changer

- Eight samples mounted on a caroussel-type changer, few seconds to bring the next one into the measurement position;

- Independent sample rotation mechanism – for reducing the preferred orientation aberrations.

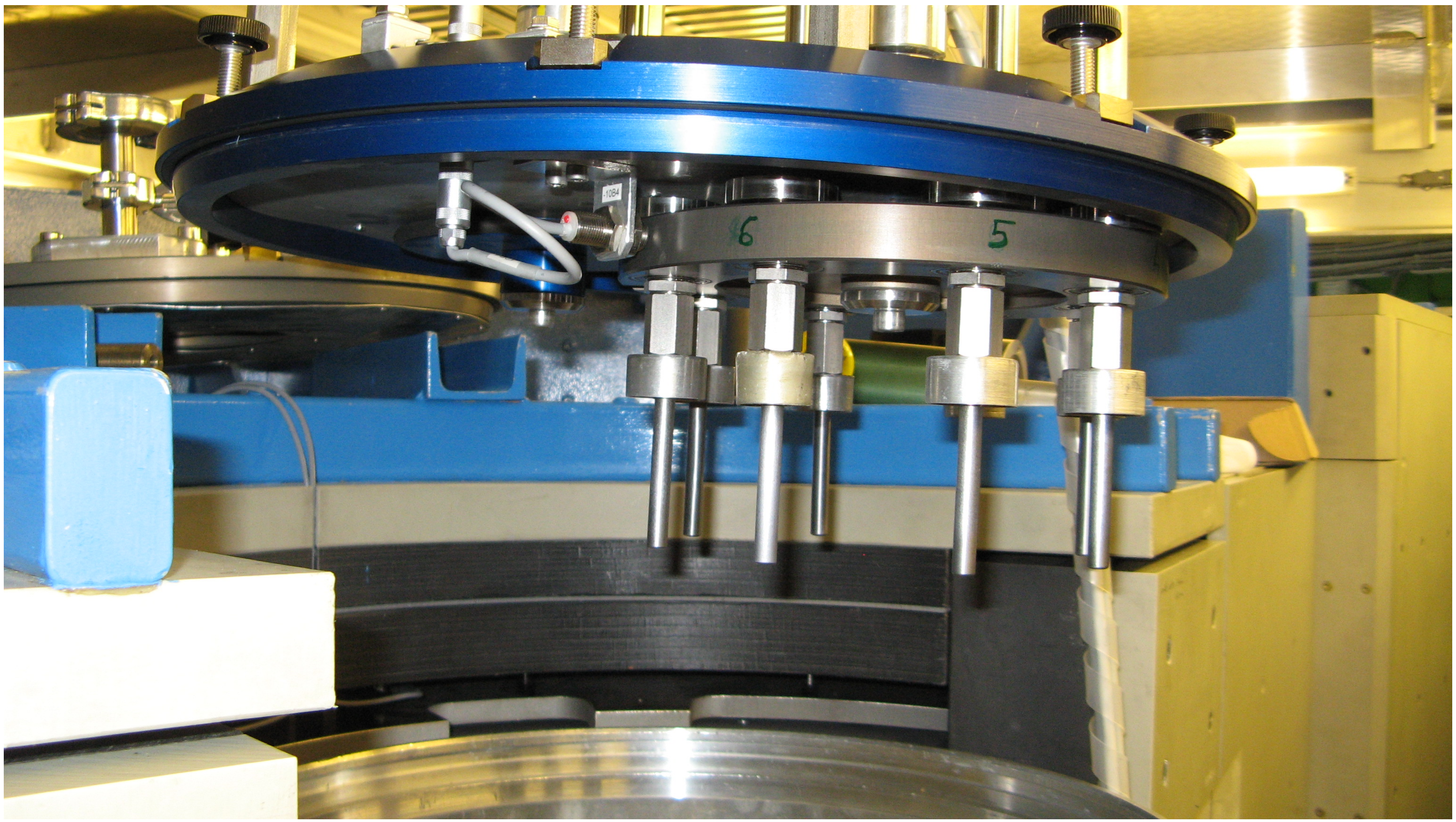

Fully loaded with 8 samples, the sample changer is ready to be installed in-place on the HRPT sample table.

HRPT room temperature 8-sample changer

- Eight samples mounted on a caroussel-type changer, few seconds to bring the next one into the measurement position;
- Independent sample rotation mechanism – for reducing the preferred orientation aberrations.

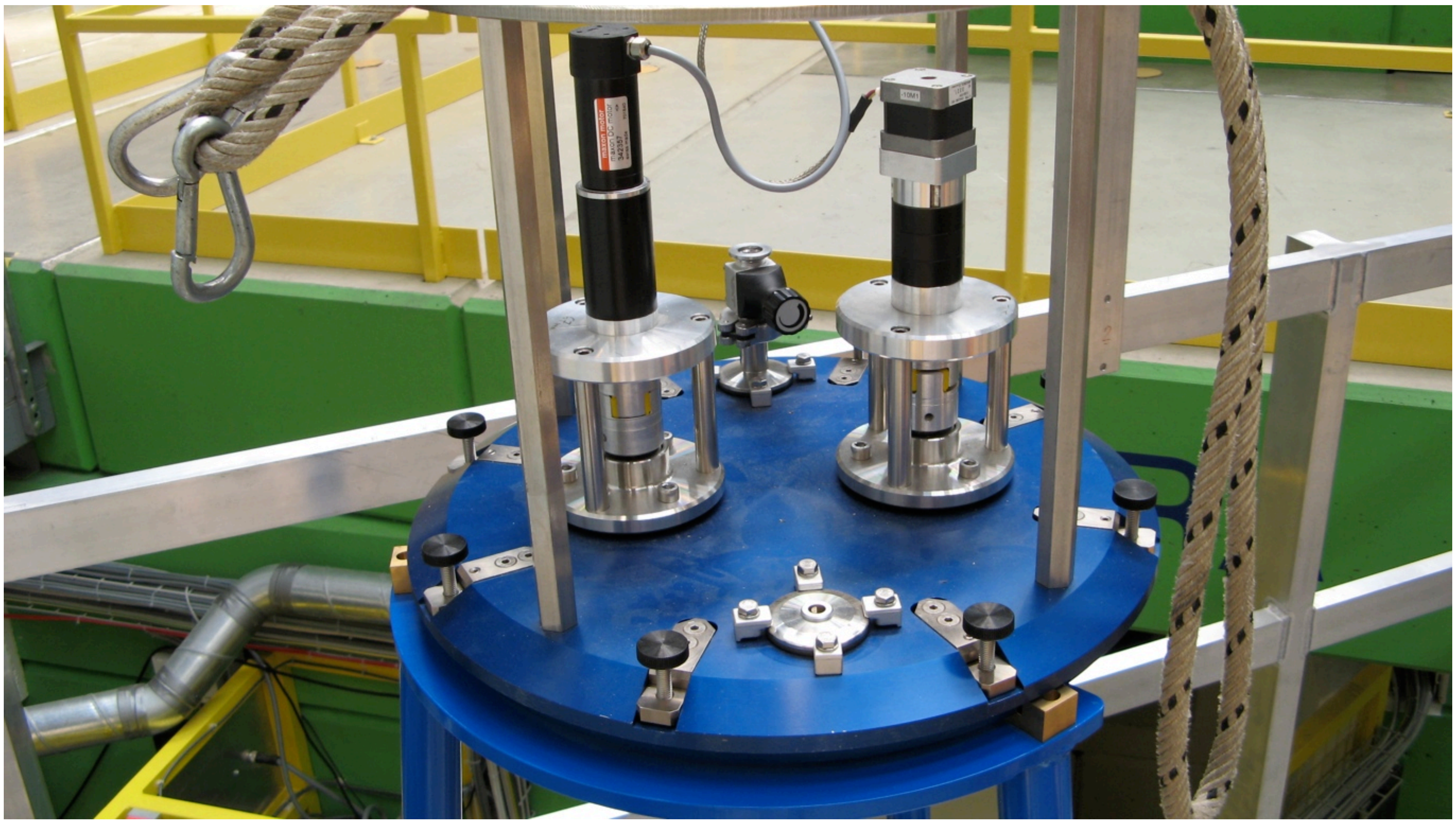

Fully loaded with 8 samples, the sample changer is ready to be installed in-place on the HRPT sample table.

HRPT room temperature 8-sample changer

- Eight samples mounted on a caroussel-type changer, few seconds to b position;

- Independer cing the preferred ori

User Experiment 20061119
"Structure of leached Raney
Ni alloys" (Nov. 2007):
~80 samples measured in
4 beam days:

20 samples/day!

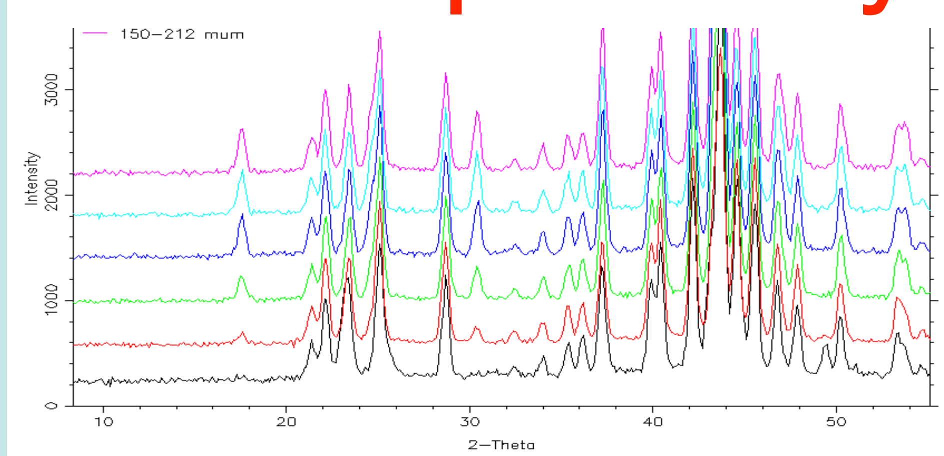

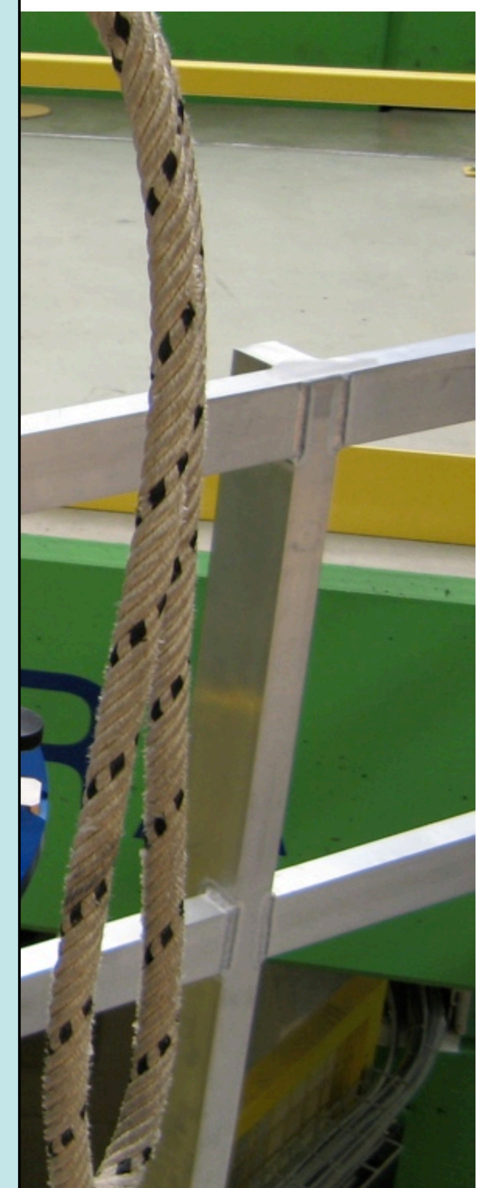

Fully loaded with 8 samples *HRPT sample table.*

HRPT low temperature 4-sample changer

A device for routine powder diffraction measurements at temperatures between 1.5K -300K.

- All samples have the same temperature, i.e. time for temperature change is saved;
- Four samples mounted on a caroussel-type changer, that is a special inset for an orange cryostat

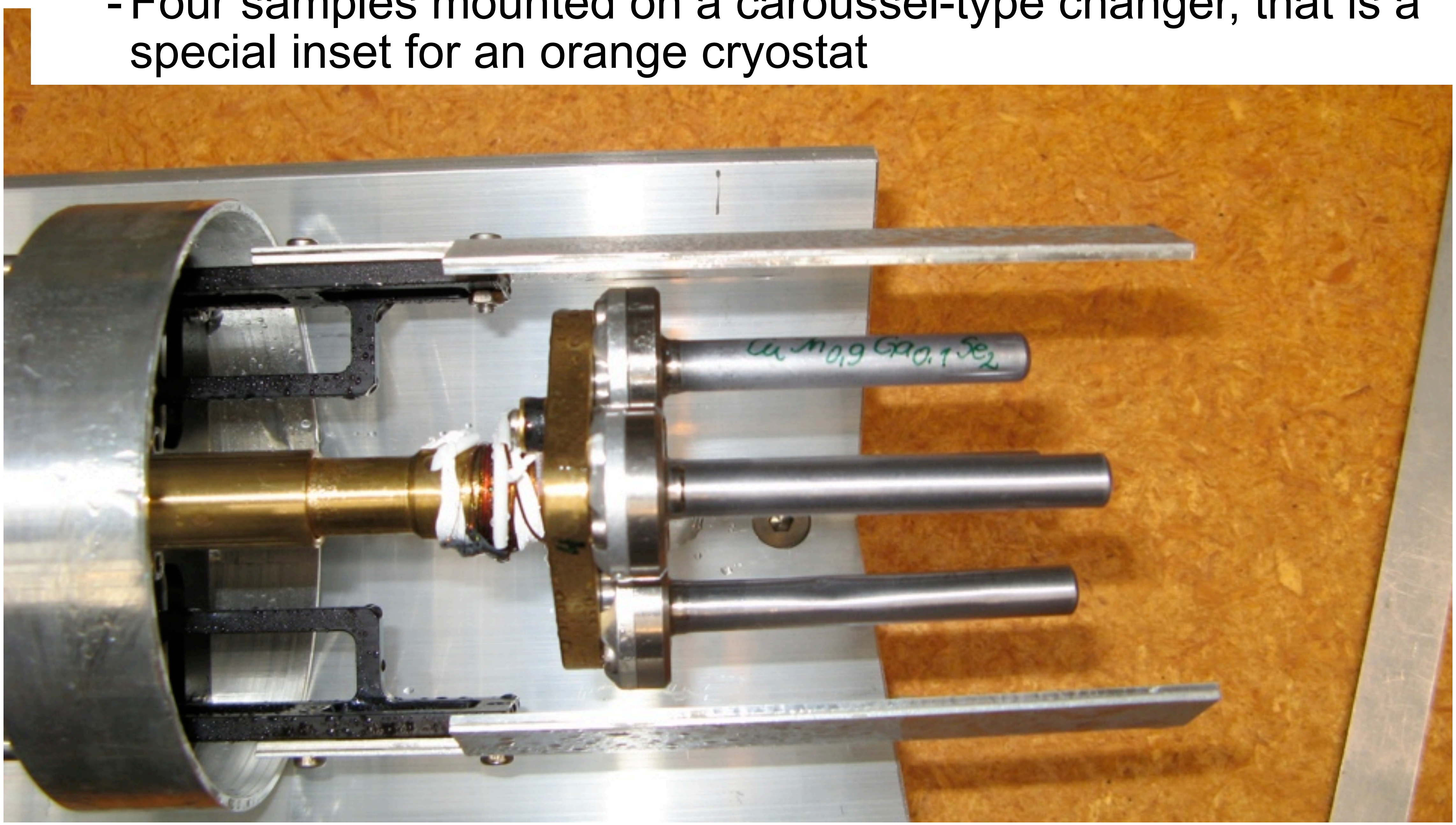

HRPT low temperature 4-sample changer

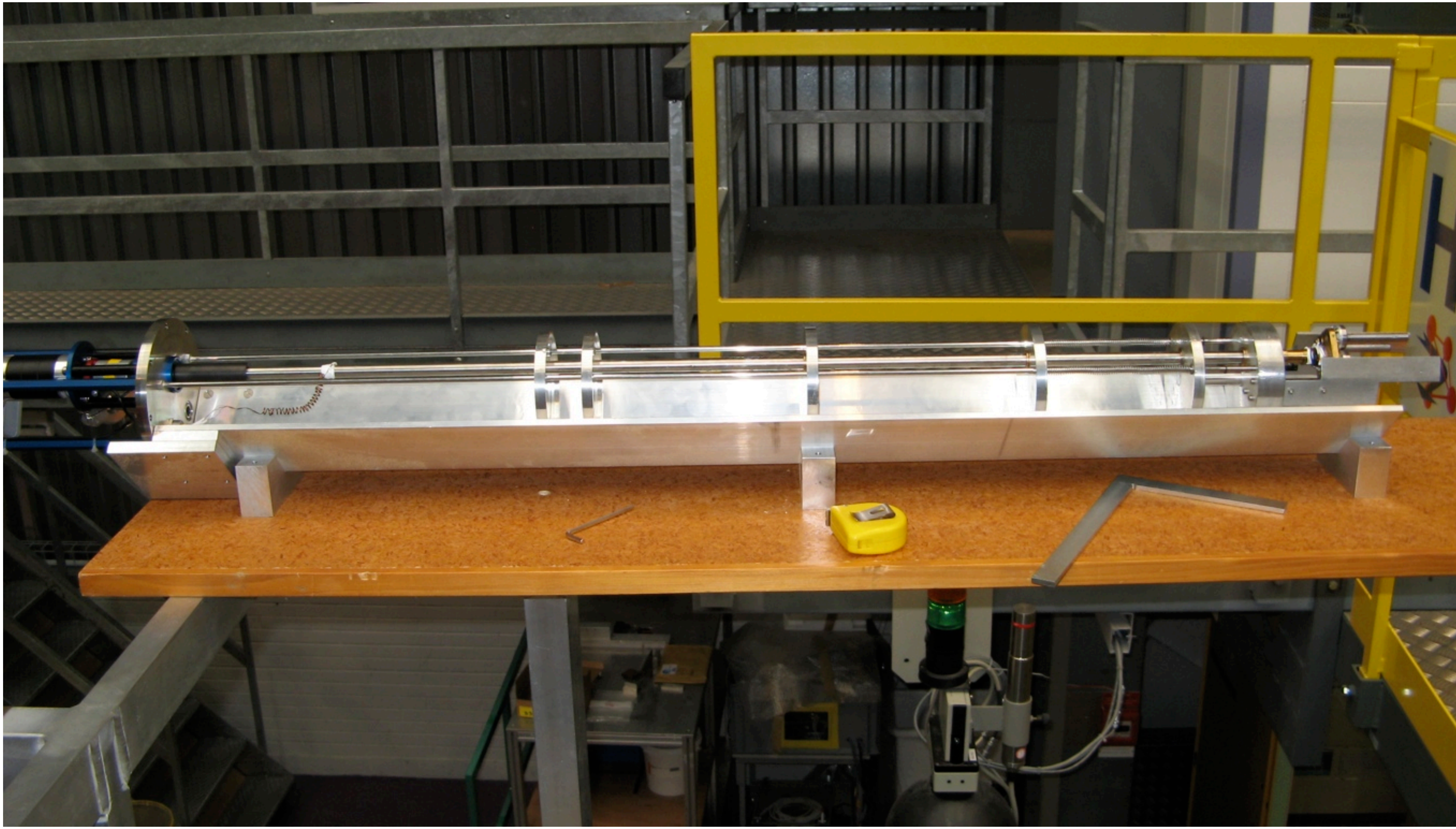

HRPT low temperature 4-sample changer

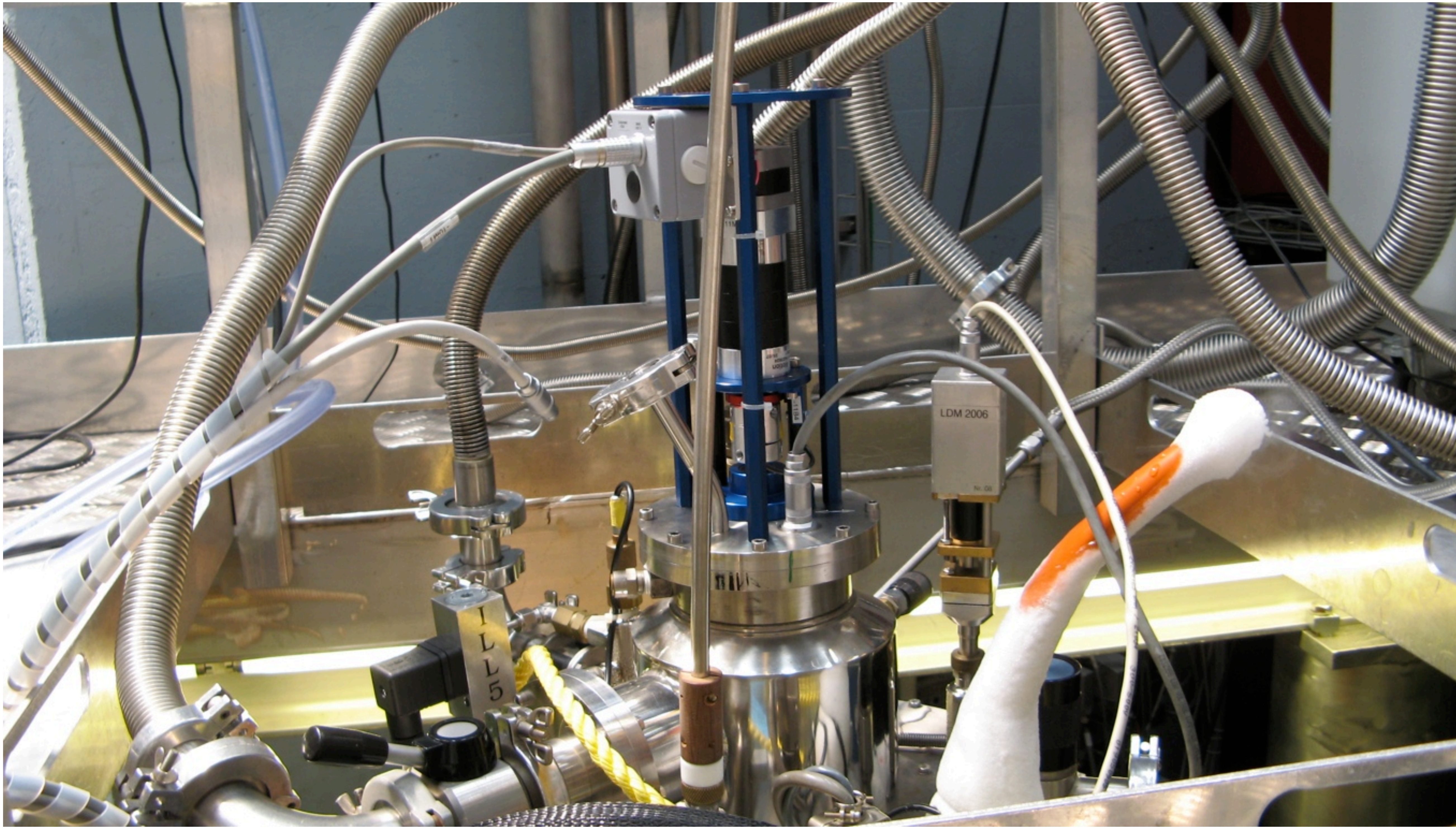

Examples of HRPT applications

Mn-O bond lengths

$(La_{1-y}Pr_y)_{0.7}Ca_{0.3}(Mn^{3+})_{0.7}(Mn^{4+})_{0.3}O_3$

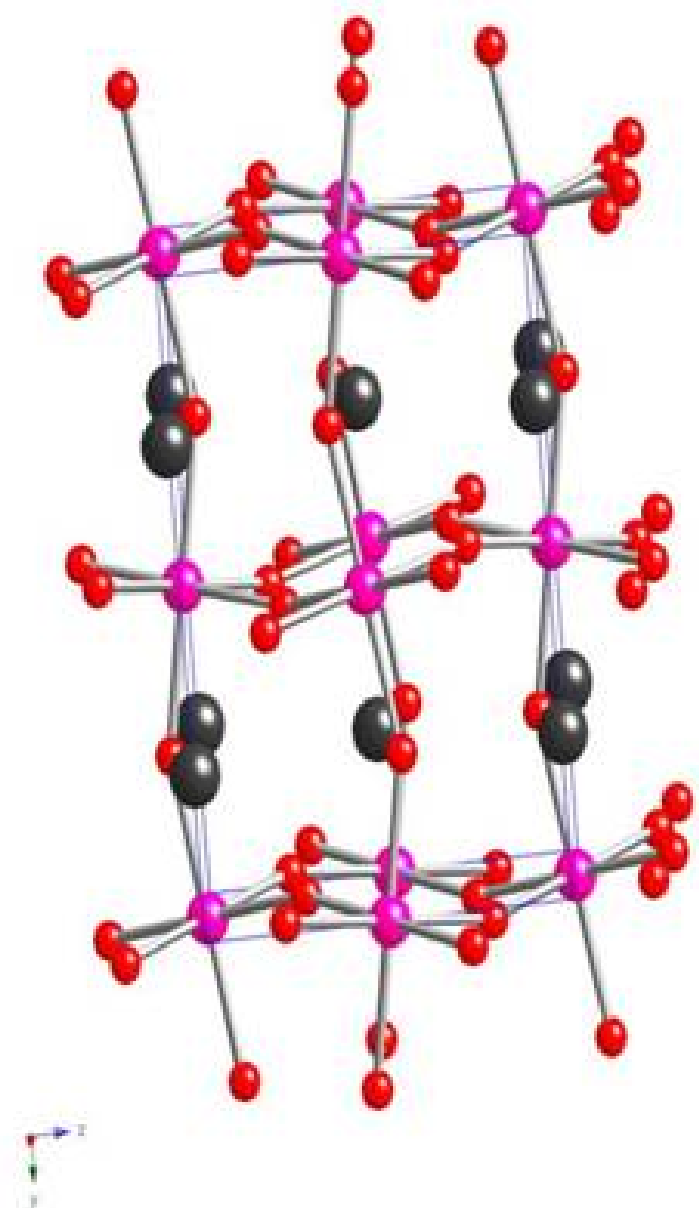

$$|\theta\rangle = \cos\frac{\theta}{2}|3z^2 - r^2\rangle + \sin\frac{\theta}{2}|x^2 - y^2\rangle$$

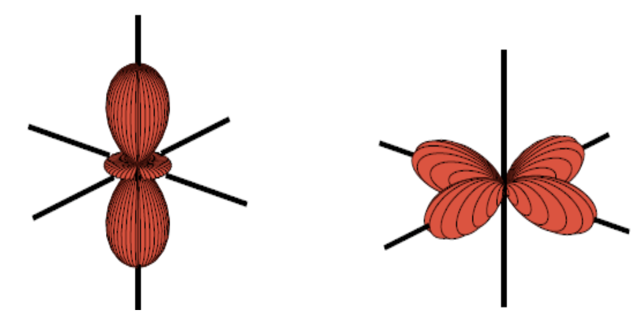

Orbital and charge ordering OO/CO

$(La_{1-y}Pr_y)_{0.7}Ca_{0.3}(Mn^{3+})_{0.7}\,(Mn^{4+})_{0.3}O_3$

$$|\theta\rangle = \cos\frac{\theta}{2}|3z^2 - r^2\rangle + \sin\frac{\theta}{2}|x^2 - y^2\rangle$$

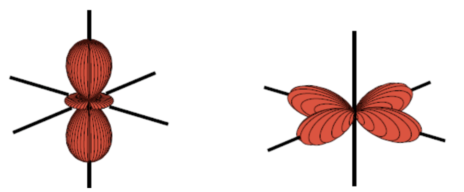

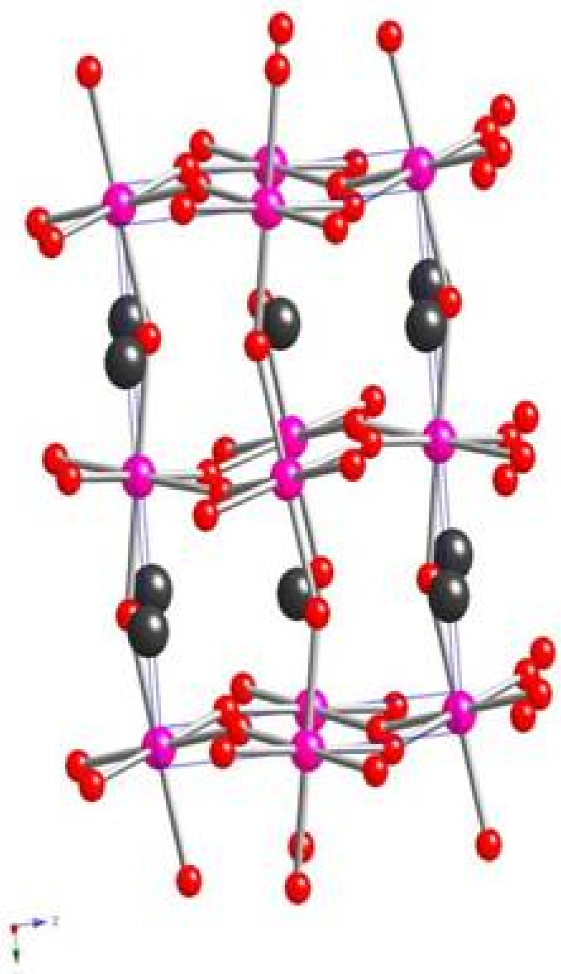

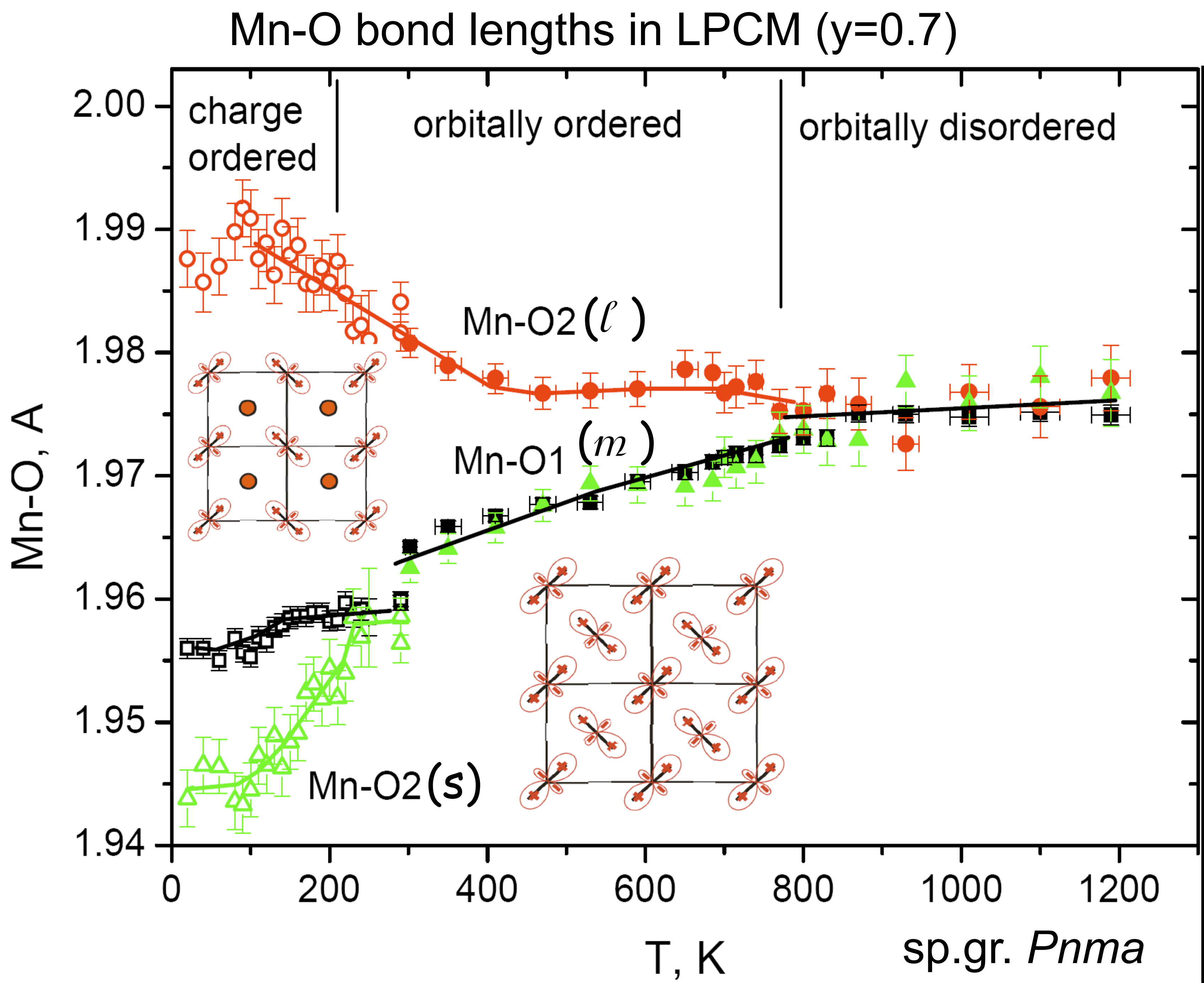

Where are Ni ions in the trimer?

$Ca_3Cu_{3-x}Ni_x(PO_4)_4$ (x=0,1,2)

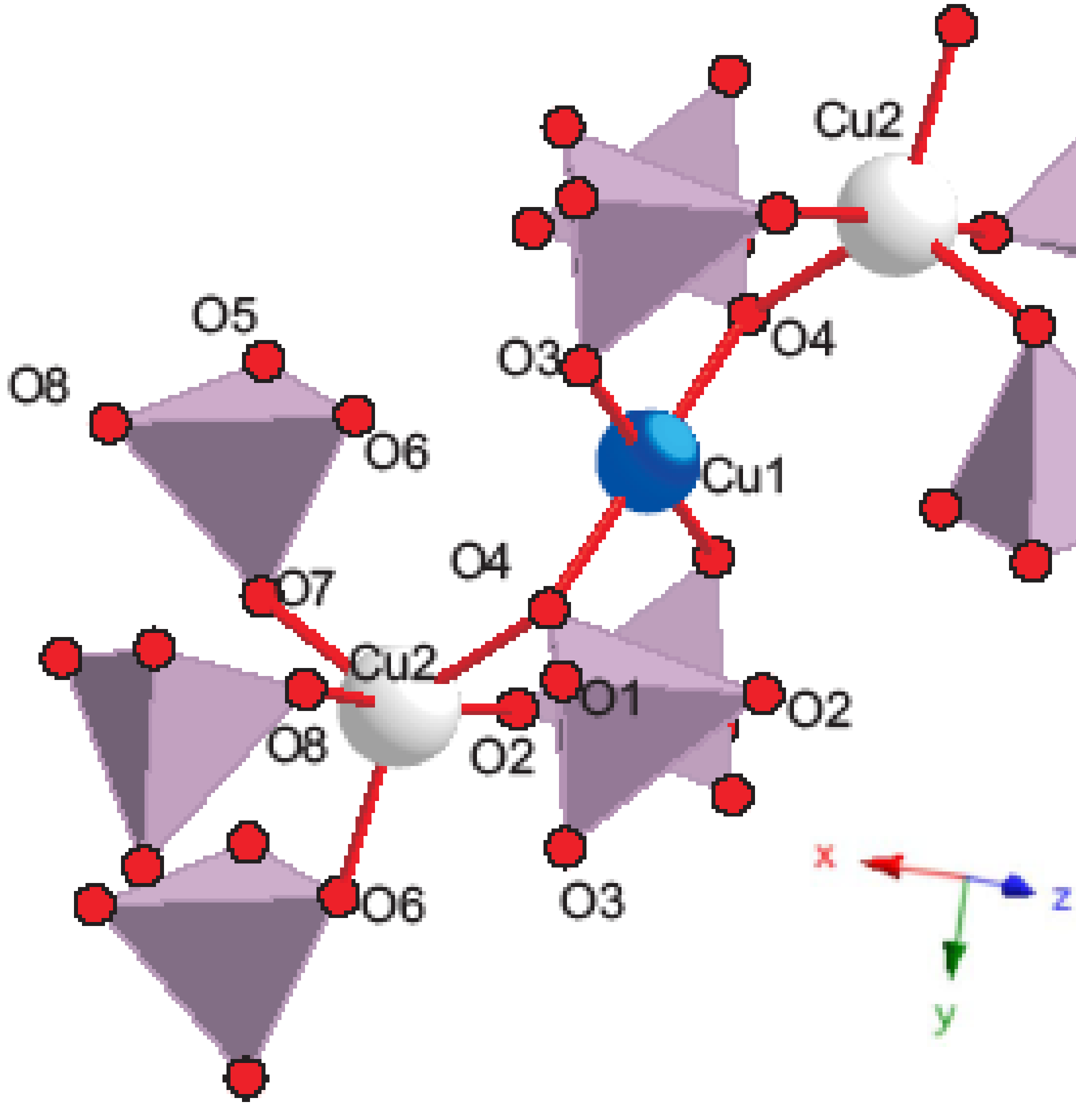

$Ca_3Cu_3(PO_4)_4$ is a novel quantum spin trimer system in which the three Cu^{2+}(S = 1/2) spins are antiferromagnetically coupled giving rise to a doublet ground state. By substituting a Cu^{2+} spin in the trimer by Ni^{2+} (S = 1) a singlet ground state could be in principle realized offering the observation of the Bose-Einstein condensation in a quantum spin trimer system.

Crystal and magnetic structures and magnetic excitations spin-trimer system $Ca_3Cu_{3-x}Ni_x(PO_4)_4$ (x=0,1,2)

Where are Ni ions in the trimer?

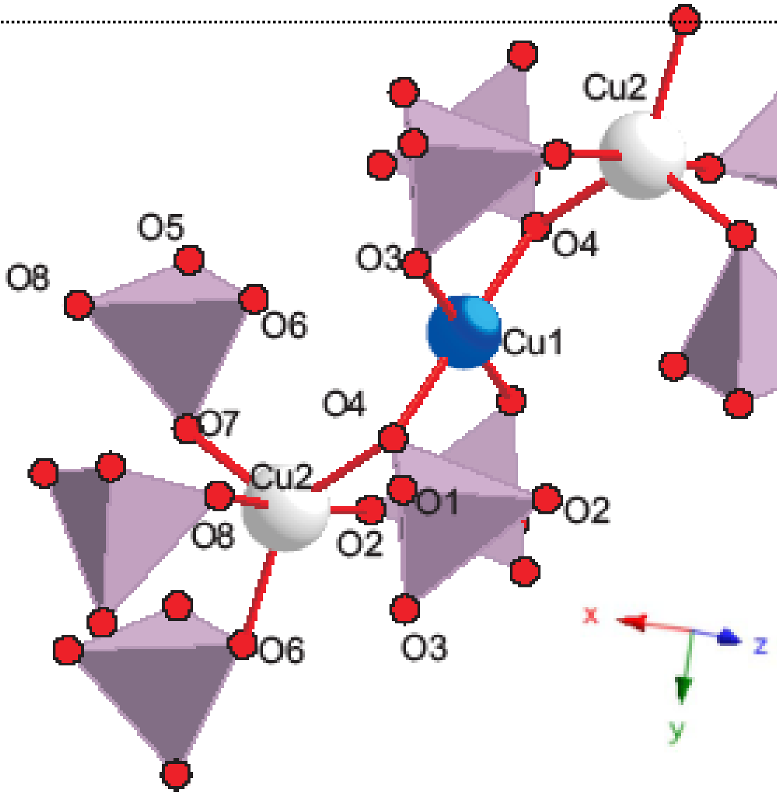

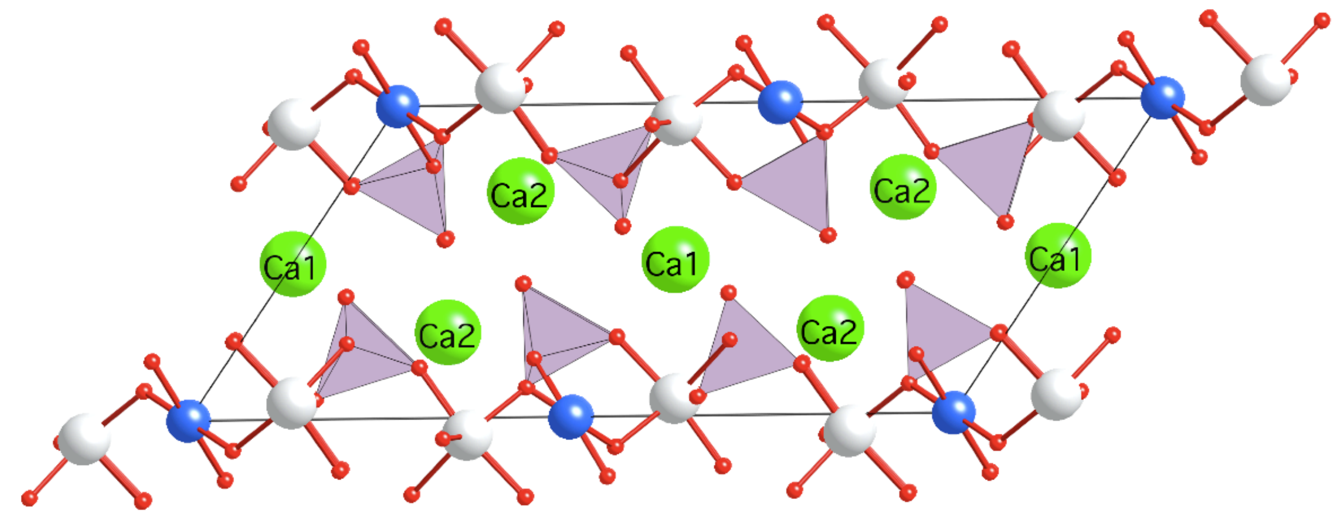

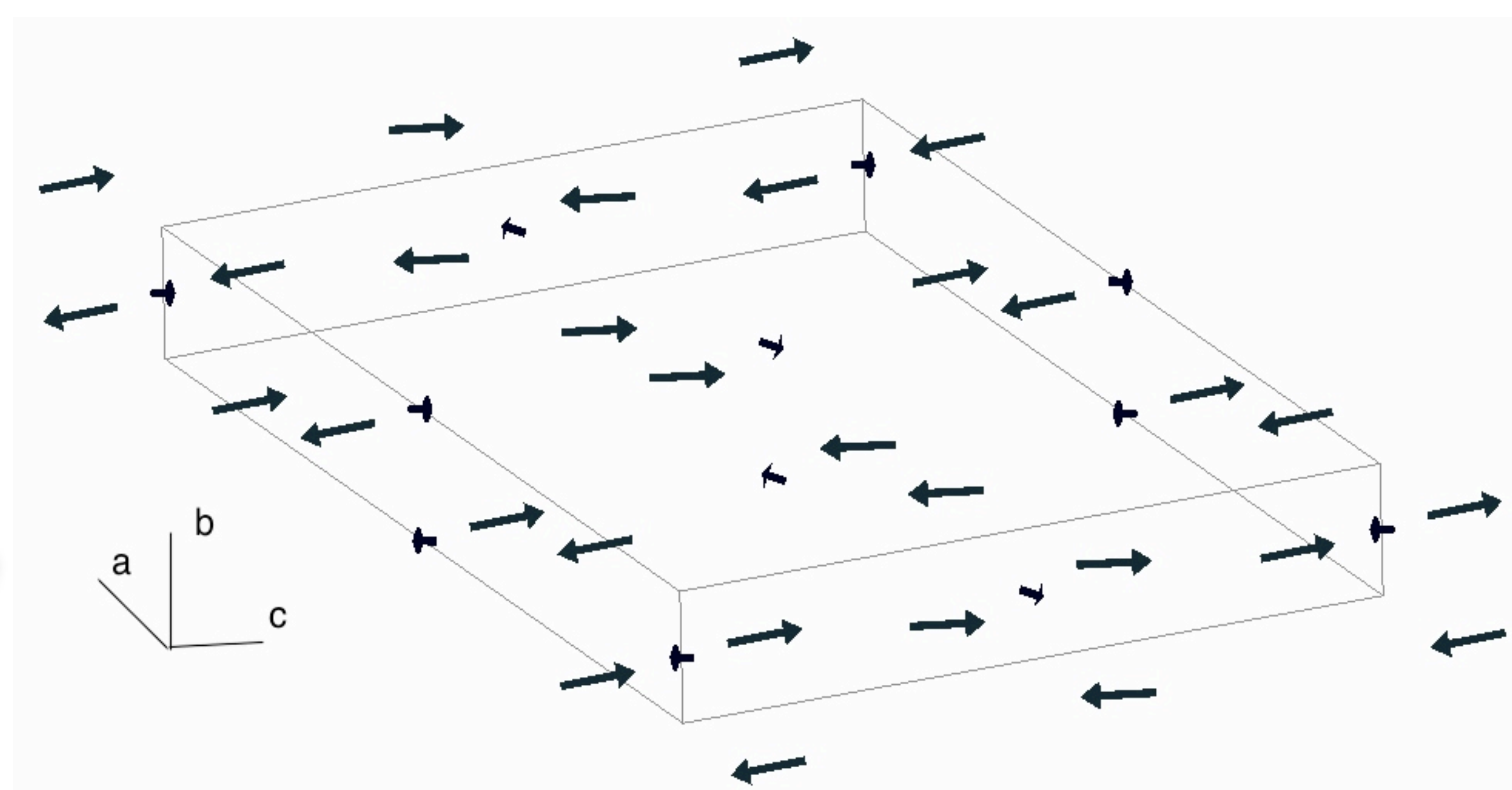

$Ca_3Cu_3(PO_4)_4$ is a novel quantum spin trimer system in which the three Cu^{2+}(S = 1/2) spins are antiferromagnetically coupled giving rise to a doublet ground state. By substituting a Cu^{2+} spin in the trimer by Ni^{2+} (S = 1) a singlet ground state could be in principle realized offering the observation of the Bose-Einstein condensation in a quantum spin trimer system.

C(CrBr)$_4$-liquid in gas pressure cell. T-P phase diagram

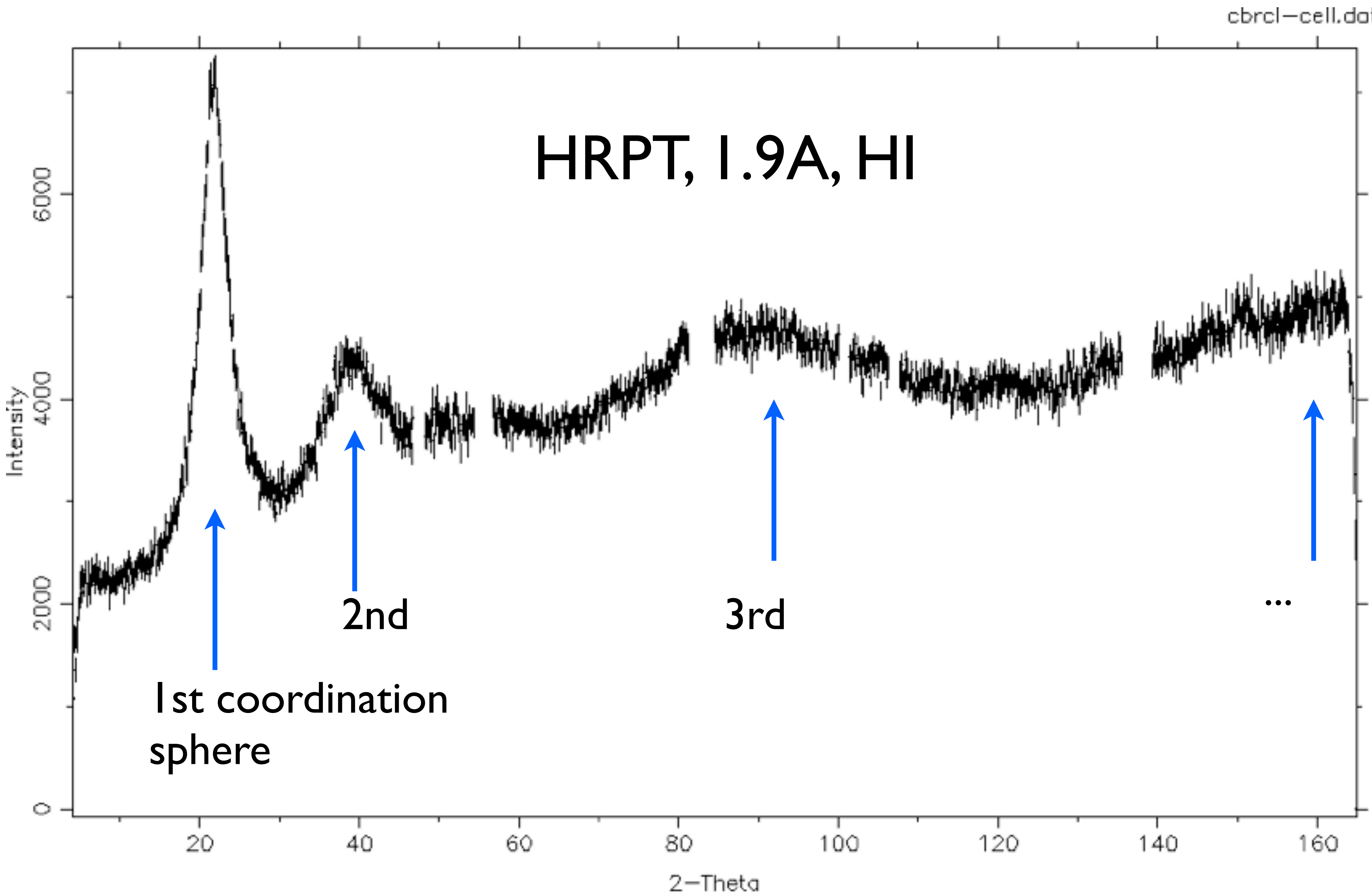

M.Barrio, et al (2009)

High pressure structure transition in quantum dimer system $SrCu_2(BO_3)_2$

Anvil pressure cell installed at HRPT diffractometer

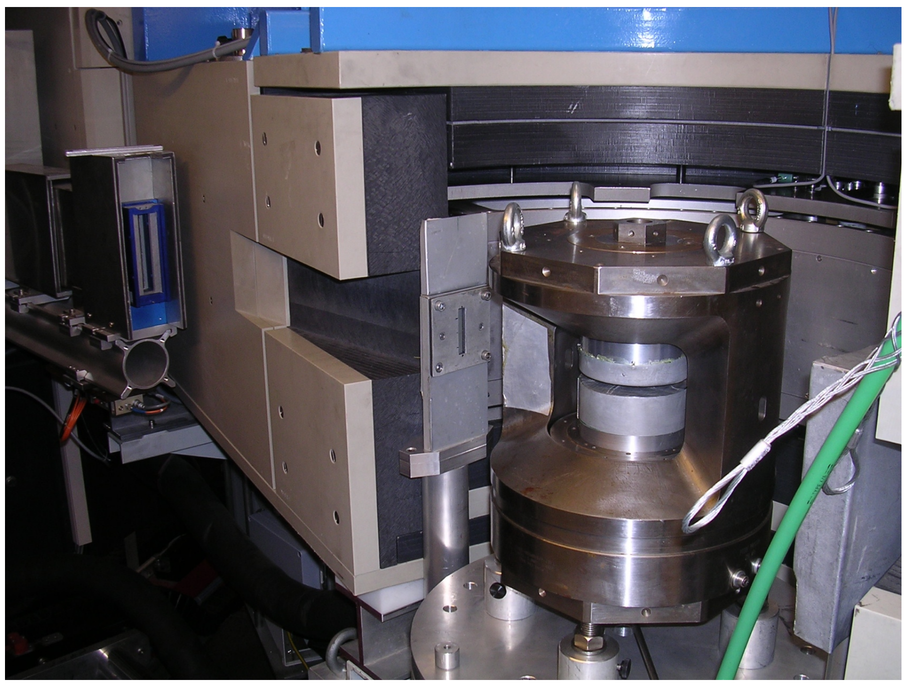

detector shielding + radial collimator + BN anvils + low noise ellectronics = excellent peak to background ratio

p=8GPa: monoclinic *C2:* the new structure solved from the HRPT data!

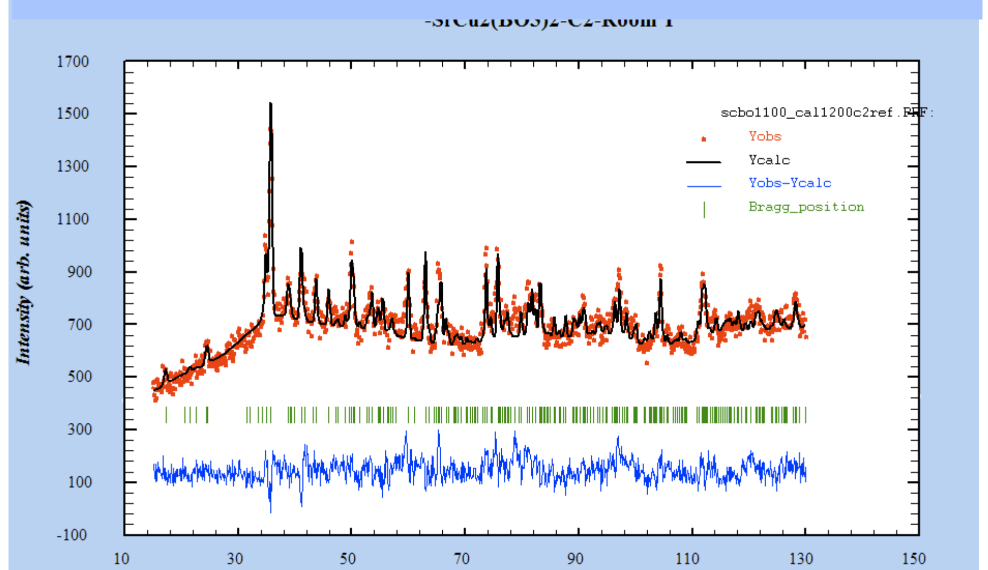

p=3.7GPa, known tetragonal *I-42m structure*

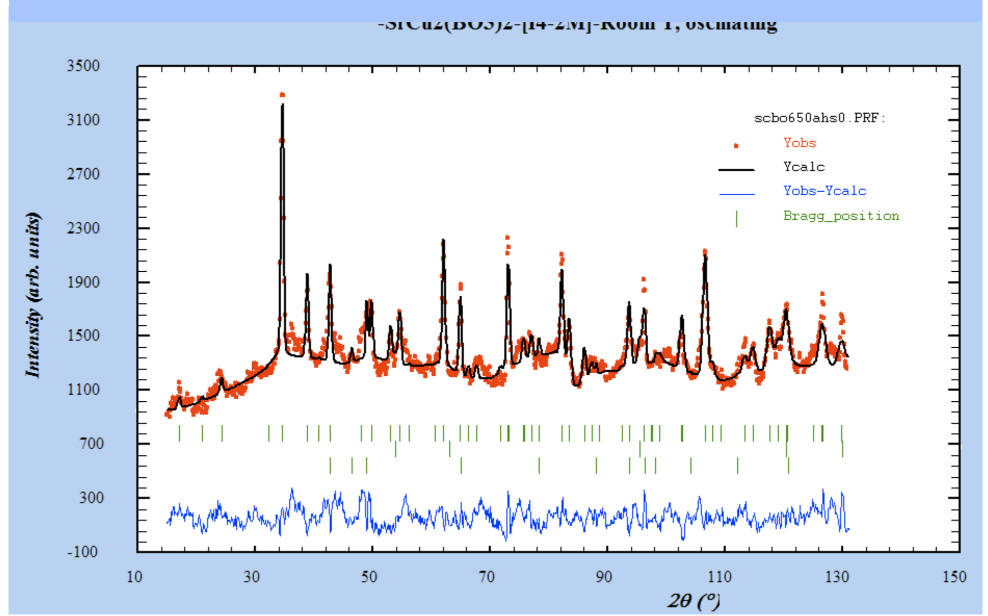

The S=1/2 moments of the Cu^{2+} ions are arranged in a 2D lattice of strongly coupled dimers (J=85 K).

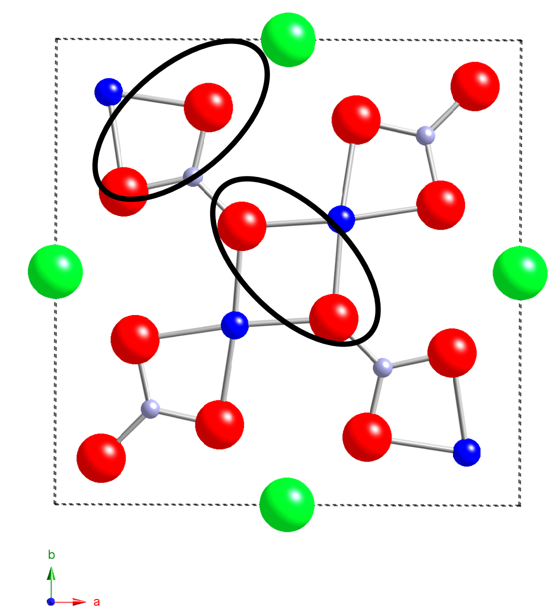

- The material is predicted to undergo a quantum phase transition by application of hydrostatic pressure.
- To fully understand the magnetic properties of the material the knowledge of the exchange paths as a function of pressure is mandatory.

LNS, PSI: V. Pomjakushin, Th. Strassle, K. Conder, E. Pomjakushina
EPFL: M. Zayed, H. Ronnow

High pressure structure transition in quantum dimer system $SrCu_2(BO_3)_2$

Anvil pressure cell installed
HRPT diffractometer

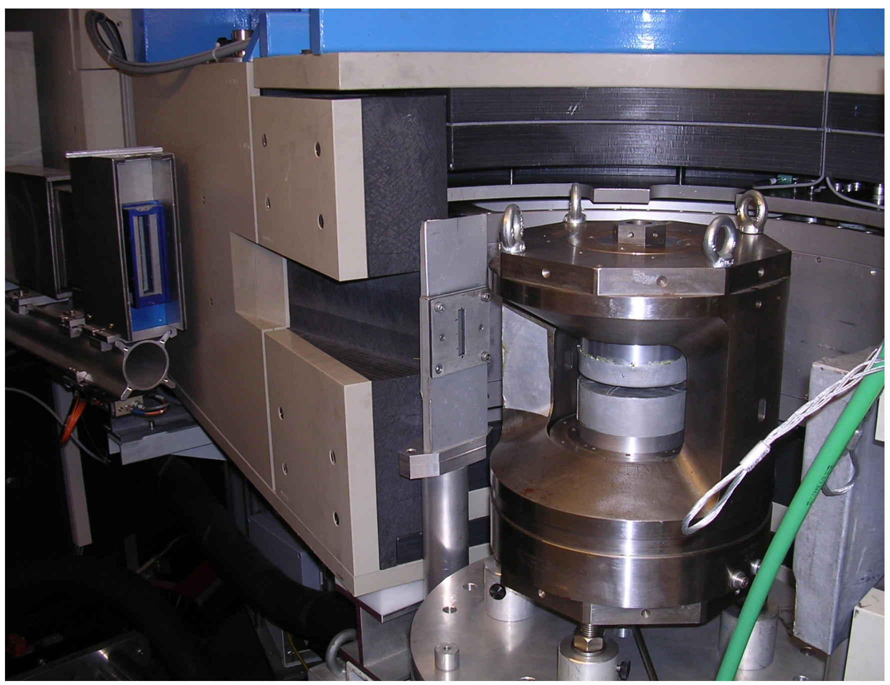

detector shielding + radial collimator + BN anvils + low noise ellectronics = excellent peak to background ratio

LNS, PSI: V. Pomjakushin, Th. Strassle, K. Conder, E. Pomjakushina
EPFL: M. Zayed, H. Ronnow

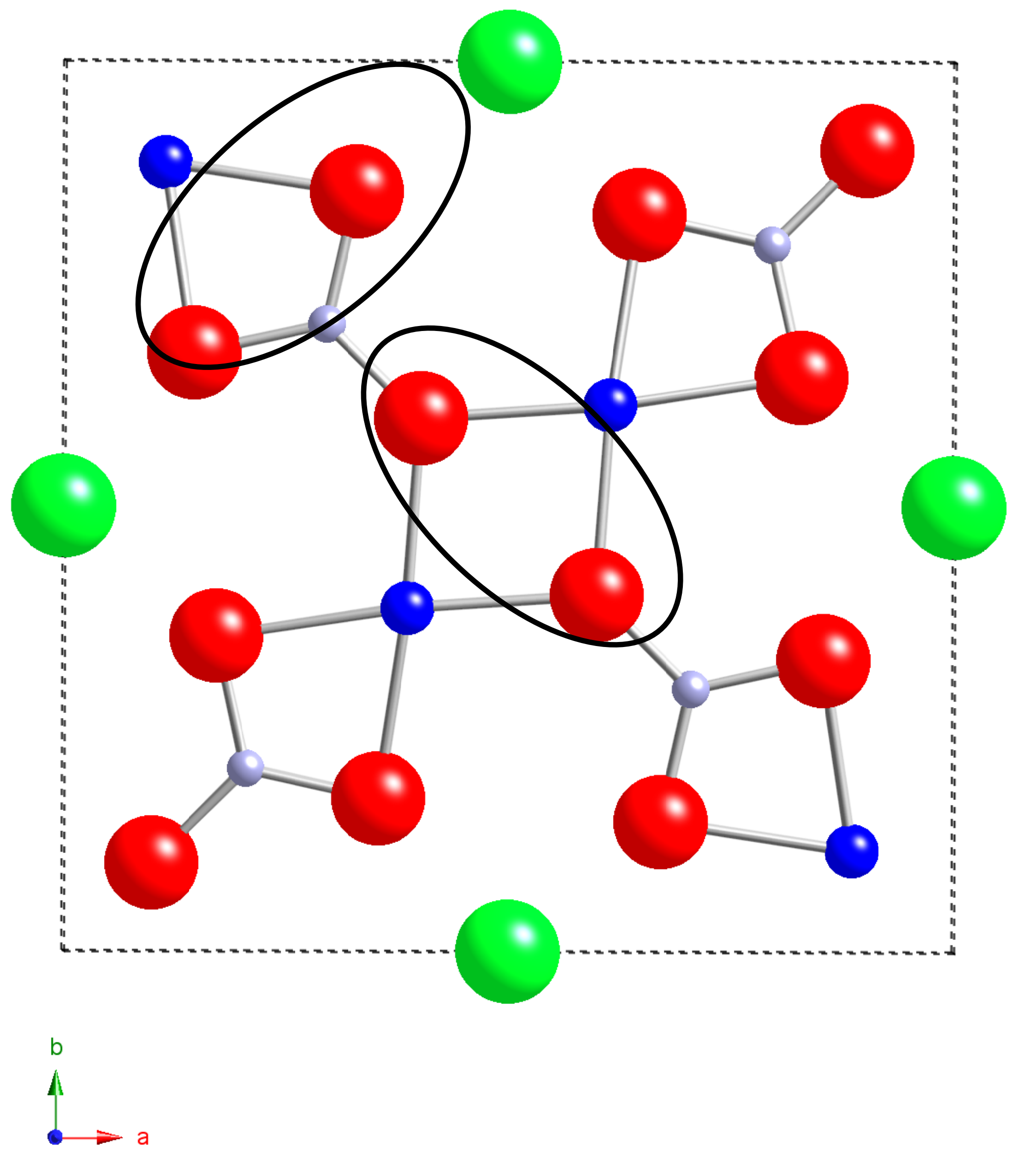

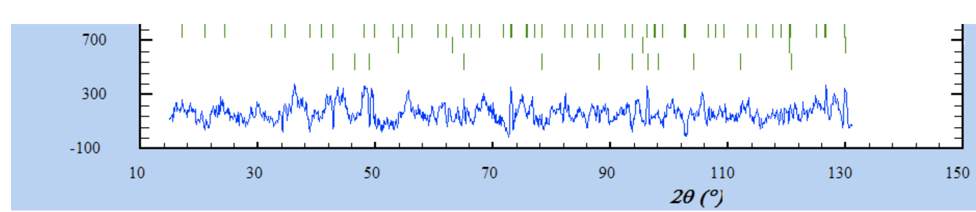

The S=1/2 moments of the Cu^{2+} ions are arranged in a 2D lattice of strongly coupled dimers (J=85 K).

- The material is predicted to undergo a quantum phase transition by application of hydrostatic pressure.
- To fully understand the magnetic properties of the material the knowledge of the exchange paths as a function of pressure is mandatory.

High pressure structure transition in quantum dimer system $SrCu_2(BO_3)_2$

p=8GPa: monoclinic *C2:* the new structure solved from the HRPT data!

p=3.7GPa, known tetragonal *I-42m structure*

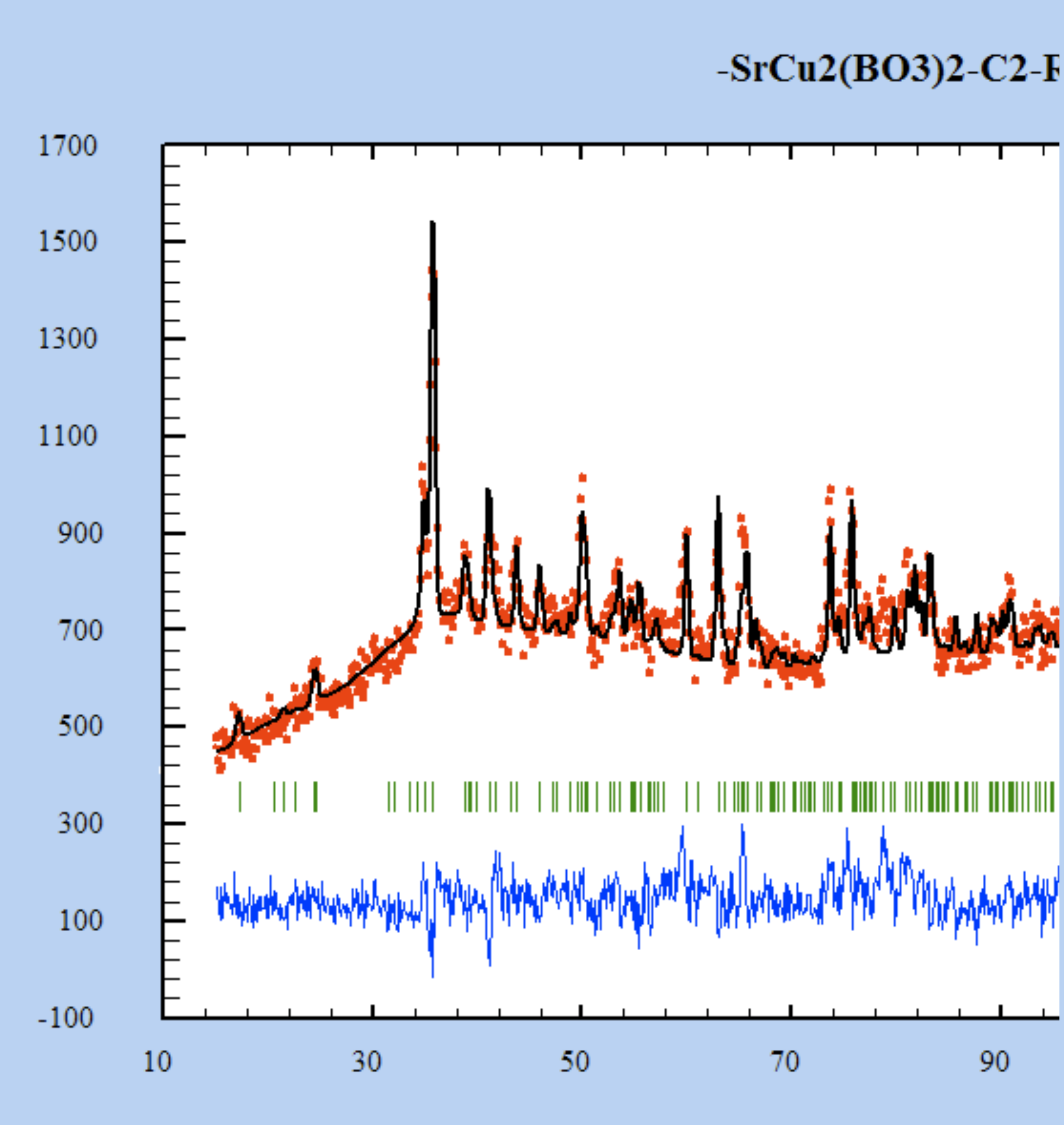

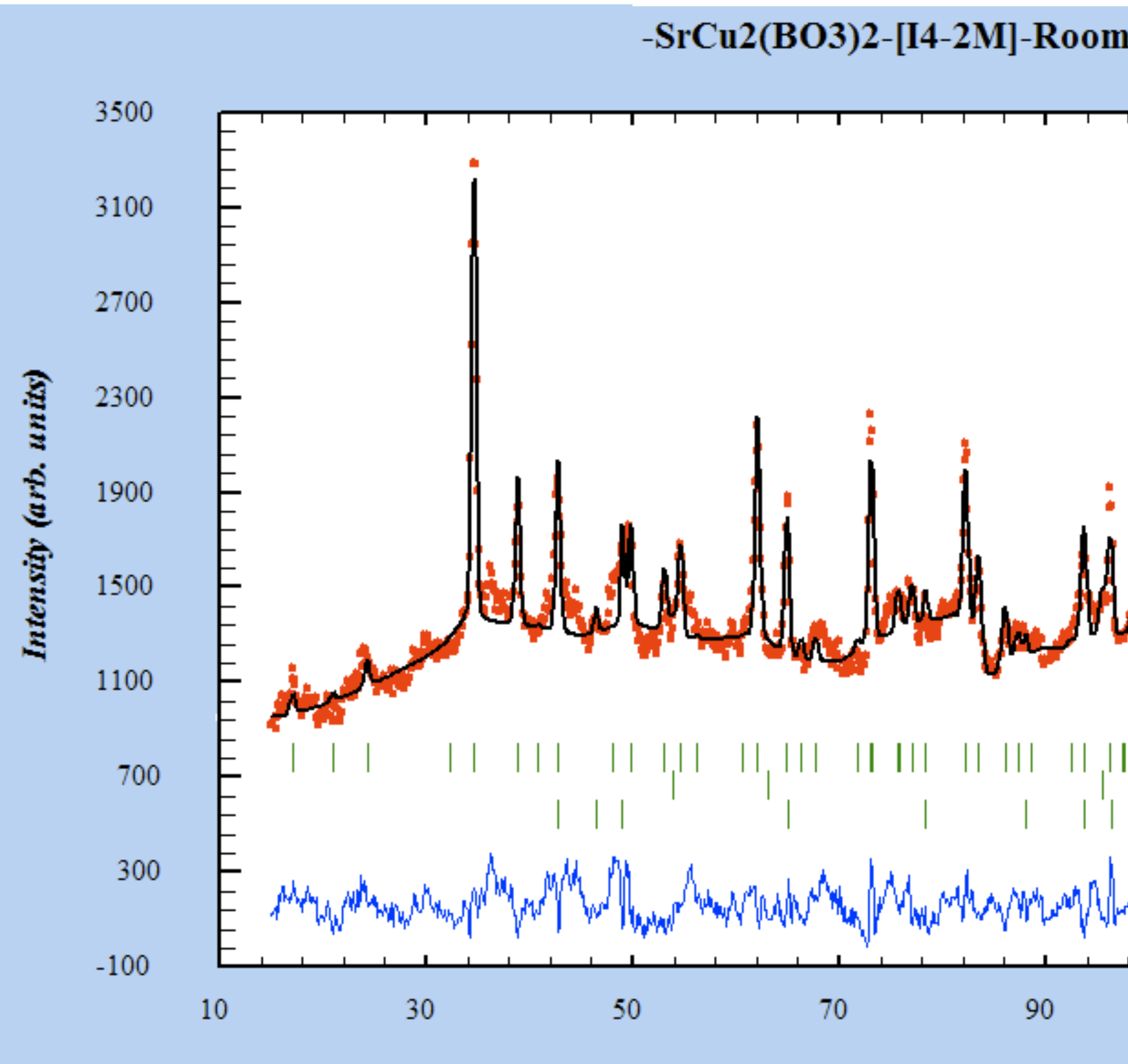

Magnetic structure of $Cu_2CdB_2O_6$ exhibiting a quantum-mechanical magnetization plateau and classical antiferromagnetic long-range order

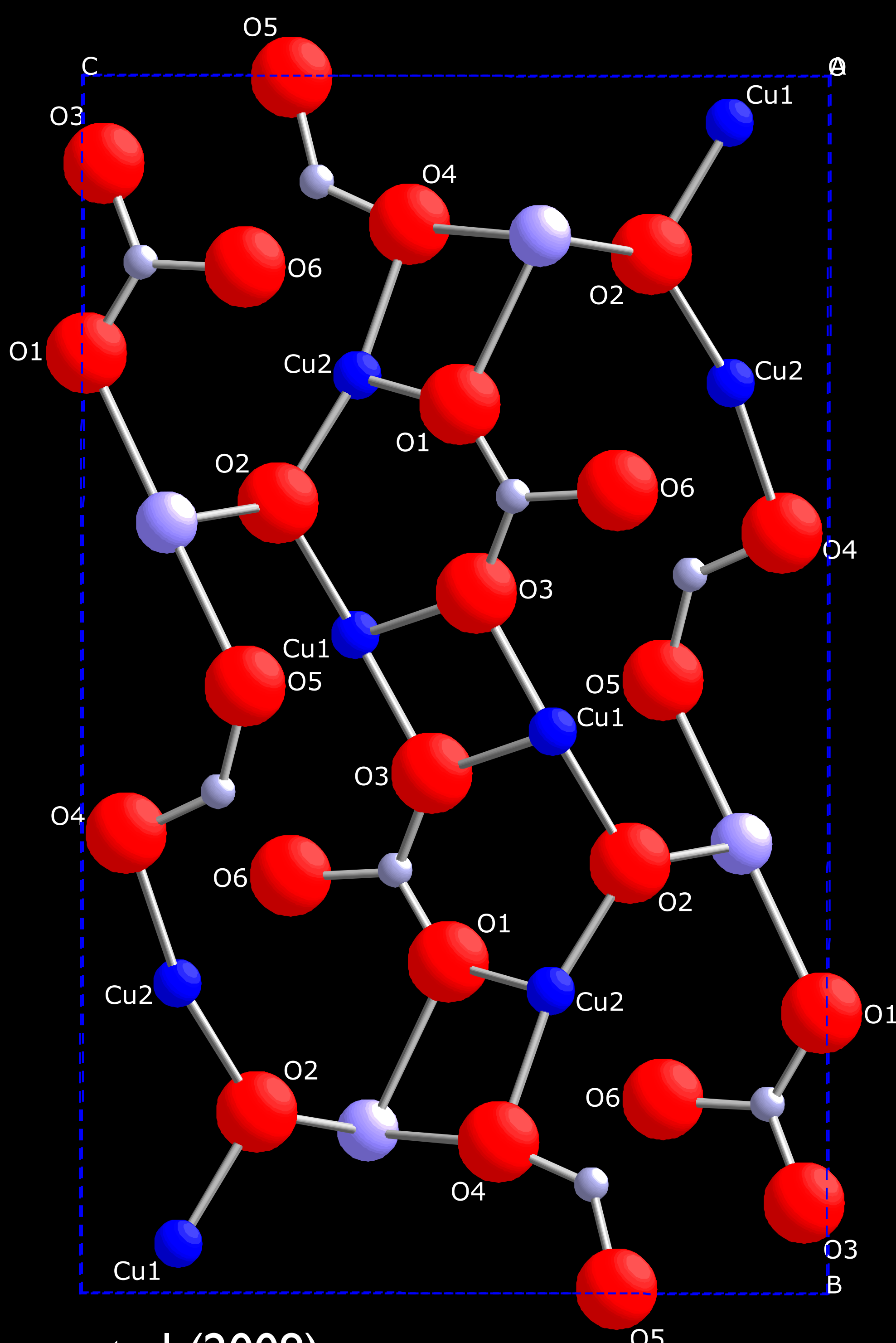

M.Hase, et al (2009)

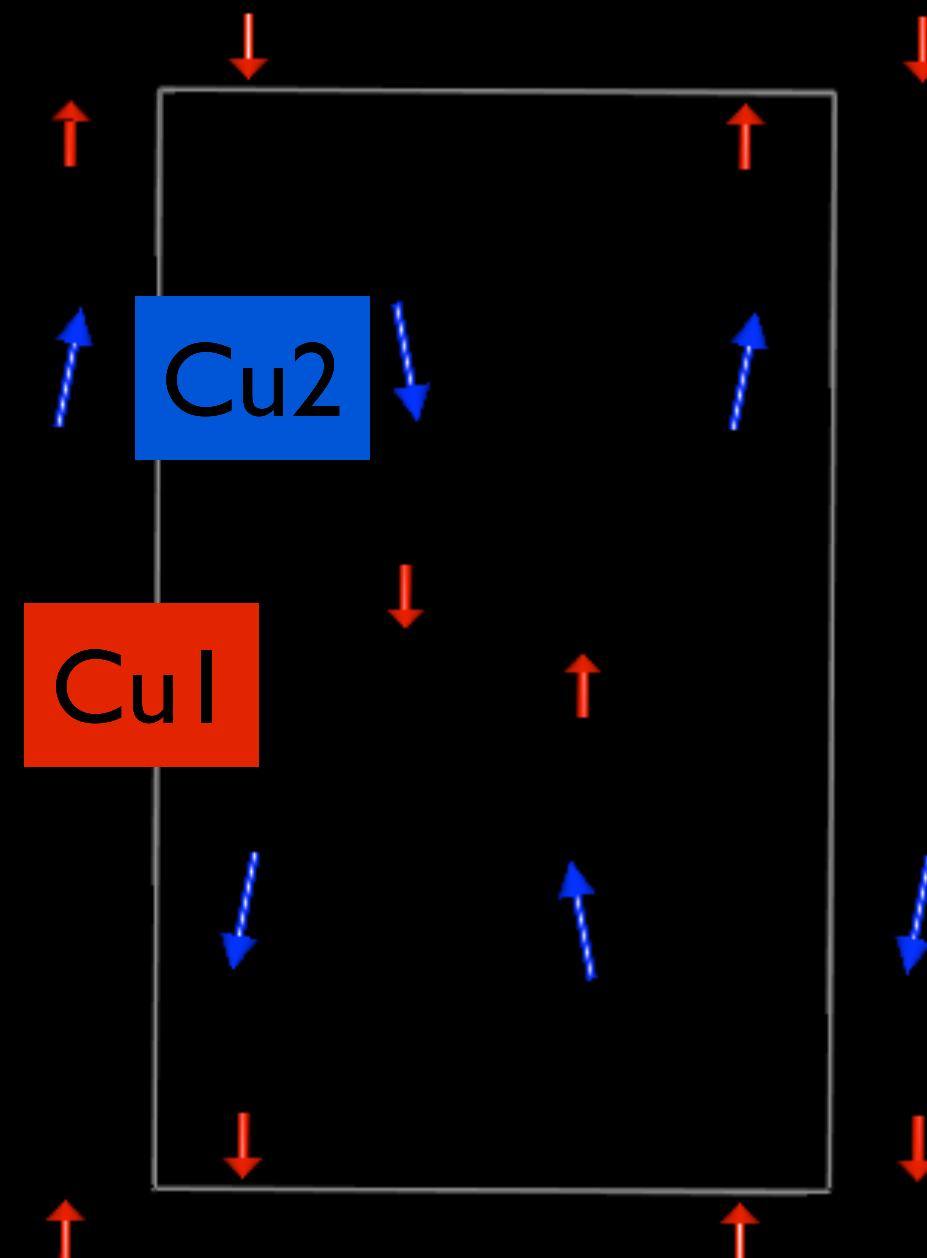

$$\mathbf{F}(\mathbf{H}) \propto \mathbf{M}_{\perp \mathrm{Cu}} \exp(2\pi i \mathbf{R}_{\mathrm{Cu}} \mathbf{H})$$

Lattice distortion (0.1%) and magnetic structure in NiO under high pressures (up to 130kbar) at HRPT

@ p=1bar: μ_{Ni}=1.73(9) μ_B, k =[½ ½ ½] in *Fm3m*

R3-m: a=2.9534(2)Å, α=60.061(2)°

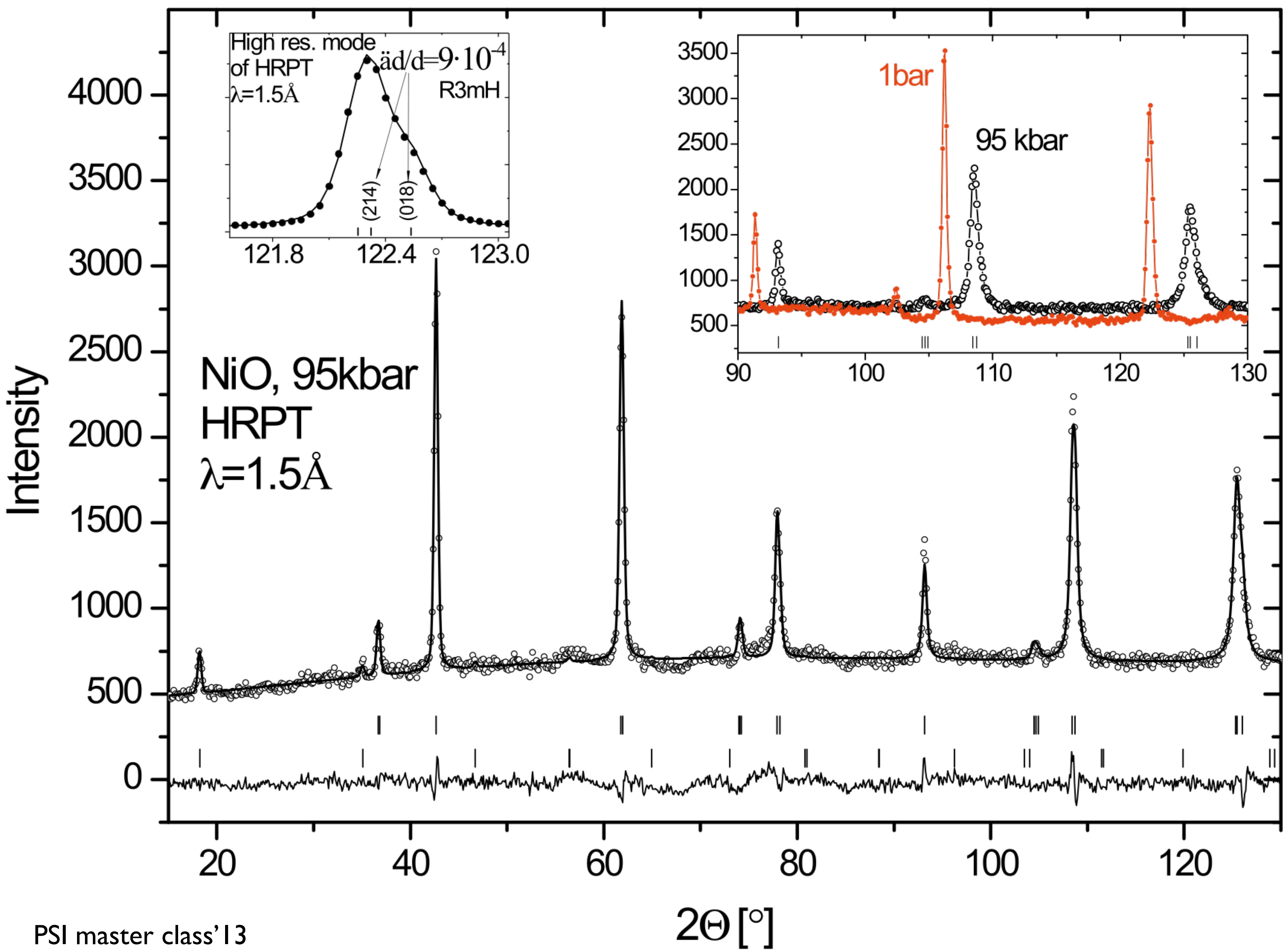

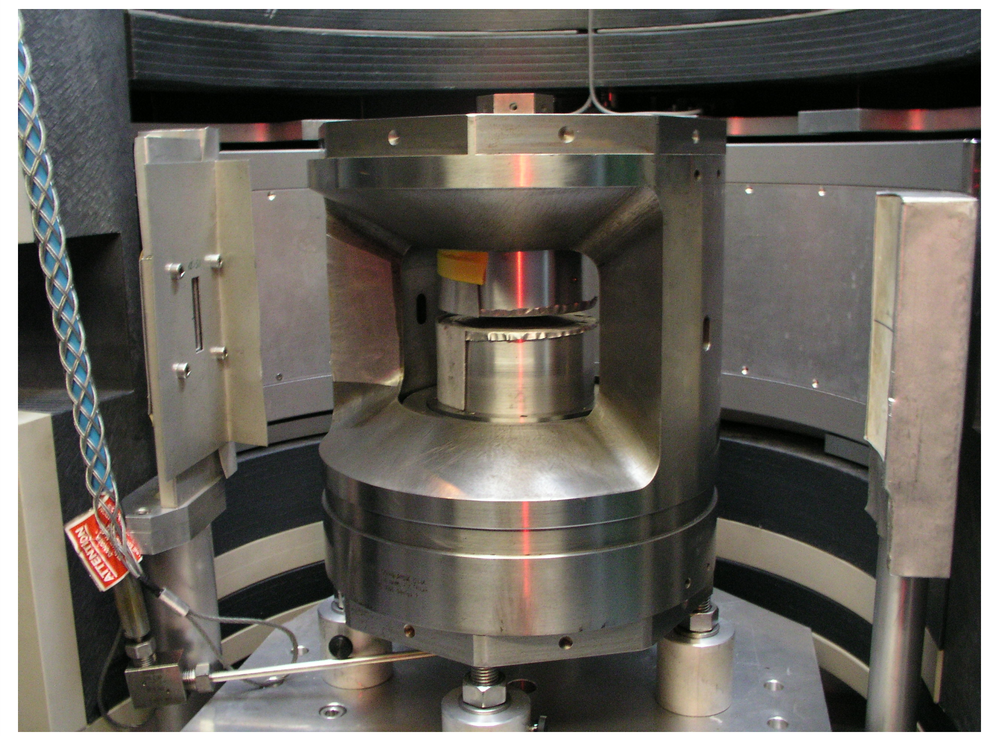

S. Klotz, Th. Strässle, G. Rousse, G. Hamel, V. Pomjakushin, *APL 2005.*

High-pressure studies of $PbMg_{1/3}Ta_{2/3}O_3$ relaxor ferroelectric

S. Gvasaliya, V. Pomjakushin, B. Roessli, Th. Strässle, S. Klotz, S. Lushnikov

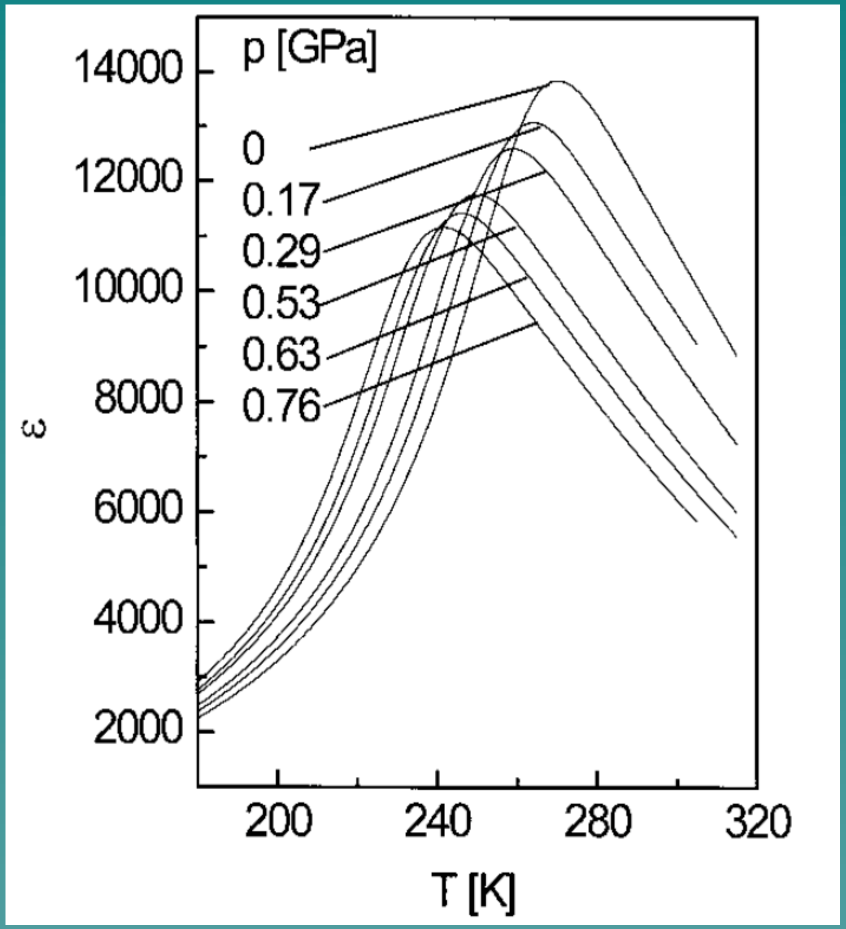

Relaxor ferroelectrics are peculiar crystals where the giant dielectric permittivity appears without structural phase transition. There is no theory which describe their properties. Among other anomalies, there is a suppression of the peak in the dielectric permittivity and of the intensity of diffuse scattering under hydrostatic pressure. In order to understand underlying physics the structure of a model relaxor was studies up to hydrostatic pressure P~7 GPa

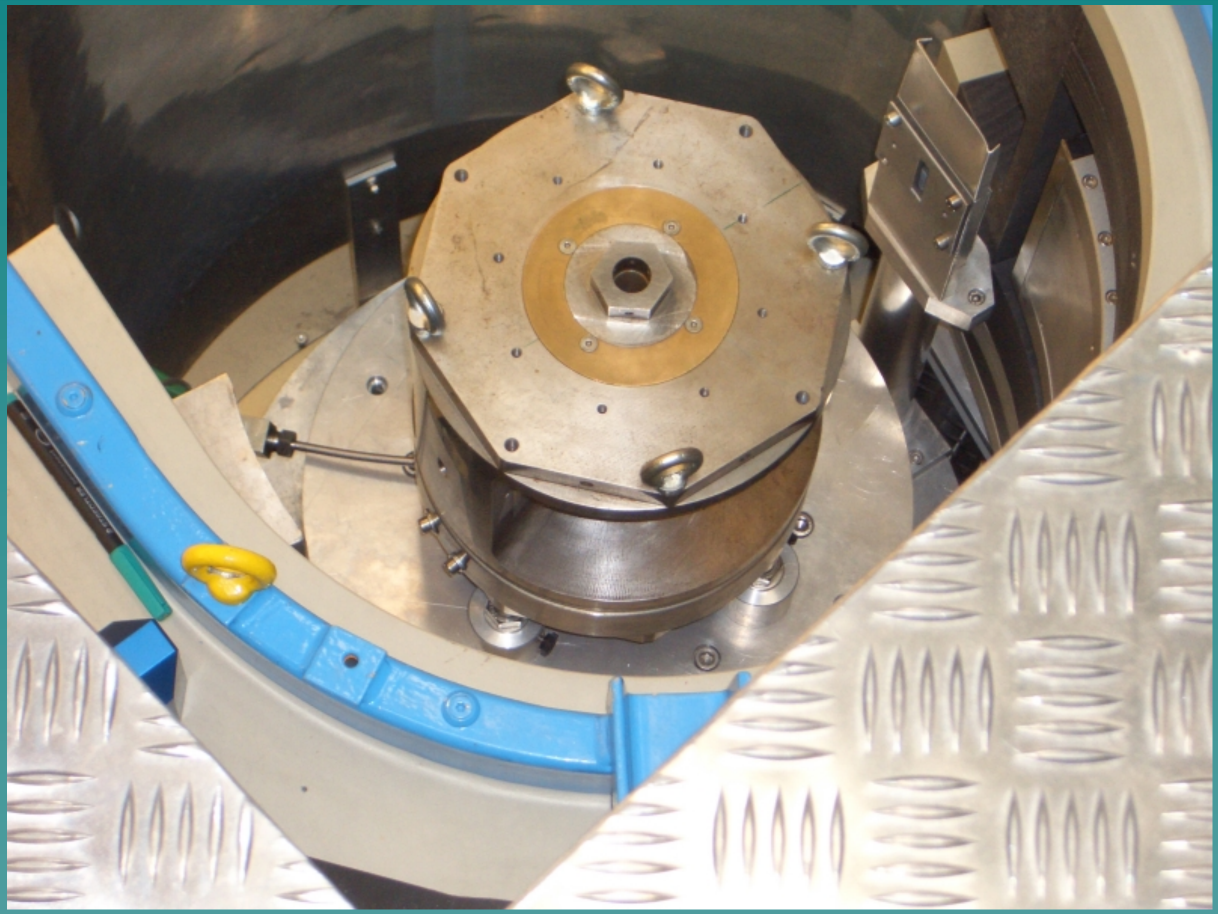

Photo of a high pressure setup using Paris-Edinburgh pressure cell at HRPT diffractometer. The sample volume is less than 100 mm^3, approximately two orders of magnitude smaller than in a standard setup.

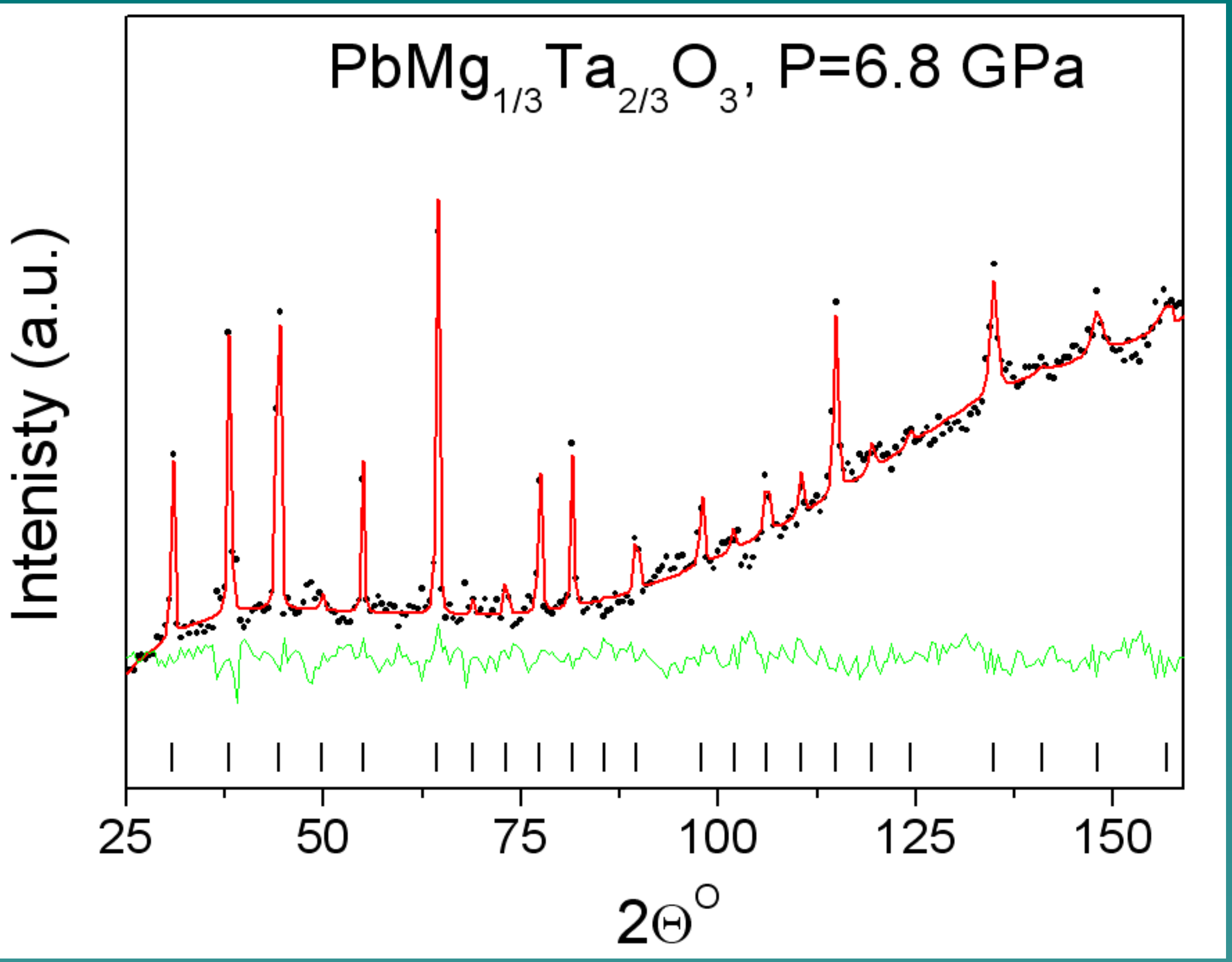

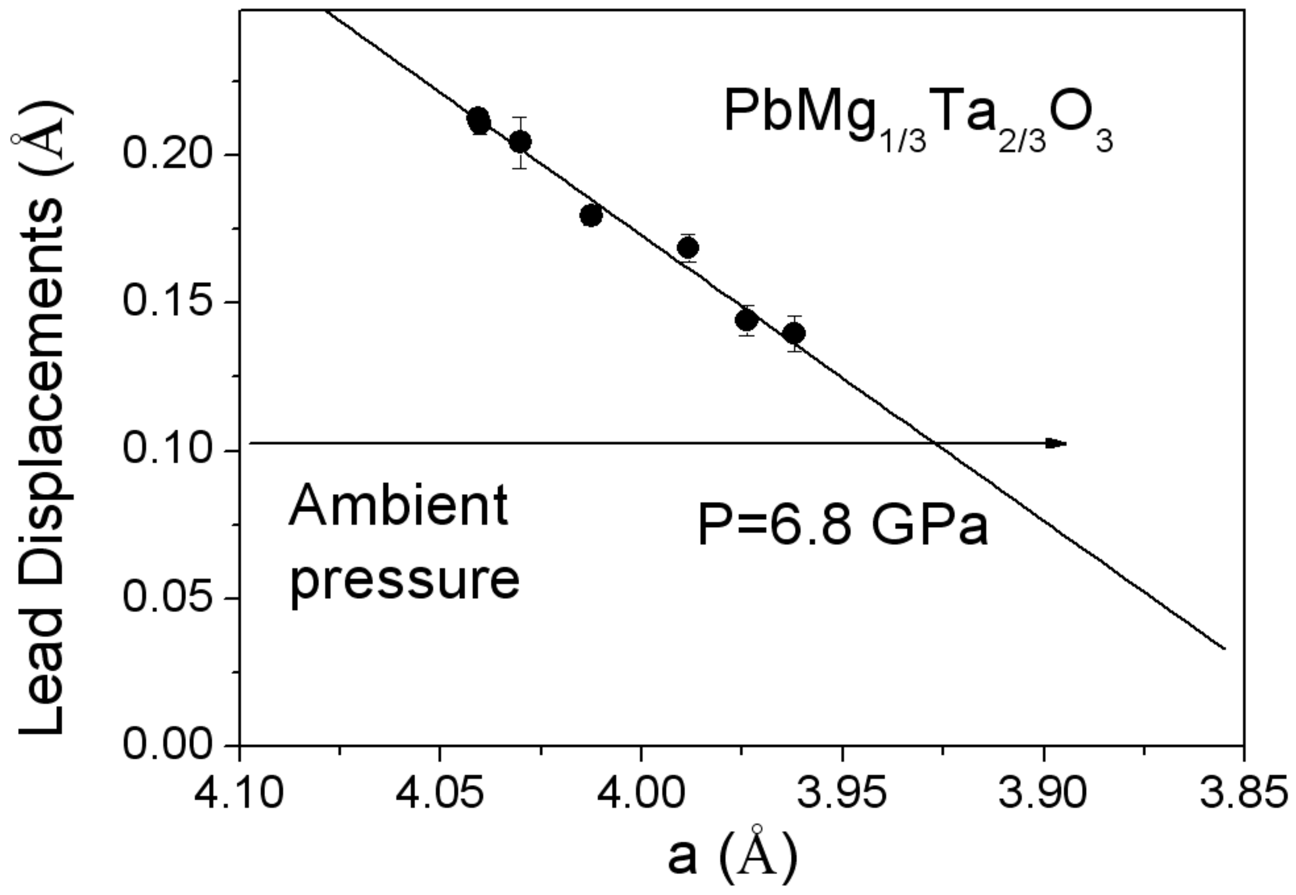

Observed and calculated diffraction spectrum from $PbMg_{1/3}Ta_{2/3}O_3$. Increased background is probably due to the unmasked part of the steel leg of the pressure cell. The crystal structure remains cubic at all pressures. The important changes are: (i) Reduction of the Lead displacements at increased pressures (ii) Appearance of the anisotropy in the Oxygen thermal motion – its ellipsoid becomes significantly elongated toward the Lead ions. Thus these change are responsible for the suppression of the peak in dielectric permittivity and of the diffuse scattering. Similar behaviors were never reported earlier.

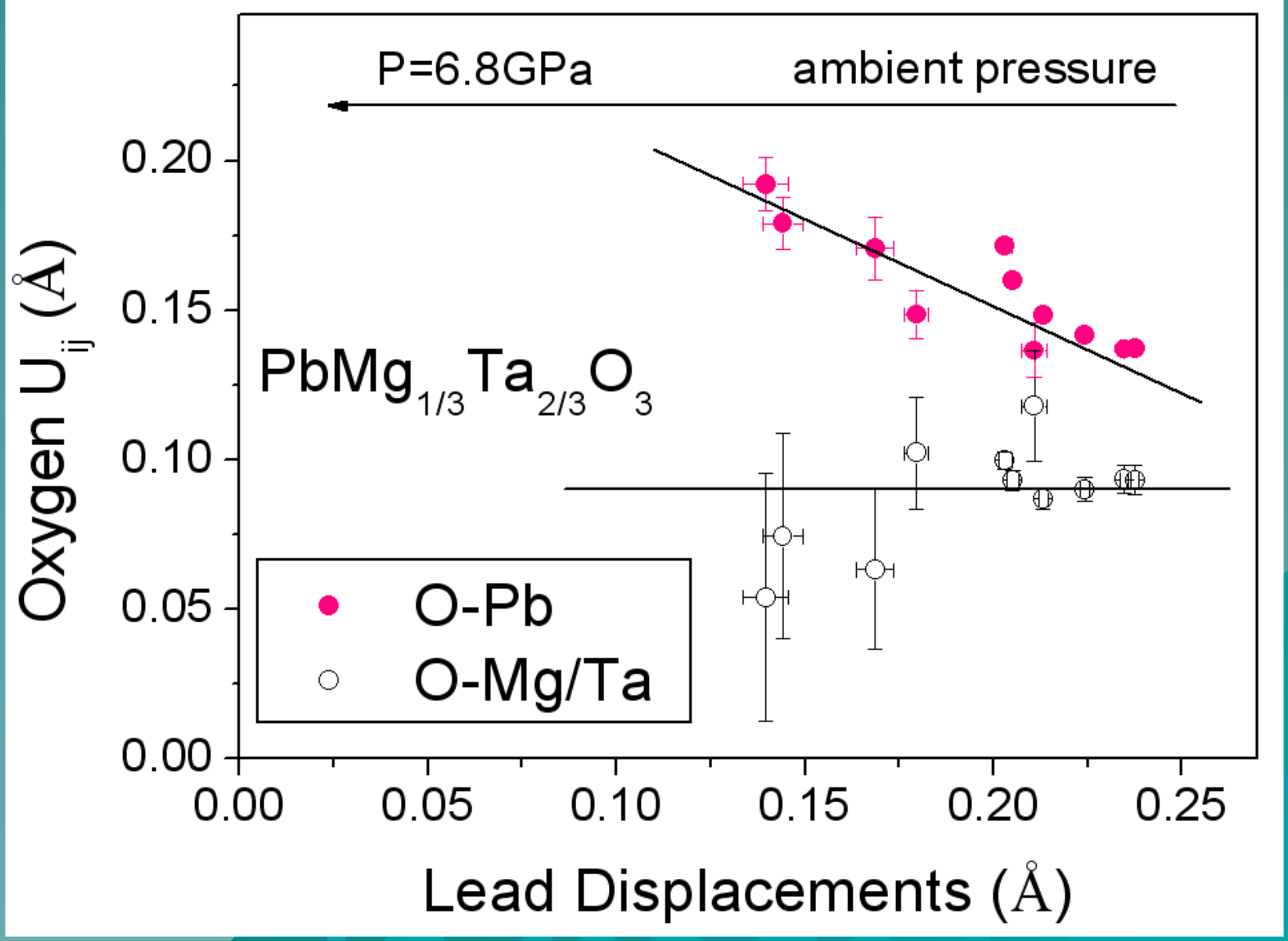

More information about HRPT

http://sinq.web.psi.ch/hrpt

OR

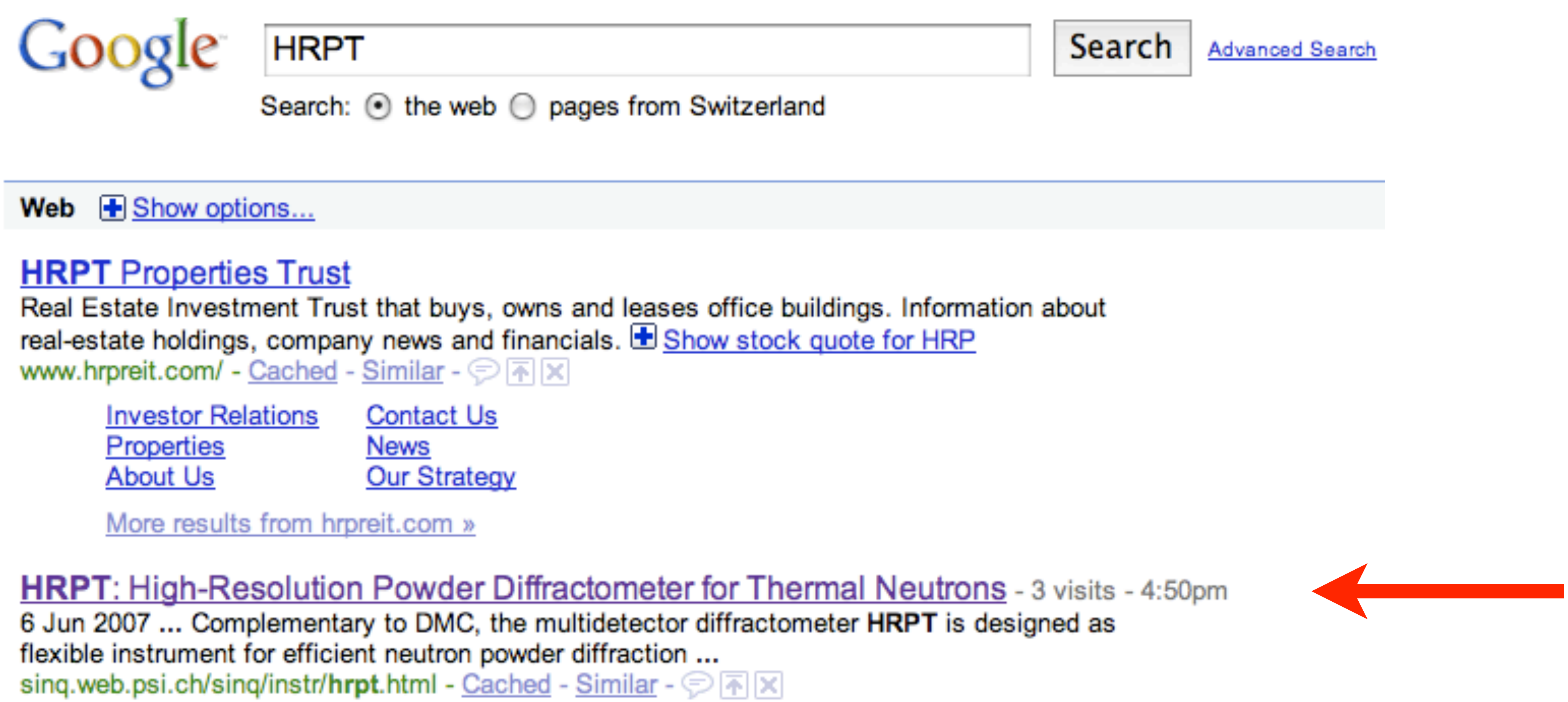

The End